

ELECTRON TRANSPORT PROPERTIES THROUGH A SERIALY CONNECTED CHAIN
OF NANORINGS

A THESIS

SUBMITTED TO THE GRADUATE SCHOOL

IN PARTIAL FULFILLMENT OF THE REQUIREMENTS

FOR THE DEGREE

MASTER OF SCIENCE

BY

MATTHEW B. ORVIS

DR. ERIC HEDIN – ADVISOR

BALL STATE UNIVERSITY

MUNCIE, INDIANA

JULY 2015

*Dedicated to my mom and dad,
for always pushing me and believing in me.*

*To my brother,
for letting me “practice physics” on him.*

*To my wife (fiancée at the time of writing),
for inspiring my every day.*

*And to Jesus Christ,
who gave me a mind and created a world worth exploring.*

TABLE OF CONTENTS

ABSTRACT	i
ACKNOWLEDGMENTS	iii
LIST OF FIGURES	iv
1. INTRODUCTION.....	1
1.1 Context	1
1.2 System	4
1.3 Aharonov-Bohm Effect.....	9
1.4 Zeeman Effect.....	16
2. METHODS	25
2.1 Tight-Binding Formalism.....	25
2.2 Dispersion Relation.....	30
2.3 Simple 1 Dimensional Lattice Example	32
2.4 Computational Method.....	37
3. NON-MAGNETIC RESULTS.....	42
3.1 Changing coupling parameter	42
3.2 Changing leads	45
3.3 Changing system size	48

4. MAGNETIC RESULTS	57
4.1 Sharpened AB Oscillations.....	57
4.2 Magnetic flux effect on energy bandgaps.....	65
4.3 Coupling parameters effect on magnetic flux sensitivity.....	73
4.4 Zeeman Effect impact on bandgap.....	79
5. CONCLUSION	84
6. REFERENCES.....	88
7. APPENDIX A	91
8. APPENDIX B	100
9. APPENDIX C	110
10. APPENDIX D	114

ABSTRACT

THESIS PROJECT: Electron Transport Properties through a Serially Connected Chain of Nanorings

STUDENT: Matthew B. Orvis

DEGREE: Master of Science

COLLEGE: Sciences and Humanities

DATE: July 2015

PAGES: 130

The field of spintronics differs from classical electronics in that it uses the spin of the electron, rather than the charge, to convey binary information. Certain topics of study in this field are the transmission properties of coupled molecular and mesoscopic rings, and in particular the electron-spin transport in semiconductor nanostructures and nanoscale electronic devices. Experimental work has shown magnetic effects on these mesoscopic rings, showing interesting flux dependence of the total wave function. The Aharonov-Bohm (AB) Effect has been studied and shown to impact transmission resonances in the transport through multiple rings. The Zeeman Effect has also been theoretically and experimentally shown to split energy levels and provide the possibility of clear spin filtering through quantum dots (QDs) in an externally applied magnetic field.

In this thesis, a system of multiple nanorings with embedded quantum dots connected serially will be explored. Each ring consists of a hexagonal structure of 6 QDs, coupled to the adjacent rings at each end in the “arm chair” configuration. The transmission of an electron

through a specified number of rings via a Tight-Binding computational model will be solved. The effect of an applied external magnetic field is modeled by including the Zeeman Effect and AB Effect in the system Hamiltonian. The AB Effect introduces a phase shift into the system, modifying the band structure, while the Zeeman Effect splits the electron transmission energy levels according to spin. Along with these magnetic effects, the effect of altering the site energies and hopping integrals of individual QDs will also be investigated. The number of rings connected serially will also be altered and its effect analyzed. Finally, these results will be generalized and applied towards learning more about transmission effects through graphene, the 2-dimensional application of this system's 1-dimensional nanoring chain.

ACKNOWLEDGMENTS

I would, first and foremost, like to acknowledge and thank my advisory, Dr. Eric Hedin. He has put almost as much time into my work as I have, from teaching me and giving me a foundational understanding of the topics, to developing programs to check mine, to editing my papers. He has pushed me, guided me, taught me, and corrected me. He has shown patience and creativity in facilitating me doing this thesis work. Dr. Yong Joe has also contributed greatly, as he has provided many ideas and corrections to me and Dr. Hedin.

I would like to thank the rest of the professors who taught me in graduate classes at Ball State. Dr. Cancio has been a frequent professor of mine, and one who has been incredibly inspiring and helpful in my academic endeavors. Dr. Nelson, Dr. Khatun, Dr. Islam, Dr. Jin, and Dr. Grosnick have all taught me in classes and have all helped instruct me in the art of physics.

I would like to thank my committee members, Dr. Hedin, Dr. Joe, Dr. Jordan, and Dr. Cancio for being willing to put up with me and for their help in producing this thesis.

I would like to thank my fellow graduate physics students at Ball State. They have been there through times of head scratching in basements and bars and have become some of my closest friends.

Finally, I would like to thank the Ball State Physics and Astronomy Department for giving me a place to study and research. Thank you for helping me in my endeavors to contribute and grow as a human being.

LIST OF FIGURES

Figure 1-1 Diagram of a chain of 2 serially connected nanorings with no magnetic field. There are 2 QDs on each arm, and one on either side, for a total of 6 QDs per ring. Each ring is connected via a single lead, and leads run into and out of the system. The number of rings connected serially, N , may also be varied as a parameter in the computation.	6
Figure 1-2 Diagram of system with applied magnetic field. Note each QD splits into 2 energy levels, with the difference plus or minus the Zeeman energy. Also note the flux passing through the center, which shifts the phase according to the AB effect.	7
Figure 1-3 Plot showing the potential barriers of a quantum dot a function of position. Each QD is modeled as two potential barriers, which can be shown to create a resonant energy which allows for quasi-bound states to be formed. [22].....	7
Figure 1-4 Plot showing transmission vs energy for a single quantum dot. Notice there is a single transmission peak, which corresponds to the resonant energy created by the 2 potential barriers of the QD. [22].....	8
Figure 1-5 Depiction of the relationship between a constant magnetic field B in a finite region of space and magnetic vector potential A [23].....	9
Figure 1-6 (a) Depiction of electron beam split around a solenoid. When the beam recombines, it is experienced a phase shift due to the presence of the magnetic vector potential. (b) Shows direction of phase shift, where A is vector potential and k is electron wave vector. [25]	11
Figure 1-7 Illustration of the alignment of the spin angular momentum and magnetic dipole moment (red) with the applied external magnetic field (black) for a g -factor less than 0. Spin up electrons will align parallel with the field, while spin down electrons will align antiparallel. [22]	22
Figure 1-8 Illustration of quantum dot with unperturbed energy ε_0 , with a perturbing magnetic field producing spin-split energy levels ε_a with spin down and ε_b with spin up. With a g -factor less than zero, the spin up state has decreased in energy, while the spin down state has increased. [25].....	23
Figure 1-9 Plot of transmission vs energy for a single quantum dot with an applied external magnetic field. Notice the Zeeman Effect has split the single transmission peak into 2 spin-split peaks, the lower energy peak corresponding to spin up electrons and the higher energy peak corresponding to down electrons. [22].....	24
Figure 2-1 1-dimensional period lattice of quantum dots. Each is separated by a distance “ a ”. [38].....	25
Figure 2-2 1-dimensional periodic lattice structure. Sites are numbered relative to site “ n ”, and hopping integrals determine the electron’s ability to transmit between sites.	29
Figure 2-3 System with a single nanoring with magnetic flux passing through it. Ring consists of parallel wires between sites and no quantum dots in them. [25].....	31
Figure 2-4 Periodic lattice with a single quantum dot formed by a double barrier resonance structure. All hopping integrals are at V_0 except for those part of the barriers, which are at V_1 . [38].....	33

Figure 2-5 Energy spectrum of 1-dimensional lattice with 1 QD. $\varepsilon_A = 0$ and $V_1 = 0.3$. Plot includes the transmission coefficient T (Blue, Solid), reflection coefficient R (Red, Dashed), and the sum of the two, $T+R$ (Black, Dot-Dashed) which should be a constant value of 1.....	36
Figure 3-1 Transmission spectrum for a 12 ring system where the site energy parameters are all set at 0. The hopping integrals V_L , V_R , and V_{in} are all at 0.5, and the hopping integral V_m is incremented from 0.1 to 0.9 in increments of 0.2 (with $V_m = 1.0$ added at the end) from (a) - (f).	44
Figure 3-2 Plot of current vs voltage for the 12 ring system of Figure 3-1 where $V_m = 0.3$ (Solid, Blue), 0.5 (Dashed, Orange), and 1.0 (Dotted, Black). Note the central bandgap as well as the ohmic regions. This corresponds to the bandgap in the transmission bands of Figure 3-1. Data modeled at room temperature, or $T=293$ K.	45
Figure 3-3 Transmission spectrum of a 4 ring system where the site energy parameters are all set at 0 and the hopping integrals V_m , V_{in} , and V_R all are set at 0.4. V_L is incremented from 0.3 to 0.8 in steps of 0.1 from (a) - (f).....	47
Figure 3-4 Contour plot of 4 ring system of transmission probability over V_L and V_R vs Energy. The site energy parameters are set at 0, while the hopping integrals V_{in} and V_m are both set at 0.3. This plot shows how the transmission spectrum is affected when the two lead values, V_L and V_R , are incremented. Of greatest note is the fact that, as the hopping integrals are increased, the number of peaks per band decreases from 8 to 6.	48
Figure 3-5 Transmission spectrum of nanoring chain with increasing number of rings. The site energy parameters are all set at 0, the hopping integrals V_m and V_{in} are at 0.3, while V_L and V_R are maxed out at 1. The number of rings, N , is incremented in steps of 1 from $N = 3$ to $N = 8$ from (a) - (f).	50
Figure 3-6 Variation of $T(\varepsilon_{QD})$ with the number of series-coupled rings for six different values of inter-ring coupling, V_m . The site energies are all set at 0, while the hopping integrals are all at 0.3, except for V_m	52
Figure 3-7 The contour plot shows the transmission of the multi-ring system for $N = 10$, as a function of energy and system-leads coupling, V_{leads} . The line plot depicts the broad band of nearly 100% transmission for the particular case of $V_{leads} = 0.77$. The inter-ring coupling is $V_m = 0.6$. The site energies are set at 0, while $V_{in} = 0.3$	53
Figure 3-8 Exponential decay of $T(\varepsilon_{QD})$ as the number of rings increases, for $V_m = 0.55, 0.5$, and 0.4. The site energies are all set at 0, while $V_{in} = V_{leads} = 0.3$	54
Figure 3-9 (a) Contour plot of the transmission as a function of electron energy for different numbers of rings in series. (b) Line plot of the transmission for the specific case of 8 rings, for which $T(\varepsilon_{QD})$ attains full transmission. Site energies are all set at 0, while $V_m = 0.8$ and $V_{in} = V_{leads} = 0.3$	55
Figure 3-10 Dependence of $T(\varepsilon_{QD})$ on V_m for six different numbers, N , of rings in series. (a) $V_{leads} = 0.3$; $N = 5$ (thick solid), 8 (long dashes), 12 (short dashes), 16 (dash-dot), 20 (dash-double dot), 24 (thin solid). (b) $V_{leads} = 0.775$ (note difference in horizontal scaling). Same values of N , except $N = 80$ (thin solid). The site energies are all set at 0, while $V_{in} = 0.3$	56
Figure 4-1 Transmission vs flux plot for a system showing sharpened AB oscillations. These can be seen as transmission peaks at integer flux quantum values of the magnetic flux.	58

Figure 4-2 Transmission spectrum of a 4 ring system with site energy parameters all set at 0 and hopping integrals all set at $V_n = 0.4$, seen without magnetic flux in (a). A small amount of magnetic flux, at $\Phi/\Phi_0 = 0.05$, results in sensitive magnetic flux effects at the hopping integral value of 0.4, seen in (b) and (c).	59
Figure 4-3 Transmission spectrum of nanoring chain with increasing number of rings. The site energy parameters are all set at 0, and the hopping integrals all are set at $V_n = 0.4$. The number of rings, N , is incremented in steps of 1 from $N = 4$ to $N = 9$ from (a) - (f). A small amount of magnetic flux, at $\Phi/\Phi_0 = 0.05$, results in sensitive magnetic flux effects at the hopping integral value of 0.4. Notice the number of peaks added by the AB Effect increases in proportion to the number of rings.	61
Figure 4-4 Transmission plots of 4 ring system showing sensitive magnetic flux effects with different lead values. (a) has no flux with leads symmetric with the rest of the system. (b) introduces flux, with both leads still symmetric. (c) has 1 lead set at full transparency, while (d) has both leads set to full transparency. Note the switching of peak to valley of the location of the flux effects.	62
Figure 4-5 Transmission vs Energy plot of a 6 ring system with hopping integrals set at $V_{leads} = V_m = 0.4$ and a magnetic flux of 0.02 flux quanta present. V_{in} is set at 0.38 (Black, Dotted), 0.4 (Blue, Solid), and 0.42 (Red, Dashed). Note the position of the bandgap as V_{in} is altered.	63
Figure 4-6 Transmission vs Energy plot of a 6 ring system with hopping integrals set at $V_{leads} = V_{in} = 0.4$ and a magnetic flux of 0.05 flux quanta present. V_m is set at 0.2 (Red, Dashed), 0.4 (Blue, Solid), and 0.8 (Black, Dotted). Note the width of the bandgap as V_m is altered.	64
Figure 4-7 Transmission spectrum of nanoring chain with increasing magnetic flux. The site energy parameters are all set at 0, and the hopping integrals all are set at $V_n = 0.3$. The magnetic flux is incremented in uneven steps from $\Phi/\Phi_0 = 0.02$ to $\Phi/\Phi_0 = 0.4$ from (a) - (f). When a small flux is first introduced, sensitive flux effects can be seen as a bandgap is introduced. When $\Phi/\Phi_0 = 0.38$, the middle energy bandgap disappears and merges into a transmission peak.	66
Figure 4-8 Contour plot of transmission as a function of magnetic flux and energy for a system of 4 nanorings. All site energies are set at 0 and all hopping integrals at 0.3. Notice the growing bandgaps at the hopping integral values, and the merging middle bandgap into a peak.	67
Figure 4-9 Contour plots of Figure 4-8 showing transmission as a function of the imaginary and real portions of energy, with increasing magnetic flux from $\Phi/\Phi_0 = 0.0$ (a), to $\Phi/\Phi_0 = 0.08$ (b), to $\Phi/\Phi_0 = 0.2$ (c). Notice a bandgap appearing, flanked by multiple peaks. The white portions represent poles in the complex energy going to infinity.	68
Figure 4-10 Contour plots of Figure 4-8 showing the transmission as a function of the imaginary and real portions of energy, with increasing flux. Notice for the second plot, the merging of the middle bandgap into a peak. The white portions represent poles in the complex energy going to infinity.	69
Figure 4-11 IV plots of the system of Figure 4-7, with the magnetic flux set at $\Phi/\Phi_0 = 0$ (a) and $\Phi/\Phi_0 = 0.38$ (b). Notice that the system goes from a semi-conductor to being ohmic over the middle region.	70

Figure 4-12 Contour plot of transmission as a function of electron energy and magnetic flux. This is a system of 3 nanorings, with site energies set at 0 and hopping integrals at 0.3. Notice the 6 sets of transmission peaks created by the increasing flux. Black boxed area expanded to show detail in next figure.....	71
Figure 4-13 Contour plot of transmission as a function of energy and magnetic flux. This is for the system of Figure 4-11, zoomed in on a set of peaks to show detail.....	71
Figure 4-14 Contour plot of transmission as a function of energy and magnetic flux. This is for a 6 ring system with site energies at and hopping integrals at 0.3. Notice the preserved overall structure, and the increased peaks per set. Black box area expanded in next figure to show detail.	72
Figure 4-15 Contour plot of transmission as a function of energy and magnetic flux. This is for the system of Figure 4-13, zoomed in on a set of peaks to show detail.....	73
Figure 4-16 Contour plots showing the transmission, $T(\varepsilon_{QD})$, as a function of magnetic flux and the lead couplings. This is a 4 ring system, with all site energies set to 0 and hopping integrals at 0.3. The plots have different ring coupling values, of $V_m = 0.3$ (a) and $V_m = 0.6$ (b). Notice that the larger coupling causes a greater flux sensitivity.	75
Figure 4-17 Contour plots showing the transmission, $T(\varepsilon_{QD})$, as a function of magnetic flux and the ring couplings. This is a 4 ring system, with all site energies set to 0 and hopping integrals at 0.3. The plots have different lead coupling values, of $V_{leads} = 0.3$ (a) and $V_{leads} = 0.775$ (b). Notice that the larger coupling causes a greater flux sensitivity.	76
Figure 4-18 Resonant transmission, $T(0)$, as a function of flux and ring coupling parameter V_m . Notice the effect that changing the ring coupling strength has, and that, when $V_m = V_0 = 1$, the peaks are at flux values of $\Phi/\Phi_0 = 1/3$ and $\Phi/\Phi_0 = 2/3$ indicated by the purple lines. This is a 4 ring system, with all site energies set at 0 and hopping integrals $V_n = V_0 = 1$	78
Figure 4-19 Resonant transmission, $T(0)$, as a function of flux and leads parameter V_{leads} . Notice the effect that changing the lead strength has, and that, when $V_{leads} = V_0 = 1$, the peaks are at flux values of $\Phi/\Phi_0 = 1/3$ and $\Phi/\Phi_0 = 2/3$, indicated by the purple lines. This is a 4 ring system, with all site energies set at 0 and hopping integrals $V_n = V_0 = 1$	78
Figure 4-20 Transmission of resonant energy $T(0)$ as a function of magnetic flux for systems of 3 rings (Blue, Solid), 6 rings (Red, Dashed), and 20 rings (Black, Dotted). Site energies as set at 0, and all hopping integrals are set at $V_0 = 1$. Notice the transmission peaks are found at values of $\Phi/\Phi_0 = 1/3$ and $\Phi/\Phi_0 = 2/3$, and the locations of the peaks does not change with system size.	79
Figure 4-21 Contour plot of electron transmission as a function of energy and Zeeman Energy ε_Z . This is for a 4 ring system with all QD site energies set at 0 and all hopping integrals set at 0.3. Notice the spin up and spin down bands merging and creating mixed spin state bands with the increase of the Zeeman Energy. Also notice the pure spin state bands diverging from center.	81
Figure 4-22 Transmission vs energy line plots for the system described in Figure 4-17. The Zeeman Energy is changed from $\varepsilon_Z = 0.2$ (a) to $\varepsilon_Z = 0.4$ (b). Notice in (a) there is no middle bandgap, while in (b), there are clear bandgaps, with band structures on either side.....	81

- Figure 4-23** IV plot of the system of Figure 4-17 with a Zeeman Energy of $\varepsilon_Z = 0.2$ and Fermi Energy set at 0. The system is completely ohmic, but with portions that are spin-polarized, such as the outer edges, and portions that are mixed, such as the center. 83
- Figure 4-24** IV plot of the system of Figure 4-17 with the Zeeman Energy set to $\varepsilon_Z = 0.4$ and Fermi Energy set at 0. Notice the ohmic and conducting regions, especially the spin-polarized ohmic regions around ± 1.5 V. 83

1. INTRODUCTION

1.1 Context

Over the past two decades, remarkable advances have been made in the field of quantum transport in mesoscopic systems. Much study has been put into the different geometries of quantum wires and their effect on electron propagation. Of particular note are the transmission properties of coupled mesoscopic rings [1] [2], and the electron-spin transport in semiconductor nanostructures and nanoscale electronic devices [3] [4]. At low temperatures, the phonon scattering of mesoscopic systems becomes insignificant and the phase coherence length of the electrons becomes large compared to the size of the system. The scattering of the system then becomes phase coherent elastic scattering, and the sample becomes equivalent to an electron waveguide [5] [6] [7]. Then, it can be assumed that the transmission properties are primarily dependent on quantum tunneling and interference, the geometry of the system, and the impurities present within it.

The field of spintronics differs from classical electronics in that it uses the spin of the electron, rather than the charge, to convey binary information [8]. Experimental work has shown magnetic effects on these mesoscopic rings [9], showing interesting flux dependence of the total wave function [10]. The Aharonov-Bohm (AB) Effect has been studied and shown to impact transmission in the transport through multiple rings, [11] creating a measureable phase shift and interference. The Zeeman Effect has also been theoretically [12] and experimentally [13] shown to split energy levels and provide clear spin filtering through quantum dots (QDs) in an

externally applied magnetic field. This spin-splitting allows for the transmission and manipulation of pure spin states.

Previous work has included research on both serial and parallel arrangements of rings [14] [15], with differing numbers of scattering sites per ring. These studies range from considering scattering only at the junctions between rings [11] [16] to 2 QDs per ring [17], to an arbitrary number of QDs per ring [2]. Each of these arrangements is used to describe a physical system, such as graphene or a GaAs heterostructure. Series configurations of rings have been shown to facilitate higher current amplitudes than parallel-coupled rings [14]. This counter-intuitive result is explored further in our model as a function of inter-ring and system-leads couplings.

System size studied in previous works has also varied, with analysis of the transmission through 1 or 2 rings [18] to an arbitrary number of rings [11] [15] [19]. The overall features of the band structure appear to be independent of the number of rings in series [11], although resonant transmission, when the electron energy matches the QD site energy values, shows a strong dependence upon the number of rings in series [2] [15] and their couplings. Rings coupled in series without leads between them, or direct-contact rings, produce a transmission spectrum without a bandgap unless a magnetic flux penetrates the rings [16] [19]. As has been previously demonstrated, we also show that rings in series which are coupled with an intervening segment develop a transmission bandgap, even in the absence of external flux [19]. Of much interest, therefore, has been the study of magnetic flux, or lack thereof, through the system [9] [10] [11] [12] [13] [20]. Interest has also been shown in the type of boundary conditions of the system, with 2 external leads to the system [16] or 3 terminals allowing transmission [1]. Each of these

system parameters and geometries has been shown to have an impact on the electron transmission, especially the band structure [19] [21] and current-voltage characteristics [14].

In this thesis, a system of multiple mesoscopic rings connected serially with embedded QDs will be explored, as can be seen in Figure 1-1 and Figure 1-2. Each ring consists of a hexagonal structure of 6 QDs, which is coupled to the adjacent rings at each end in the “arm chair” configuration. There are 2 QDs per arm, and 2 external leads entering and exiting the system. We solve for the electron transmission through a variable number of rings via a Tight-Binding computational model, which has been shown to effectively model systems in which incoherent effects may be ignored [1]. The current through the system is also found as a function of the applied voltage. In this thesis, first investigated will be the system only in the absence of an applied external magnetic field. In this way, the properties and effects of each QD, or “atom”, can then be isolated and observed. Then a magnetic field will be introduced into the system the results of several interesting effects will be documented and analyzed.

In the non-magnetic portion, results are given in the form of graphical output with the electron transmission coefficient as a function of various system parameters and observables. We investigate the inter-ring coupling and the effect this has on the band structure of the transmission. An I/V plot is presented to show the semiconductor-to-metallic transition that is made with the change in inter-ring coupling. The effects of the leads are observed, with the coupling strength to one or both leads being altered. We also look at the system size, as the number of rings connected serially is incremented to demonstrate the effect on the transmission bandgap and the resonant transmission. The resonant transmission is also analyzed for unique system properties, demonstrating a strong dependence of the resonance transmission on an interplay between the relative values of inter-QD couplings within a ring, inter-ring couplings,

and system-leads couplings. Longitudinal system strain has been implicated as a possible method of producing these effects through its role in shifting the relative values of the system coupling constants. The effects on the resonance transmission of varying the coupling constants are found to be further modulated by incrementing the number of rings in series. Overall, these results demonstrate the flexibility of the transmission characteristics of series-coupled rings in the absence of an externally imposed magnetic field.

In the magnetic results section, an external magnetic field is applied to the system. Sharpened AB oscillations are observed and analyzed first, creating small bandgaps related to the flux and certain system parameters. As the flux is increased through the rings, these bandgaps are shown to increase, while the middle bandgap commonly found in these systems decreases until it merges into a transmission peak. Also shown relating to the increase in magnetic flux is a decrease in the coupling parameter strength needed to achieve maximum resonant transmission. As these related coupling parameters are increased, the system sensitivity and response to the magnetic flux also increases. Applying a magnetic field in a way that only utilizes the Zeeman Effect shows a different way to control the bandgap. Through increasing the Zeeman Energy, the middle bandgap will be seen to disappear, changing the material from a semi-conductor to a metal. It also causes 2 spin-polarized transmission bands to arise, showing the possibility of ohmic conductance of completely spin-polarized electrons.

1.2 System

The Tight-Binding Approximation method is used to model the electron wavefunction as it passes through the system of QDs. This approximation assumes only nearest neighbor

interactions between sites, and has been shown to effectively model electron transport through mesoscopic structures consisting of coupled rings with embedded QDs [15]. The Tight-Binding Approximation to the Schrödinger Equation can be written as

$$- [V_{n,n-1}\psi_{n,n-1} + V_{n,n+1}\psi_{n,n+1}] + \varepsilon_n\psi_n = E\psi_n, \quad (1-1)$$

where ψ_n is the electron wavefunction at site number n . This approximation assumes a quantized system with discrete sites. Since the observed system of interconnected QDs or atomic sites matches well with those assumptions, this approximation works well in modeling the interactions. The Tight-Binding Method will be discussed at length in a later section.

There are multiple physical properties which can be parameterized in the model and manipulated to alter the transmission spectrum, as can be seen in Figure 1-1. $V_{i,j} = V_n$ represents the hopping integrals between sites. These take a value between 0 and 1, and are a measure of an electron's ability to pass unreflected to the next QD, with 0 giving complete reflection and 1 giving complete transmission. Four parameters (V_L, V_R, V_{in} , and V_m) represent hopping integrals or sets of hopping integrals within the system. V_L and V_R are the couplings to the left and right leads, which serve as the source and drain of the system, coupling the chain of rings to probes. V_m represents the hopping integral between each ring on the segment coupling one ring to another. The parameter V_{in} represents the rest of the hopping integrals, which are all the couplings within the rings themselves, 6 per ring. The site energies of each QD are represented by the parameter ε_n . There are 6 sites per ring, with $\varepsilon_L, \varepsilon_{TL}, \varepsilon_{TR}, \varepsilon_{BL}, \varepsilon_{BR}$, and ε_R , corresponding to each of the six QDs on a ring. The ε_n are allowed to take any value between $-2V_0$ and $2V_0$ within the energy window set by the Tight-Binding dispersion relation,

$$E = \varepsilon_0 - 2V_0 \cos(\theta). \quad (1-2)$$

$V_0 = 1.0$ is the coupling between sites in the leads and is used throughout as a unit of energy. The site energies determine resonance conditions, and therefore which incoming electron energy values are most easily passed through each QD.

In Figure 1-2, we see this system with a magnetic field applied to it. Each QD's site energy is then split into a higher and lower energy, with a difference of $\pm\epsilon_Z$, the Zeeman Energy. Now each site has 2 resonant energies. Due to the Zeeman Effect, which will be discussed later, these two energies correspond to exclusively spin up ($-\epsilon_Z$) or spin down ($+\epsilon_Z$) electron states, which do not interact with each other. Thus, as can be seen from Figure 1-2, the system is essentially doubled, with separate, non-interacting paths for spin up and spin down electrons. Also of note in Figure 1-2 is the flux passing through the middle of the ring. Due to AB Effect, this flux will cause a shift in the phase of each electron as it passes through the ring.

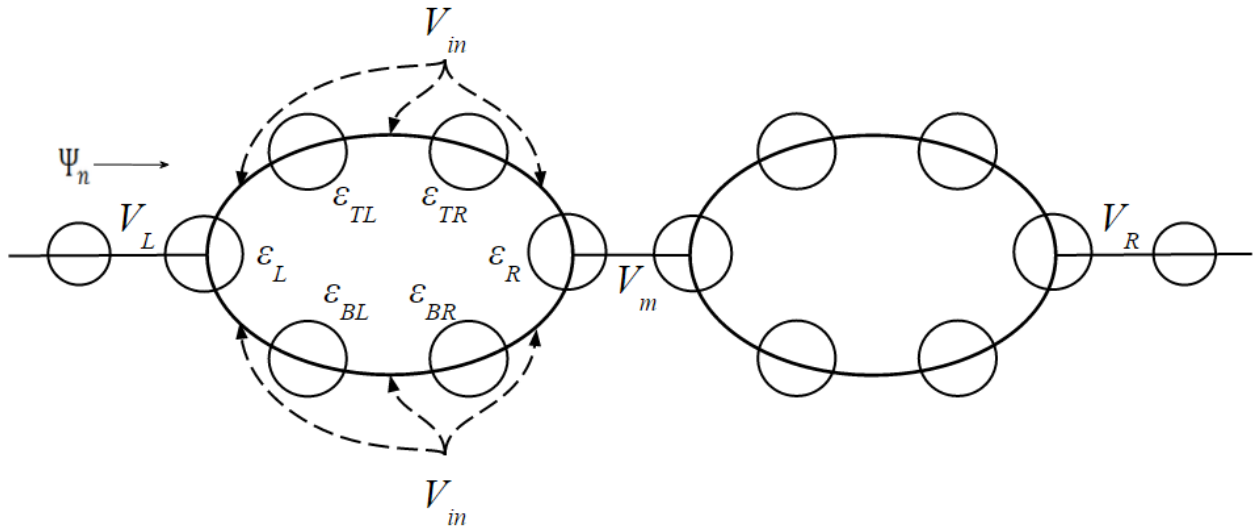


Figure 1-1 Diagram of a chain of 2 serially connected nanorings with no magnetic field. There are 2 QDs on each arm, and one on either side, for a total of 6 QDs per ring. Each ring is connected via a single lead, and leads run into and out of the system. The number of rings connected serially, N , may also be varied as a parameter in the computation.

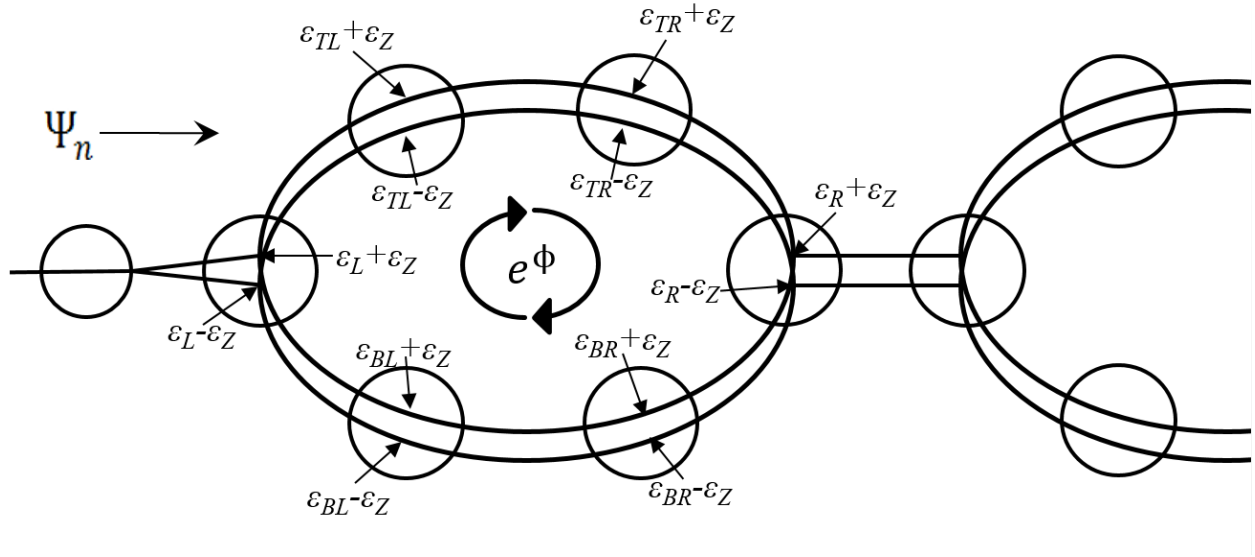


Figure 1-2 Diagram of system with applied magnetic field. Note each QD splits into 2 energy levels, with the difference plus or minus the Zeeman energy. Also note the flux passing through the center, which shifts the phase according to the AB effect.

Each of these rings consists of a series of QDs, which represent atoms. These atoms can be assumed to be atoms of several physical system which can take this form, however we will assume the rings are either GaAs heterostructures or graphene.

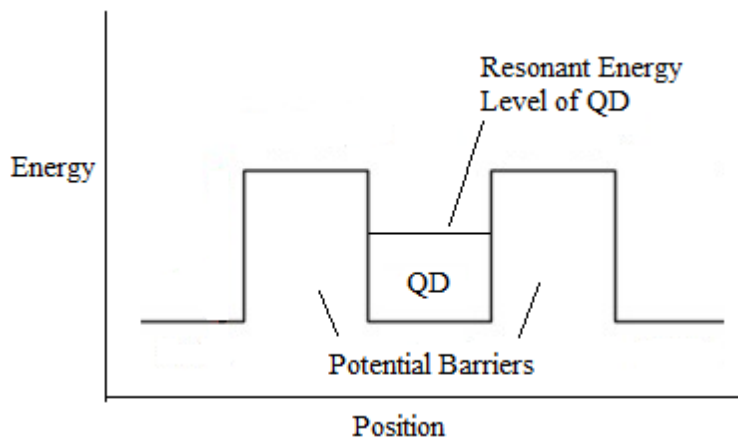


Figure 1-3 Plot showing the potential barriers of a quantum dot as a function of position. Each QD is modeled as two potential barriers, which can be shown to create a resonant energy which allows for quasi-bound states to be formed. [22]

These QDs are modeled as a simple double potential barrier, which is a well-known system. An illustration of this can be seen in Figure 1-3. Each of these double potential barrier systems has, due to the confining nature and “well” formed by the barriers, quasi-bound states which form in it. These standing waves cause certain electron energies to be passed much more favorably than others, resulting in what we observe as resonant energies. Each QD has its own resonant site energy, labeled ϵ_n , which dictates the energy that the system passes with the highest probability. In Figure 1-4, the energy transmission of a single QD can be seen. As can be guessed from observing the figure, the QD site energy is set at $\epsilon_{QD} = 0.0$. It is at this value that we see the transmission peak centered on, showing that this energy has the most favorable transmission probability.

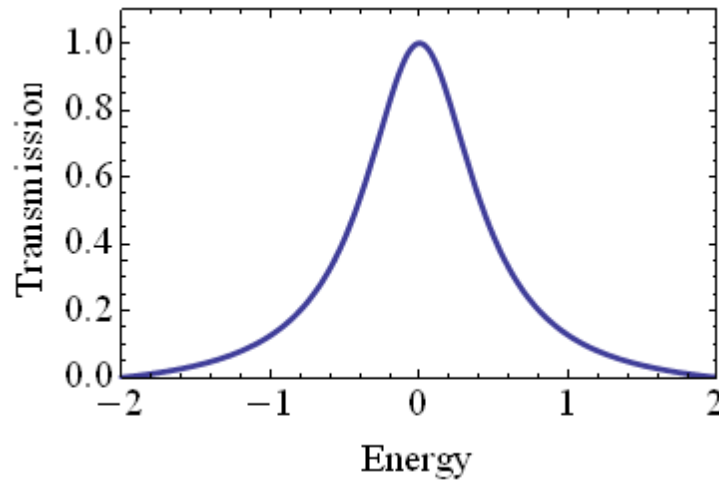


Figure 1-4 Plot showing transmission vs energy for a single quantum dot. Notice there is a single transmission peak, which corresponds to the resonant energy created by the 2 potential barriers of the QD. [22]

1.3 Aharonov-Bohm Effect

Maxwell's Equations thoroughly describe electric and magnetic fields (\vec{E} and \vec{B}). These fields are the main contributing forces to the motion of charged particles. This electromagnetic force can be expressed as $\vec{F} = q(\vec{E} + \vec{v} \times \vec{B})$. Both of these two fields can be simplified and expressed in terms of a more fundamental potential. The electric field can be thought to be derived from the electric scalar potential, V , and is expressed as the gradient function $\vec{E} = -\vec{\nabla}V$. The magnetic field likewise can be thought to arise from the curl of the magnetic vector potential, \vec{A} , taking the form $\vec{B} = \vec{\nabla} \times \vec{A}$. \vec{A} is defined in the integral $\oint \vec{A} \cdot d\vec{x} = \int \vec{B} \cdot d\vec{a} = \Phi$, where Φ is the magnetic flux through the area a . With a time varying charge distribution, this vector potential also contributes to the electric field, changing it to $\vec{E} = -\vec{\nabla}V - \partial\vec{A}/\partial t$.

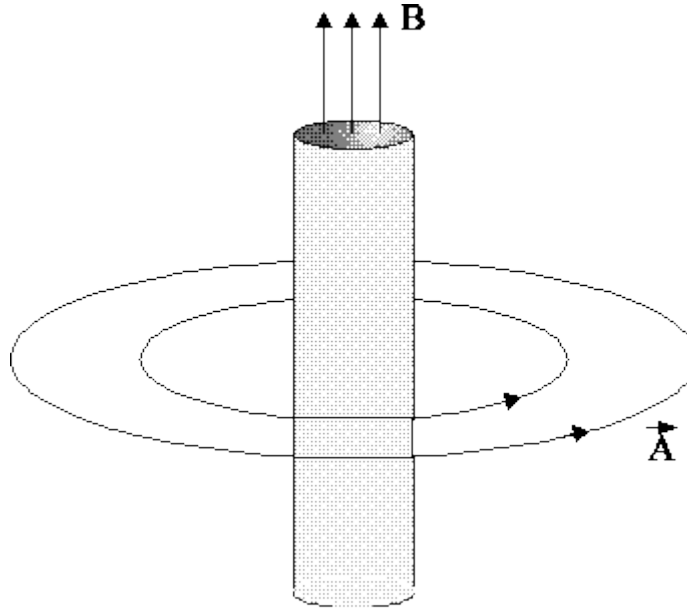


Figure 1-5 Depiction of the relationship between a constant magnetic field \vec{B} in a finite region of space and magnetic vector potential \vec{A} [23]

Considering Figure 1-5, let us find an expression for the magnetic vector potential. Recalling the previous definition $\oint \vec{A} \cdot d\vec{x} = \Phi$ and integrating over a circle of radius $r > a$ (where a is the radius of the cylinder containing the magnetic field), we find that

$$\vec{A} = \frac{\Phi}{2\pi r} \hat{\phi} \quad (1-3)$$

and is proportional to the magnetic flux. It can be seen from this example that the vector potential is non-zero outside of the cylinder, and will always be as any path must contain the flux inside of the cylinder. It is important to note that the region of $r > a$ contains zero magnetic field, but a nonzero magnetic potential.

Until the beginning of the 20th century, this magnetic vector potential was thought of purely as mathematical construct, one which contained no physical significance and only played a part in the simplification and expression of other equations. However, with the rise of quantum mechanics, and the fact that the Schrödinger Equation uses potentials, and not fields, this view came into question. Yakir Aharonov and David Bohm proposed an experiment to uncover the significance of the magnetic vector potential, and in 1959 discovered what is called the Aharonov-Bohm Effect [24].

Aharonov and Bohm found that a charged particle responded to the presence of a vector potential, even when there was no magnetic field in the region. It was theorized, and proven, that the wavefunction of an electron would experience a phase shift due to the electron's interference with this potential. The Aharonov-Bohm Effect is what describes this phase shift. In the most commonly observed case, an electron, or coherent electron beam, travels toward a solenoid cylinder. This can be seen in Figure 1-6(a). The solenoid is long enough that the magnetic field is confined to the inside of the cylinder, and is zero everywhere else. Because of this configuration,

there exists a magnetic vector potential outside of the solenoid oriented tangentially to the surface. The beam is split into two parts, and forced to travel on either side of the solenoid, never encountering the magnetic field but passing through a region of nonzero magnetic vector potential. The beam then recombines, and a resulting phase shift is observed in the combined beam. This case has been thoroughly experimentally observed.

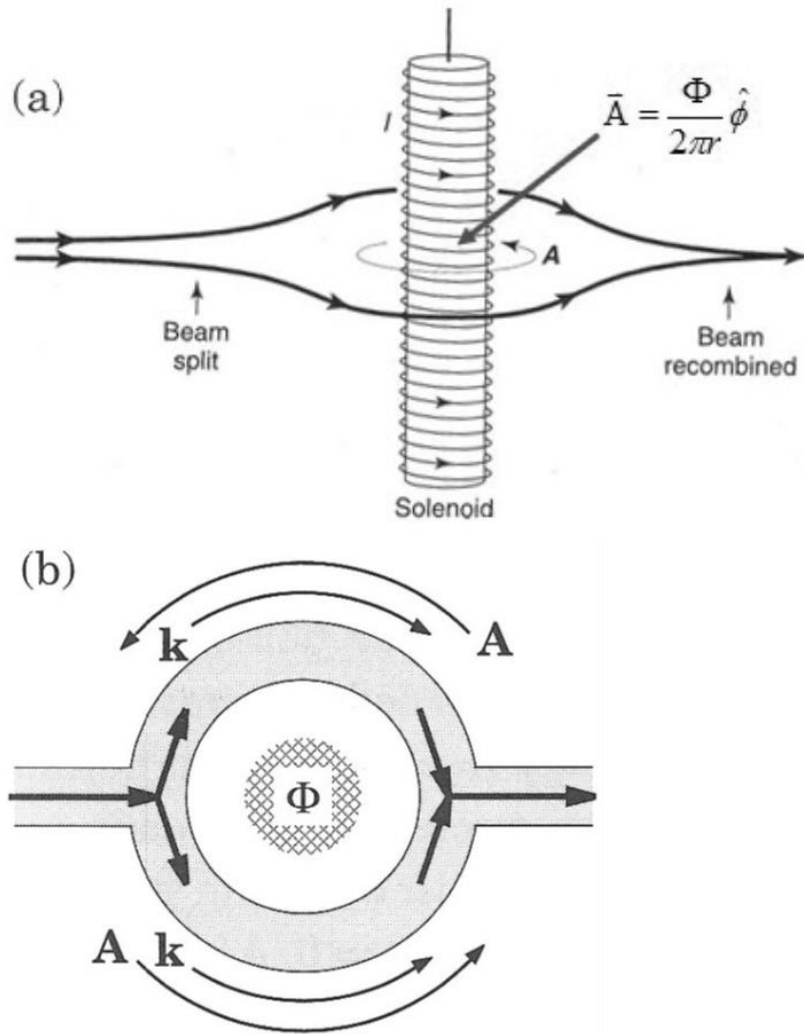


Figure 1-6 (a) Depiction of electron beam split around a solenoid. When the beam recombines, it experiences a phase shift due to the presence of the magnetic vector potential. (b) Shows direction of phase shift, where \vec{A} is vector potential and \vec{k} is electron wave vector. [25]

A cross sectional view of this setup can be seen in Figure 1-6(b). The electron wavevector, \vec{k} , points along each arm of the ring. Due to the magnetic flux, the vector potential points in a counter-clockwise direction around the ring. The total mechanical momentum for this system can be given as

$$\hbar\vec{k} = \vec{p} + e\vec{A}, \quad (1-4)$$

where \vec{p} is the canonical momentum of the electron and e is the electron charge in MKS units. Because of this relation, it can then be shown that the portion of the wavefunction passing through the upper arm gains momentum, and its phase shift changes more quickly. The wavefunction through the lower arm loses momentum, and this phase shift changes more slowly. When these wavefunctions recombine, there is a resulting difference in phase that has been caused by the magnetic vector potential [26].

Let us now mathematically derive the phase difference and its effect on an electron's wavefunction for a system similar to the one described above and shown in Figure 1-6(a). Much of this derivation follows what is outlined in Aharonov and Bohm's paper [24]. First, let us assume that an electron is traveling inside of a Faraday cage and subject to the Hamiltonian $H = H_0 + V(t)$, where H_0 is the Hamiltonian when $V(t)$, a time varying potential, is zero and $V(t) = e\varphi(t)$. If $\psi_0(x, t)$ is a solution to the Hamiltonian H_0 , then H can be shown to have the solution

$$\psi(x, t) = \psi_0(x, t)e^{-iS/\hbar} \quad (1-5)$$

where

$$S = \int V(t)dt = e \int \varphi(t)dt. \quad (1-6)$$

This comes from applying the equation

$$H\psi = (H_0 + V)\psi = i\hbar \frac{\partial \psi}{\partial t} \quad (1-7)$$

$$\left(i\hbar \frac{\partial \psi_0}{\partial t} + \psi_0 \frac{\partial S}{\partial t} \right) e^{-iS/\hbar} = i\hbar \frac{\partial \psi}{\partial t} \quad (1-8)$$

where the only difference between ψ , and ψ_0 is the phase factor S .

Let us now extend this to a 2 branch system, with the same Hamiltonian and time varying potential. We will break the wavefunction of the electron into two parts, one for each arm that it passes through. Let $\psi^0(x, t) = \psi_1^0(x, t) + \psi_2^0(x, t)$ be the wavefunction when no potential is present. Then the results of the previous example can be generalized to this case, where

$$\psi = \psi_1^0 e^{-iS_1/\hbar} + \psi_2^0 e^{-iS_2/\hbar} \quad (1-9)$$

and

$$S_1 = e \int \varphi_1(t) dt, \quad S_2 = e \int \varphi_2(t) dt. \quad (1-10)$$

Thus, it can be shown that when the wavefunctions recombine after passing through each arm, the interference will result in the phase difference

$$\theta = (S_1 - S_2) / \hbar. \quad (1-11)$$

As the electrons can now be thought of as traveling in a circular path, this can also be expressed as the integral over a closed loop in space

$$\frac{S_1 - S_2}{\hbar} = \frac{e}{\hbar} \oint \varphi dt. \quad (1-12)$$

The relativistic generalization of this integral is, expressed in CGS units,

$$\frac{S_1 - S_2}{\hbar} = \frac{e}{\hbar} \oint \left(\phi dt - \frac{\vec{A}}{c} \cdot d\vec{x} \right), \quad (1-13)$$

where the region of integration covers any closed loop in space-time.

We can now finally apply this example to the case described in Figure 1-6(a). As shown above, the 2 branches which the electron wavefunction passes through travel around a tightly wound cylindrical solenoid which creates a magnetic field \vec{B} . The solenoid is long enough that the magnetic field is zero outside of the solenoid, and thus is zero in the space traversed by the electron. The vector potential here is nonzero outside of the solenoid, as shown above. Given the conditions in this case, we can consider this integral to be constant in time, and only integrates over space. This eliminates the time dependent portion of the integral, making it

$$\frac{S_1 - S_2}{\hbar} = -\frac{e}{\hbar c} \oint \vec{A} \cdot d\vec{x}. \quad (1-14)$$

The Hamiltonian for this case is

$$H = \frac{[\vec{P} - (e/c)\vec{A}]^2}{2m}. \quad (1-15)$$

Here, there is a similar solution to the corresponding Schrödinger Equation, where

$$\psi = \psi_1 + \psi_2. \quad (1-16)$$

If ψ_0 is the solution when $\vec{A} = 0$,

$$\psi_1 = \psi_1^0 e^{-iS_1/\hbar}, \quad \psi_2 = \psi_2^0 e^{-iS_2/\hbar} \quad (1-17)$$

and

$$S_1 \text{ and } S_2 = \frac{e}{c} \int \vec{A} \cdot d\vec{x} \quad (1-18)$$

integrated along their respective branches. This confirms the above phase difference equation which, when using previous results, becomes

$$\frac{S_1 - S_2}{\hbar} = \frac{e}{\hbar c} \oint \vec{A} \cdot d\vec{x} = \frac{e}{\hbar c} \Phi \quad (1-19)$$

The phase difference of the electron beam, once recombined, can then be expressed as

$$\theta = \frac{S_1 - S_2}{\hbar} = \frac{e}{\hbar c} \Phi = 2\pi \frac{e}{\hbar c} \Phi = 2\pi \frac{\Phi}{\Phi_0} \quad (1-20)$$

where

$$\Phi_0 = \frac{hc}{e}$$

$$\text{in MKS units: } \Phi_0 = \frac{h}{e} = 1.33 * 10^{-17} \text{ gauss cm s} \quad (1-21)$$

and is considered the “flux quantum”. This phase difference has been confirmed and experimentally verified [27] [28], and does indeed produce a measurable interference.

Due to the size of nanoscale devices, in order for the flux to approach the same order of magnitude as the flux quantum, a huge amount of magnetic field would need to be present. This will be calculated shortly. In order to overcome this, many times heterostructures of GaAs are fabricated. These can be formed to create large rings which can capture flux on the scale of a flux quantum. Graphene is a material of great interest, and with a hexagonal structure, resembles the chain we are investigating. In fact, the chain of hexagonal nanorings used in this paper, with appropriate values, could be considered a 1 dimensional graphene ribbon in the “arm-chair”

configuration. Graphene is known to have a distance of 1.42\AA between carbon atoms [29], which can be considered the side length of the hexagonal structure used as our nanoring. Using this side length results in an enclosed area of $S = 0.0524\text{ nm}^2$. We recall the definition of flux in terms of magnetic field from earlier, where $\Phi = \int \vec{B} \cdot d\vec{a}$. If we assume a perpendicular magnetic field, this becomes $\Phi = B * S$, where S is the enclosed area. In order to pass 1 flux quantum (which in SI units is $\Phi_0 = 4.136 * 10^{-15}\text{ T m}^2$) through one graphene ring, a magnetic field of $7.89 * 10^4\text{ T}$ must be used. This is far greater than is practical to use, especially in a nanoscale device. Therefore, if we want to find magnetic results which can apply to graphene, a very small magnetic flux must be used.

This Aharonov-Bohm Effect plays a large part in the results found here and has a large impact on which electronic energy states are transmitted. It is commonly used as way to probe and to change the coherence of the electron's wavefunction. This effect will be used to specify certain states parameters of the system, and it will be varied to measure the magnetic effect on a system.

1.4 Zeeman Effect

When a magnetic field is applied to a quantum system, its spectral lines and particular electron energy levels are split. This is called the Zeeman Effect [30], and is commonly used in astrophysics to determine stars' magnetic fields, and in nanotechnology to separate electronic spin states. In our application, we will be using the Zeeman Effect to manipulate electron transmission, and to separate electron spin states to create spin-polarized energy transmission

peaks. Electrons exhibit degeneracy, where electrons in the same system have the same total energy. These degenerate electrons can have different quantum numbers, though. When the system is perturbed by an applied external magnetic field, it is these different quantum numbers which can cause the degeneracy to be broken. This is because electrons with different quantum numbers, although having the same overall energy, react differently to an applied magnetic field. Therefore, while electrons may be degenerate without a magnetic field present, when the magnetic perturbation via the field is introduced, it causes the degeneracy to lift and separates the electron energy levels according to their quantum numbers.

The coupling of the electron spin and angular momentum is at the heart of the Zeeman Effect. The total magnetic moment, $\vec{\mu}$, of an electron can be expressed as

$$\vec{\mu} = \vec{\mu}_L + \vec{\mu}_S \quad (1-22)$$

where $\vec{\mu}_L$ is the part of the moment due to orbital angular momentum and $\vec{\mu}_S$ is the spin angular momentum, or magnetic dipole moment [31]. Initially, the total magnetic moment was thought to be able to be described only by the orbital angular momentum. However, the Stern-Gerlach experiment demonstrated otherwise [32]. This experiment showed that electrons, along with other elementary particles, possess an intrinsic property that we call spin. Along with this, it was demonstrated that the total magnetic moment is quantized. Because of this, we then had to begin thinking of the total magnetic moment in terms of both orbital angular momentum and spin. The intrinsic spin property adds what is called the magnetic dipole moment $\vec{\mu}_S$.

Initially, as researchers were discovering and experimenting with the Zeeman Effect, they noticed additional magnetic effects that could not be explained. These were called the Anomalous Zeeman Effect [33], and eventually this effect was discovered to be due to the spin

characteristics of the electron. It is this Anomalous Zeeman Effect which we will be using, and I will refer to it as simply the Zeeman Effect. This is valid because the orbital angular momentum contribution to the total magnetic moment is negligible, due to the restrictions imposed by the system and the horizontal magnetic field [34]. Once an electron enters the system, it is confined to a 2 dimensional electron gas (2DEG) for this configuration. With the applied magnetic field, the electron is acted upon by the Lorentz Force

$$F = q \vec{v} \times \vec{B}, \quad (1-23)$$

where q is the electron charge in MKS and \vec{v} is the velocity of the electron. In the heterostructures forming the substrate for the QDs, the magnetic field is typically parallel to the substrate plane in these simulations. Therefore, because of the cross product in the Lorentz Force, the force on the electrons will be perpendicular to the 2DEG plane. The impedance faced by the electrons confines their movement in the vertical direction, and eliminates electron movement perpendicular to this plane. Then the orbital degrees of freedom of the electron are restricted, and the orbital angular momentum term can be ignored. Therefore, the total magnetic moment can now be simplified to only depend on the magnetic dipole moment, or the spin orbital momentum

$$\vec{\mu} = \vec{\mu}_S. \quad (1-24)$$

Now, let us use the magnetic moment of the electron to characterize the Zeeman Energy, or the energy by which the electron energy levels are split. The Hamiltonian of an atom in the presence of a magnetic field is

$$H = H_0 + V_m \quad (1-25)$$

where H_0 is the Hamiltonian of the unperturbed system, and V_m represents the potential energy of the magnetic perturbation. The potential energy created by the interaction of the applied external magnetic field and the magnetic dipole moment of the electron is given as

$$V_m = -\vec{\mu}_S \cdot \vec{B} = \varepsilon_Z, \quad (1-26)$$

where the potential energy V_m is the Zeeman Energy, ε_Z . The magnetic dipole moment can be expressed in terms of electron spin as

$$\vec{\mu}_S = -\frac{e}{m_e} \vec{S}, \quad (1-27)$$

where e is the charge of the electron, m_e is its mass, and \vec{S} is the spin angular momentum. This relationship, however, is approximate, and only holds when there is a constant charge to mass ratio. If this ratio is not constant, then a new factor, called the g-factor, must be altered to account for the uneven charge to mass ratio.

The g-factor multiplies the gyromagnetic ratio, γ . This ratio describes the relationship between the electron's magnetic moment $\vec{\mu}$ and its spin angular momentum \vec{S} , and is the ratio between the two [35]. The gyromagnetic ratio can be expressed as

$$\gamma = \frac{e}{2m_e} \quad (1-28)$$

which is then multiplied by the g-factor. Rewriting $\vec{\mu}_S$ in terms of these new terms results in

$$\vec{\mu}_S = -g \frac{e}{2m_e} \vec{S} \quad (1-29)$$

where g must be equal to 2. We are, for the moment, considering a free electron. This has a g-factor of $g = 2.0023$, which we will approximate as 2, just as we would expect. A common

heterostructure used in these experiments is GaAs, which has a g-factor of $g = -0.44$ [36]. Experiments have shown that graphene has a g-factor around 2 [37], making the free electron a good approximation to the Zeeman Effect of an electron in graphene.

Let us take the z-axis as the direction of the applied external magnetic field, giving

$$\vec{B} = B_z \hat{z}. \quad (1-30)$$

Because of the dot product, we only need to think about the z component of the spin angular momentum, S_z . This S_z represents the two different spin orientations for this axis, spin up or spin down, and is given by

$$S_z = m_s \hbar. \quad (1-31)$$

Here, m_s is the spin magnetic quantum number and can either $\frac{1}{2}$ for spin up or $-\frac{1}{2}$ for spin down.

This means that the spin angular momentum can be

$$S_z = \pm \frac{\hbar}{2}. \quad (1-32)$$

These magnetic dipoles will always orient so that the spin magnetic moment is aligned with the magnetic field, either parallel or antiparallel [26]. When the spin is parallel with the field, it is considered spin up and S_z is positive. Conversely, when the spin is antiparallel, it is spin down and S_z is negative.

Now, let us plug Equation (1-32) into Equation (1-27) to find an expression for the z component of the magnetic dipole moment in terms of the spin angular momentum:

$$\mu_{S,Z} = -g \frac{e}{2m_e} m_s \hbar. \quad (1-33)$$

A fundamental unit to express the electron spin magnetic moment in terms of is the Bohr Magneton, $\vec{\mu}_B$. This is a numerical constant with the relationship

$$\mu_B = \frac{e\hbar}{2m_e}. \quad (1-34)$$

Expressing the z component of the magnetic dipole moment in terms of this gives us the simple expression

$$\mu_{S,Z} = \pm \frac{g}{2} \mu_B. \quad (1-35)$$

As can be seen, if the g-factor for a free electron is used, the z component of the magnetic dipole moment is equal in magnitude to the Bohr Magneton.

Going back to the potential energy, or Zeeman Energy term, of Equation (1-26), we take the dot product and substitute in the value for the magnetic dipole moment which we have derived thus far:

$$\varepsilon_Z = -\vec{\mu}_S \cdot \vec{B}$$

$$\varepsilon_Z = -\mu_{S,Z} B_Z$$

$$\varepsilon_Z = g m_s \mu_B B_Z. \quad (1-36)$$

When substituting in the values for the spin magnetic quantum number m_s , we then have a Zeeman Energy of

$$\varepsilon_Z = \pm \frac{g}{2} \mu_B B_Z. \quad (1-37)$$

As you can see, the Zeeman Energy ε_Z splits each QD energy state into a higher and lower energy level according to the electron spin, with a Zeeman splitting energy of

$$\Delta\varepsilon_Z = \frac{g}{2}\mu_B B_Z. \quad (1-38)$$

When the g-factor of a material is less than 0, such as for bulk GaAs, the spin angular momentum and the magnetic dipole moment align normally with the applied external magnetic field. A spin up electron will align parallel to the field, while a spin down electron will align antiparallel, as can be seen in Figure 1-7.

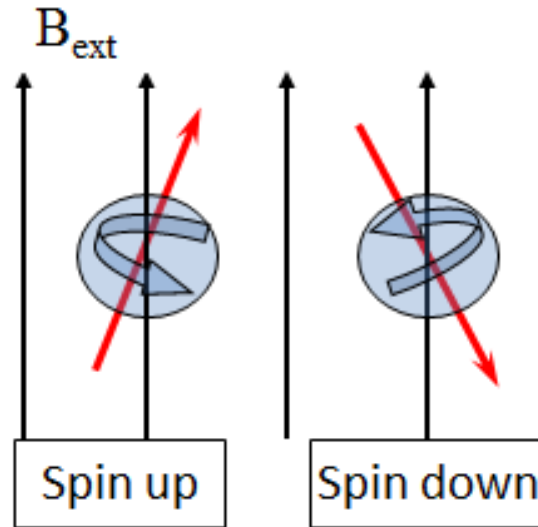


Figure 1-7 Illustration of the alignment of the spin angular momentum and magnetic dipole moment (red) with the applied external magnetic field (black) for a g-factor less than 0. Spin up electrons will align parallel with the field, while spin down electrons will align antiparallel. [22]

Each QD has an unperturbed resonant energy value of ε_0 . As we have seen, when there is a perturbing applied external magnetic field, for our conditions that energy level is split into two

energy levels by a difference of the Zeeman Energy. This gives 2 energy levels, ε_a and ε_b . These correspond to the spin down and spin up states respectively, and are given by

$$\varepsilon_a = \varepsilon_0 - \frac{g}{2} \mu_B B_Z \quad (1-39)$$

$$\varepsilon_b = \varepsilon_0 + \frac{g}{2} \mu_B B_Z. \quad (1-40)$$

For a g-factor greater than 0, the spin down state decreases in energy while the spin up state increases. However, for materials such as bulk GaAs, with a g-factor less than zero, the spin down state state increases in energy, while the spin up state decreases. This can be seen illustrated in Figure 1-8.

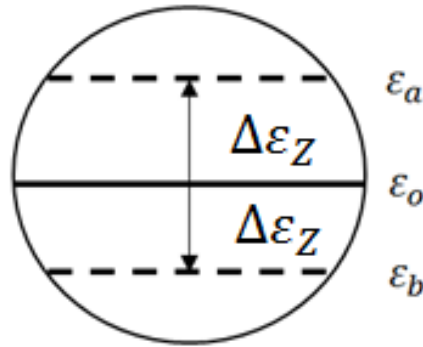


Figure 1-8 Illustration of quantum dot with unperturbed energy ε_0 , with a perturbing magnetic field producing spin-split energy levels ε_a with spin down and ε_b with spin up. With a g-factor less than zero, the spin up state has decreased in energy, while the spin down state has increased. [25]

Recall from Section 1.1, the transmission vs energy spectrum for a single QD showed a single transmission peak corresponding to the resonant energy of that QD (Figure 1-4). This is in the absence of a magnetic field. When an external magnetic field is applied, and Zeeman splitting takes place, this single peak is spin-split into 2, a higher and lower energy peak corresponding to spin down and spin electron states, respectively. These peaks are different from

the original resonant peak by energies of $\pm\epsilon_Z$ [36]. Note that this assumes a g-factor less than 0. In effect, the Zeeman splitting causes each QD to have 2 resonant energies, or 2 energies which are more likely to be transmitted without reflection, as is clearly seen in Figure 1-9.

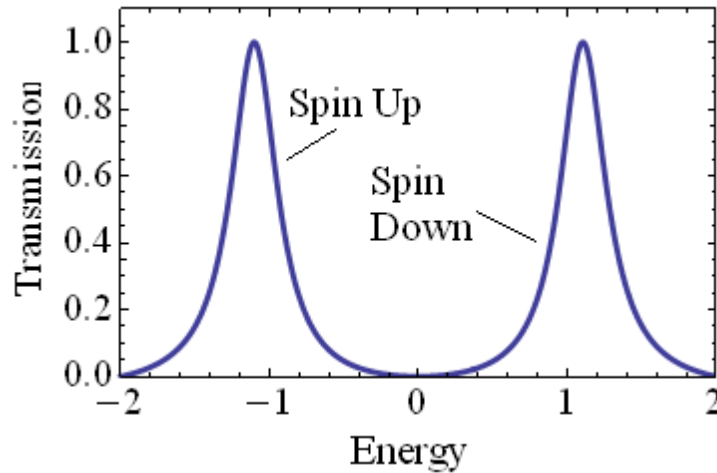


Figure 1-9 Plot of transmission vs energy for a single quantum dot with an applied external magnetic field. Notice the Zeeman Effect has split the single transmission peak into 2 spin-split peaks, the lower energy peak corresponding to spin up electrons and the higher energy peak corresponding to down electrons. [22]

2. METHODS

2.1 Tight-Binding Formalism

In order to analytically characterize the transmission of the system, we used the Tight-Binding Method. This is a 1 electron approximation to the Schrödinger Equation. As described above, our system consists of chains of QDs, with certain segments connected in parallel to form ring structures. As the electron travels along these chains, it interacts with each QD. When the electron is in one QD, the QDs are spaced far enough part to cause the wavefunction to only overlap with the sites directly before and after the occupied QD. It is because of this that the Tight-Binding Approximation is valid for our system. The Tight-Binding Approximation assumes only nearest neighbor interactions, and any influence from sites beyond those directly adjacent the site occupied by the electron is considered negligible. In this section, our form of the Tight-Binding Approximation and its application in our system will be derived.

Let us consider a 1-dimensional periodic lattice of QDs, as can be seen in Figure 2-1. This is a simple crystal structure with a near infinite repetition of atoms. Due to the periodic nature of this lattice, the interaction between atoms can be considered identical over the structure.

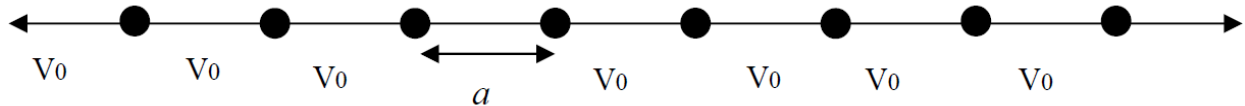


Figure 2-1 1-dimensional period lattice of quantum dots. Each is separated by a distance “ a ”. [38]

The total wavefunction of the electron in this periodic lattice can be expressed as

$$\Psi(x) = \sum_n c_n \varphi_n(x), \quad (2-1)$$

where φ_n are separable solutions of the Schrödinger Equation corresponding to each site of the lattice. According to Bloch's Theorem [35], the wavefunction of an electron in a periodic lattice can be given as

$$\varphi_n(x) = \varphi_0(x - na), \quad (2-2)$$

where a is distance between sites in the lattice, and n represents the numbering of individual sites. Correspondingly, we can view the potential as a superposition of potential barriers. Each of these has a height of v and is centered on the lattice point located at $x = \pm na$. Then the potential is

$$V(x) = \sum_n v(x - na). \quad (2-3)$$

This means that the Hamiltonian of the lattice can now be constructed. The Hamiltonian of the crystal lattice around each site is approximated to be a single atom, given as

$$H = \frac{p^2}{2m} + \sum_n v(x - na). \quad (2-4)$$

Here, p is the momentum operator in the kinetic energy term. As mentioned earlier, the Tight-Binding Approximation only considers nearest neighbor interactions as contributing, so this becomes the Hamiltonian of the site n ,

$$H_n = \frac{p^2}{2m} + v_{n-1} + v_n + v_{n+1}. \quad (2-5)$$

This also means that the wavefunction at site n , $\Psi_n(x)$, can be rewritten as

$$\Psi_n(x) = c_{n-1}\varphi_{n-1} + c_n\varphi_n + c_{n+1}\varphi_{n+1}. \quad (2-6)$$

We can now consider the Schrödinger Equation,

$$H_n \Psi_n = E_n \Psi_n. \quad (2-7)$$

Using the Hamiltonian above, this becomes

$$\left(\frac{p^2}{2m} + v_{n-1} + v_n + v_{n+1} \right) \Psi_n = E_n \Psi_n. \quad (2-8)$$

Then, using the expression of the wavefunction, this becomes

$$\begin{aligned} & \left(\frac{p^2}{2m} + v_{n-1} + v_n + v_{n+1} \right) (c_{n-1}\varphi_{n-1} + c_n\varphi_n + c_{n+1}\varphi_{n+1}) \\ &= E_n (c_{n-1}\varphi_{n-1} + c_n\varphi_n + c_{n+1}\varphi_{n+1}). \end{aligned} \quad (2-9)$$

We allow that the wavefunction at each site satisfies the equation

$$\left(\frac{p^2}{2m} + v_n \right) c_n \varphi_n = \varepsilon_n c_n \varphi_n, \quad (2-10)$$

which is simply the Schrödinger equation for each point in the lattice, where ε_n is the individual site energy. This simplifies the above equation to

$$\begin{aligned} & \varepsilon_{n-1} c_{n-1} \varphi_{n-1} + \varepsilon_n c_n \varphi_n + \varepsilon_{n+1} c_{n+1} \varphi_{n+1} \\ &+ c_n v_{n-1} \varphi_n + c_{n+1} v_{n-1} \varphi_{n+1} \\ &+ c_{n-1} v_n \varphi_{n-1} + c_{n+1} v_n \varphi_{n+1} \end{aligned}$$

$$\begin{aligned}
& +c_{n-1}v_{n+1}\varphi_{n-1} + c_nv_{n+1}\varphi_n \\
& = E_n(c_{n-1}\varphi_{n-1} + c_n\varphi_n + c_{n+1}\varphi_{n+1}).
\end{aligned} \tag{2-11}$$

Notice in the above equation that there are cross terms, meaning terms associated with site $(n+1)$ paired with terms associated with site $(n-1)$. Remember that the Tight-Binding Approximation assumes only nearest neighbor interactions, meaning only terms that pair site $(n+1)$ and (n) , or $(n-1)$ and (n) should survive. Therefore we let the terms pairing sites $(n+1)$ with $(n-1)$ be dropped, and are left with

$$\begin{aligned}
& \varepsilon_{n-1}c_{n-1}\varphi_{n-1} + \varepsilon_nc_n\varphi_n + \varepsilon_{n+1}c_{n+1}\varphi_{n+1} + c_nv_{n-1}\varphi_n \\
& + c_{n-1}v_n\varphi_{n-1} + c_{n+1}v_n\varphi_{n+1} + c_nv_{n+1}\varphi_n \\
& = E_n(c_{n-1}\varphi_{n-1} + c_n\varphi_n + c_{n+1}\varphi_{n+1})
\end{aligned} \tag{2-12}$$

Now, the wavefunctions φ_n are orthonormal with each other, meaning

$$\int \varphi_n \varphi_m dx = \delta_{nm}. \tag{2-13}$$

So, if we multiply both sides by φ_n and integrate over the lattice, we obtain

$$\varepsilon_n c_n + c_n(v_{n-1})_{n,n} + c_{n-1}(v_n)_{n,n-1} + c_{n+1}(v_n)_{n,n+1} + c_n(v_{n+1})_{n,n} = E c_n, \tag{2-14}$$

where

$$c_n(v_n)_{n,n-1} = \int \varphi_n(x)v_n(x)\varphi_{n-1}(x)dx. \tag{2-15}$$

Let us write this in terms of c_n :

$$c_n(\varepsilon_n + (v_{n-1})_{n,n} + (v_{n+1})_{n,n}) + c_{n-1}(v_n)_{n,n-1} + c_{n+1}(v_n)_{n,n+1} = E c_n. \tag{2-16}$$

If we define the energy

$$\bar{\varepsilon}_n = \varepsilon_n + (v_{n-1})_{n,n} + (v_{n+1})_{n,n}, \quad (2-17)$$

then this simplifies to

$$c_n \bar{\varepsilon}_n + c_{n-1} (v_n)_{n,n-1} + c_{n+1} (v_n)_{n,n+1} = E c_n. \quad (2-18)$$

Now, we let $-V_{n,n-1} = (v_n)_{n,n-1}$ and $-V_{n,n+1} = (v_n)_{n,n+1}$, while also defining $c_n \equiv \psi_n$. The term $V_{n,n-1}$ is defined as the hopping integral between site (n) and $(n-1)$, and can be thought of as the electron's ability to pass without reflection between those sites (see Figure 2-2). $\bar{\varepsilon}_n$ is the energy of site (n) , and ψ_n is the corresponding wave function at that site. Using this new notation, we are left with

$$-[V_{n,n-1} \psi_{n-1} + V_{n,n+1} \psi_{n+1}] + \bar{\varepsilon}_n \psi_n = E \psi_n, \quad (2-19)$$

which is our approximation to the Schrödinger Equation. In a 2-dimensional system, the terms in square brackets can be extended to include all nearest neighbor terms of site (n) . Using this equation allows us to generate a matrix of equations which can be solved for the electron transmission through the system.

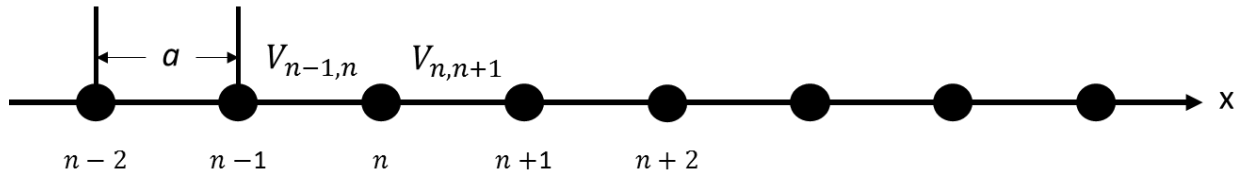


Figure 2-2 1-dimensional periodic lattice structure. Sites are numbered relative to site “ n ”, and hopping integrals determine the electron's ability to transmit between sites.

2.2 Dispersion Relation

According to Bloch's Theorem once again, we propose a periodic solution to our approximation of the Schrödinger Equation of the form

$$\psi_n = Ae^{ikan} = Ae^{i\theta n}, \quad (2-20)$$

where $\theta = ka$. If we plug this in to the Schrödinger Equation, we get the equation

$$-[V_{n,n-1}Ae^{i\theta(n-1)} + V_{n,n+1}Ae^{i\theta(n+1)}] + \bar{\epsilon}_n Ae^{i\theta n} = EAe^{i\theta n}. \quad (2-21)$$

which simplifies to

$$-[V_{n,n-1}e^{-i\theta} + V_{n,n+1}e^{i\theta}] + \bar{\epsilon}_n = E. \quad (2-22)$$

If we assume we are in a portion of the system that is completely uniform, such as the leads entering or exiting, the potential is uniform surrounding site (n). Then we can say that $V_{n,n-1} = V_{n,n+1} = V_0$, where

$$-V_0[e^{-i\theta} + e^{i\theta}] + \bar{\epsilon}_n = E. \quad (2-23)$$

Using the Euler Identity, we can rearrange this so that it has the form

$$E = -2V_0\cos(\theta) + \bar{\epsilon}_n \quad (2-24)$$

and is the dispersion relation [31] for this system. This can be applied to the leads, allowing us to simplify any expressions involving these. It also dictates that the spread of the energy levels of the system be

$$\Delta E = 4V_0. \quad (2-25)$$

Applying the magnetic effects to this system adds some complexity to it, but nothing drastic. Allowing magnetic flux to pass through the system causes us to incorporate the AB Effect. Since this adds a phase shift to the wavefunction, depending on which branch it is in, we will multiply the hopping integral by an exponential with the phase shift. If we let $\varphi = 2\pi\Phi/\Phi_0$, where Φ_0 is the flux quantum and Φ is the flux through the ring, the added exponential term is $e^{\pm i\varphi/N}$, where N is the total number of QDs in the ring. For the system shown in Figure 2-3, the hopping integral passing from site ($n = 0$) to ($n = 1$) via the upper path will be modified by $V_{0,1}(upper) = V_U e^{-i\varphi/2}$, while passing through the lower path will make it $V_{0,1}(lower) = V_L e^{i\varphi/2}$. Going backwards from site ($n = 1$) to ($n = 0$) will have a similar effect, only reversing the signs, making $V_{1,0}(upper) = V_U e^{i\varphi/2}$ and $V_{1,0}(lower) = V_L e^{-i\varphi/2}$.

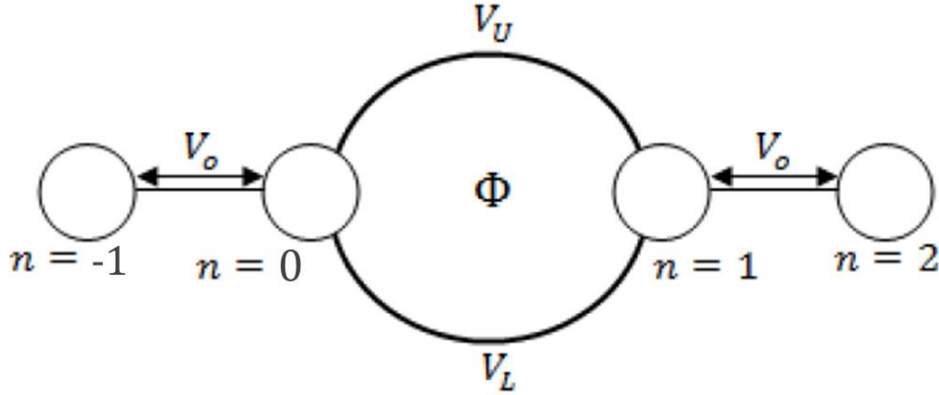


Figure 2-3 System with a single nanoring with magnetic flux passing through it. Ring consists of parallel wires between sites and no quantum dots in them. [25]

Along with the AB Effect, the Zeeman Effect must also be taken into account. Mathematically, this is a much more impactful effect. Instead of simply adding a term to each hopping integral, this effect splits each QD into 2 sites, creating a spin up and spin down state QD. Then each QD will have 2 separate equations describing it, with each spin coherent site

having its own associated wavefunction. Because of the nature of electron spin states, the spin up and spin down QDs do not interact with each other, meaning that the nearest neighbor terms in the Schrödinger Equation will only include those sites with the same spin state. In effect, mathematically this creates two parallel chains, connected only at the points where the leads touch the system. Due to the fact that chains now have double the coupling to the leads, a factor of $\sqrt{2}$ must be multiplied to the lead hopping integrals in order to match results with a non-magnetic system.

2.3 Simple 1-Dimensional Lattice Example

For the sake of example, we work through a simple application of the Tight-Binding Method. Let us consider a 1-dimensional periodic lattice structure consisting of a single quantum dot embedded at the site ($n = 0$). On either side of the QD, between sites ($n = A$) and ($n = 0$), and between sites ($n = A$) and ($n = 1$), there is a hopping integral of V_1 . Every other hopping integral in the system is V_0 . These are considered to have no effect on the wavefunction, and are set to be transparent at a value of $V_0 = 1$. Correspondingly, the site energy at each site outside of the QD is set at $\bar{\epsilon}_n = 0$. This creates a system with a single QD formed by two potential barriers, a double barrier resonance structure. This system can be seen in Figure 2-4.

Initially, we assume solutions of wavefunctions outside of the dot in sites $n \leq 0$ and $n > 0$, which we shall refer to being in the “leads”. These solutions are the well-known expressions for waves before and after barriers.

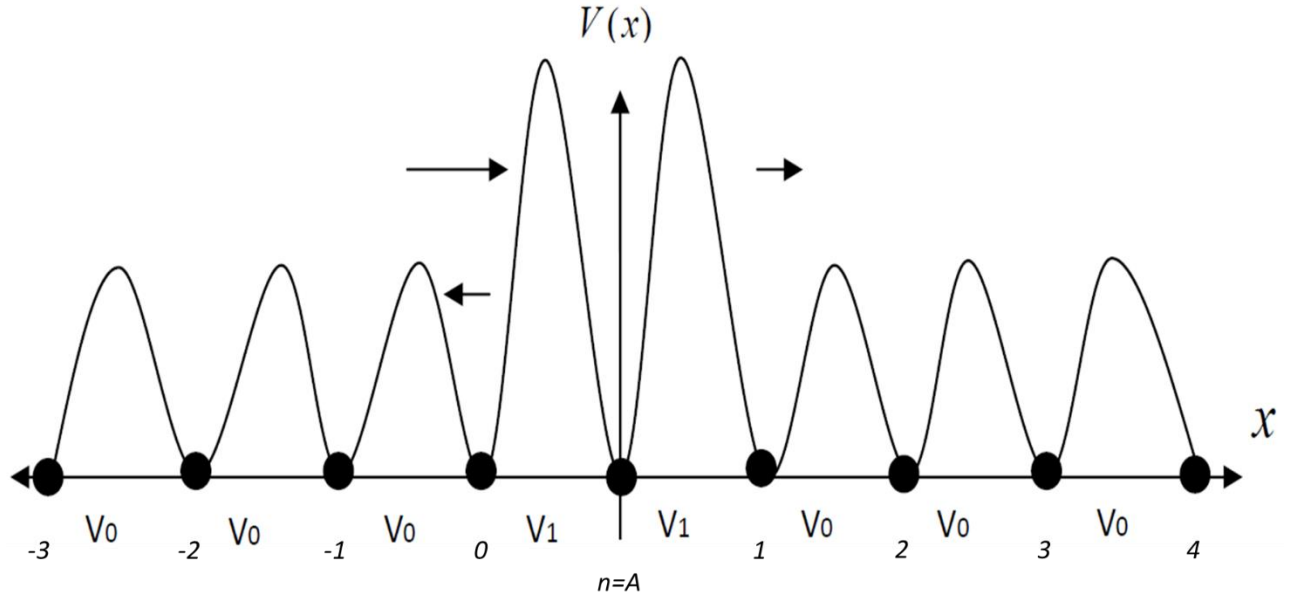


Figure 2-4 Periodic lattice with a single quantum dot formed by a double barrier resonance structure. All hopping integrals are at V_0 except for those part of the barriers, which are at V_1 . [38]

For $n \leq 0$, the wavefunctions are

$$\psi_n = e^{i\theta n} + r e^{-i\theta n} \quad (2-26)$$

and for $n > 0$, the wavefunctions are

$$\psi_n = t e^{i\theta n}. \quad (2-27)$$

Here, r is the reflection amplitude and t is the transmission amplitude. The wavefunction at the QD site, for $(n = A)$, is left as an unknown to be solved. Let us begin by applying our Tight-Binding Approximation, Equation (2-19), to site $(n = 0)$:

$$-[V_0\psi_{-1} + V_1\psi_A] + \bar{\epsilon}_0\psi_0 = E\psi_0. \quad (2-28)$$

Plugging in the values for the known wavefunctions, V_0 , and $\bar{\epsilon}_{-1}$ yields

$$-[e^{-i\theta} + re^{i\theta} + V_1\psi_A] = E(1 + r). \quad (2-29)$$

We now separate terms,

$$-r(e^{i\theta} + E) - V_1\psi_A = E + e^{-i\theta}. \quad (2-30)$$

Recall the dispersion relation for a lead, using its exponential form with the site energy at 0, with $V_0 = 1$,

$$E = -[e^{-i\theta} + e^{i\theta}], \quad (2-31)$$

and plug it in to the above equation, yielding

$$re^{-i\theta} - V_1\psi_A = -e^{i\theta}. \quad (2-32)$$

Let's now apply the Schrödinger to the QD site at ($n = A$), giving us

$$-[V_1\psi_0 + V_1\psi_1] + \bar{\epsilon}_A\psi_A = E\psi_A, \quad (2-33)$$

which, when conditions are applied, yields

$$-V_1(1 + r) - V_1te^{i\theta} + \bar{\epsilon}_A\psi_A = E\psi_A. \quad (2-34)$$

Separating terms again gives us

$$-V_1r - V_1te^{i\theta} + (\bar{\epsilon}_A - E)\psi_A = V_1. \quad (2-35)$$

We finally apply the Schrödinger to the site just beyond the QD, at ($n = 1$), yielding

$$-[V_1\psi_A + V_0\psi_2] + \bar{\epsilon}_1\psi_1 = E\psi_1. \quad (2-36)$$

Applying the known wavefunctions and other conditions gives us

$$-V_1\psi_A - te^{2i\theta} = Ete^{i\theta}. \quad (2-37)$$

Separating terms yields

$$-V_1\psi_A - te^{i\theta}(e^{i\theta} + E) = 0, \quad (2-38)$$

and plugging in the exponential form of the dispersion relation again leaves us with

$$-V_1\psi_A + t = 0. \quad (2-39)$$

We now have 3 equations with 3 unknowns, a simple matter of algebra to solve. Writing this system of equations in matrix form yields

$$\begin{pmatrix} -V_1 & e^{-i\theta} & 0 \\ \bar{\epsilon}_A - E & -V_1 & -V_1e^{i\theta} \\ -V_1 & 0 & 1 \end{pmatrix} \cdot \begin{pmatrix} \psi_A \\ r \\ t \end{pmatrix} = \begin{pmatrix} -e^{i\theta} \\ V_1 \\ 0 \end{pmatrix}. \quad (2-40)$$

This is easily solved through matrix techniques, and yields solutions for the transmission and reflections amplitude as functions of energy of

$$t(E) = \frac{V_1^2(e^{2i\theta} - 1)}{2e^{i\theta}V_1^2 - (\bar{\epsilon}_A - E)} \quad (2-41)$$

and

$$r(E) = \frac{e^{2i\theta}[(\bar{\epsilon}_A - E) - 2V_1^2\cos(\theta)]}{2e^{i\theta}V_1^2 - (\bar{\epsilon}_A - E)}. \quad (2-42)$$

After substituting the dispersion relation in for “ θ ”, these functions will be explicitly dependent only on the energy. These functions give the energy probability when the absolute value squared is taken, giving the transmission and reflection coefficients of the system. As such, they should sum to 1 when in this form, giving

$$T = \|t\|^2 \quad (2-43)$$

$$R = \|r\|^2 \quad (2-44)$$

$$R + T = 1 \quad (2-45)$$

Using $t(E)$ and $r(E)$ above to plot T and R for this 1 dimensional lattice with 1 QD gives an energy spectrum of Figure 2-5.

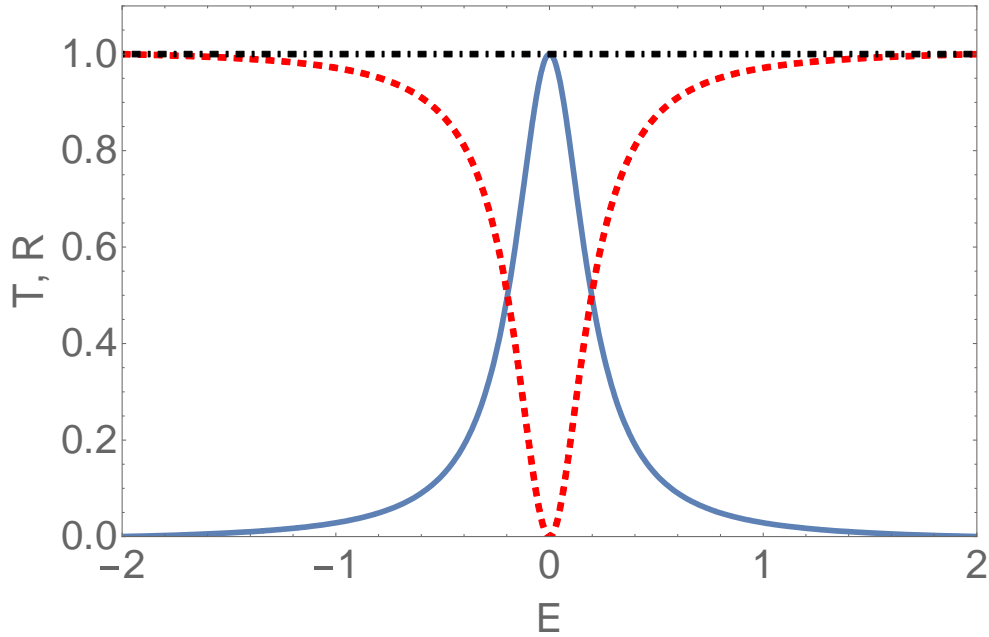


Figure 2-5 Energy spectrum of 1-dimensional lattice with 1 QD. $\varepsilon_A = 0$ and $V_1 = 0.3$. Plot includes the transmission coefficient T (Blue, Solid), reflection coefficient R (Red, Dashed), and the sum of the two, $T+R$ (Black, Dot-Dashed) which should be a constant value of 1.

As observed in the plot, when using parameter values of $\varepsilon_A = 0$ and $V_1 = 0.3$, the transmission coefficient T has a single peak centered at $E = 0$, the value of the QD site energy, ε_A . This is expected, as a double barrier potential tends create resonant conditions and allow quasi-bound states to form. These bound states are at a particular energy, and this energy is transmitted at a much higher probability than any other energy state. The reflection coefficient R

shows just the inverse of this, as we would expect, with a large dip at the resonant energy, and reflection close to 1 elsewhere. The sum should be a constant value 1, which we see to be the case, which verifies that the system is internally consistent. In our research, we focus solely on the transmission coefficient of the system, as this tells us all we need to know about the electronic properties.

2.4 Computational Method

Using the Tight-Binding Method described above, we can now solve the system for its transmission characteristics. By applying Equation (1-1), the system of Figure 1-1 and Figure 1-2 is converted into matrices. Below, Equation (2-46) shows the general form these matrices take. The first matrix contains the coefficients of the wave function at each site, $\alpha_{n,m}$. The second column vector contains the wavefunctions, ψ_n , while the third is a column of constants, C_n . In the usage of these matrices, the column of constants is combined with the other two, leaving only one matrix of wavefunction coefficients and constants along with a column vector.

$$\begin{pmatrix} \alpha_{1,1} & \alpha_{1,2} & \alpha_{1,3} & \dots \\ \alpha_{2,1} & \alpha_{2,2} & \alpha_{2,3} & \dots \\ \alpha_{3,1} & \alpha_{3,2} & \alpha_{3,3} & \dots \\ \dots & \dots & \dots & \dots \end{pmatrix} \begin{pmatrix} \psi_1 \\ \psi_2 \\ \psi_3 \\ \dots \end{pmatrix} = \begin{pmatrix} C_1 \\ C_2 \\ C_3 \\ \dots \end{pmatrix} \quad (2-46)$$

The electron transmission through this system is solved analytically, using the software *Mathematica*. In earlier work [19], this has been done by creating a large matrix, then using pattern recognition and other algorithms to fill this matrix and add the desired physics to it. However, there are drawbacks to this approach, and it is difficult to implement, leading to a

lengthy computer program. Having one large matrix also leads to longer computing times, making using this program impractical in its usage for a system composed of many rings. Also, with one matrix there is a fixed system size. In order to change the number of rings, the entire matrix must be reformulated and populated with the new specification.

Instead of creating one large matrix, this research uses an iterative computational approach. In this approach, the reflection and transmission amplitudes for one ring are obtained from the Tight-Binding equations, then the procedure is iterated multiple times, with the results of each ring being passed to the next. There are multiple benefits to this approach. It is relatively simple to code and debug, taking no more than two pages of code to implement. The actual matrix used is simply a 6×9 matrix, cutting computing time for a system of 10 rings to about a second. It offers more flexibility as well. When a ring is added to the system, the program will just iterate the loop once more, rather than reformulating the entire matrix. The only drawback to this method is that a reflection function cannot be solved for without adding complexity to the code, while with one large matrix it is a simple addition.

In order to elaborate further on this method, we give here some practical explanation using a system without any magnetic field present. 3 matrices total are needed to implement the iterative procedure, a matrix for the first ring, a matrix for the last ring, and a matrix to be iterated for all rings between those two. For this reason, the smallest number of rings that can be used is 3. These matrices are populated by the Tight-Binding Approximation to the Schrödinger Equation. Each column represents a site wavefunction, with the last 3 columns representing reflection coefficients, transmission coefficients, or a blank column added. These matrices must be separate because the dimension of the first is 7×9 , the iterated matrix is 6×9 (see Equation (2-47)) and the last is 7×8 . There are overlapping terms in each matrix. So, each matrix is row

reduced, and the overlapping terms are called from the previous matrix. These terms are associated with the coupling of the leads between rings and any constant terms. In the end, it is the transmission coefficient which is called to become the analytical solution. In this system, the iterated matrix has the form,

$$A[i] = \begin{pmatrix} \psi_L & \psi_{TL} & \psi_{TR} & \psi_{BL} & \psi_{BR} & \psi_R & \psi_L(i+1) & \text{Constants} \\ \varepsilon_L - E + V_m A[i-1][6][8] & -V_{in} & 0 & -V_{in} & 0 & 0 & 0 & V_m A[i-1][6][9] \\ -V_{in} & \varepsilon_{TL} - E & -V_{in} & 0 & 0 & 0 & 0 & 0 \\ 0 & -V_{in} & \varepsilon_{TR} - E & 0 & 0 & -V_{in} & 0 & 0 \\ -V_{in} & 0 & 0 & \varepsilon_{BL} - E & -V_{in} & 0 & 0 & 0 \\ 0 & 0 & 0 & -V_{in} & \varepsilon_{BR} - E & -V_{in} & 0 & 0 \\ 0 & 0 & -V_{in} & 0 & -V_{in} & \varepsilon_R - E & 0 & -V_m \\ 0 & 0 & 0 & 0 & 0 & 0 & 0 & 0 \end{pmatrix} \begin{matrix} n = L \\ n = TL \\ n = TR \\ n = BL \\ n = BR \\ n = R \end{matrix} \quad (2-47)$$

where matrix $A[i]$ is iterated in the body of code. The factor $A[i-1]$ contains terms from the preceding ring's matrix which are added to $A[i]$, connecting the rings by passing the information from one matrix to another. The sites ($n = L$) to ($n = R$) refer to the sites found in Figure 1-1. As mentioned above, a blank column is added to each iterated matrix. This column is added so that the term called from the first matrix will occupy the same matrix element for each iterated matrix. If this column were not added, the terms called from the first matrix would be (6,8) and (6,9), while the terms called from each iterated matrix would be (6,7) and (6,8), respectively. With the added column, these terms can remain (6,8) and (6,9), as seen in Equation (2-46).

For our particular case, only 2 terms need to be passed from each matrix to the next. When the matrix is row reduced, it will produce a diagonal of coefficients written in cascading order in terms of the coefficients below them. This means that the last coefficient of the diagonal, at the bottom of the matrix, will be written in terms of only the coefficients to the right of it. This coefficient, which in our case is for the wavefunction of the QD on the far right of the ring (ψ_R), must be written in terms of the next ring's far left QD wavefunction (ψ_L), and a

constant term which all the matrices share. Using Equation (2-47) as an example, observe first that this is a 6x9 matrix. By row reducing, this matrix is converted to row echelon form. In this form, a diagonal of 6 terms will be produced, with 3 extra columns to the right. It is clear that when this matrix is row reduced, the term associated with ψ_R (identified by the term with $\varepsilon_R - E$ in it) will be written only in terms of the final 3 columns. These last 3 columns correspond to the ψ_L of the next ring (8th column) and the constant term (9th and final column). The 7th column is blank and so contains no information to be passed. The row reduced matrix then has the form

$$\text{Row Reduced } A[i] = \begin{pmatrix} 1 & 0 & 0 & 0 & 0 & 0 & 0 & \alpha_{L,L} & C_L \\ 0 & 1 & 0 & 0 & 0 & 0 & 0 & \alpha_{L,TL} & C_{TL} \\ 0 & 0 & 1 & 0 & 0 & 0 & 0 & \alpha_{L,TR} & C_{TR} \\ 0 & 0 & 0 & 1 & 0 & 0 & 0 & \alpha_{L,BL} & C_{BL} \\ 0 & 0 & 0 & 0 & 1 & 0 & 0 & \alpha_{L,BR} & C_{BR} \\ 0 & 0 & 0 & 0 & 0 & 1 & 0 & \alpha_{L,R} & C_R \end{pmatrix} \quad (2-48)$$

where the furthest column to the right is associated with the constants, while the 2nd column from the right is associated with ψ_L , the wavefunction of the first site of the next ring.

The first row of the next matrix, which applies Equation (1-1), is initially written in terms of ψ_R of the previous matrix, and ψ_L , ψ_{TL} , ψ_{BL} , and a constant term of the next matrix. This can be written as

$$\text{site } (n = L): \quad - [V_m \psi_R + V_{in} \psi_{TL} + V_{in} \psi_{BL}] + \varepsilon_L \psi_L = E \psi_L \quad (2-49)$$

However, the previous matrix generated an expression for ψ_R in terms of ψ_L and the constant term. Taken from the bottom row of Equation (2-48) and written in general form, this is

$$\psi_R + \alpha_{L,R} \psi_L = \text{constants}$$

$$\psi_R = -\alpha_{L,R} \psi_L + constants \quad (2-50)$$

So, in essence, this expression for ψ_R can be inserted into the first row. This is done by adding each term that ψ_R contained to its matching column, and multiplying by V_m , the constant multiplying ψ_R . By substituting Equation (2-50) into Equation (2-49), we get

$$\begin{aligned} -[V_m(-\alpha_{L,R} \psi_L + constants) + V_{in}\psi_{TL} + V_{in}\psi_{BL}] + \varepsilon_L \psi_L &= E \psi_L \\ -V_{in}\psi_{TL} - V_{in}\psi_{BL} + \psi_L(\varepsilon_L - E + V_m \alpha_{L,R}) &= V_m * constants. \end{aligned} \quad (2-51)$$

The results of this process can be seen in the top left and top right of Equation (2-47). In the term for ψ_L , $\varepsilon_L - E$ has been added to the previous matrix's (6,8) term (multiplied by V_m) making it $\varepsilon_L - E + V_m A[i-1][6][8]$. The constant term in the top right initially was 0, but the (6,9) term from the previous matrix, multiplied by V_m was added, making it $V_m A[i-1][6][9]$. This new matrix no longer has any explicit mention of ψ_R of the previous matrix, and so the column associated with it can be eliminated. In this way, information can be passed from matrix to matrix, and the dimension of each matrix can be maintained in such a way that will allow it to be solved exactly after the final matrix. Results from this method have been checked against those obtained through more brute force methods and its results match exactly.

3. NON-MAGNETIC RESULTS

3.1 Changing coupling parameter

Figure 3-1 shows the transmission spectrum for a 12-ring system for various values of inter-ring coupling. The results demonstrate some interesting relationships between the inter-ring coupling parameter, V_m , and the other hopping integrals as V_m is consistently incremented. The first noteworthy effect is the decreasing of the middle bandgap. As V_m increases from 0.1 to 1.0, the central bandgap shrinks from an energy gap of about $\Delta E = 1.0$ to become almost non-existent at $V_m = 1.0$. This energy bandgap relates to a semiconductor I/V bandgap, while the transmission bands relate to ohmic regions. In the overall transmission spectrum, three bandgaps exist except for the fully symmetric case when the hopping integrals are all the same, as in Figure 3-1(c), which only has one central bandgap. Another special case occurs when $V_m = 2V_{in} = 1.0$, which closes the central bandgap, leaving only the two peripheral bandgaps, as seen in Figure 3-1.f. It is understood that the values of hopping integrals are related to inter-orbital distances, with a standard relationship determined from the semi-empirical Slater-Koster theory [39]. Longitudinal strain on a molecular nano-ribbon such as graphene can alter the relative values of the hopping integrals between sites within the ring compared to couplings between the rings [40]. Research has also shown the role of strain in modulating the values of hopping integrals, and thereby modifying the transmission spectrum, in strands of DNA [41].

Current vs. voltage curves are calculated from the transmission function using a standard formalism based on the scattering theory of transport [21]. The current, I , is calculated from the transmission, $T(E)$ as,

$$I = \frac{2e}{h} \int dE T(E) [f_L(E) - f_R(E)] \quad (3-1)$$

Here, $f(E)$ is the Fermi function given by $f_{L/R}(E) = 1/(\exp[\beta(E - \mu_{L/R})] + 1)$, where $\beta = 1/(k_B T)$ and $\mu_{L/R}$ is the electrochemical potential of the left (right) semi-infinite leads, whose values depend on the applied source-drain bias voltage V_{sd} . The temperature is set at $T = 293\text{K}$, unless specified otherwise. We assume symmetric leads and set $\mu_L = E_F + \frac{eV_{sd}}{2}$, and $\mu_R = E_F - \frac{eV_{sd}}{2}$, with the Fermi energy, E_F , a system parameter adjustable by means of an external bias voltage. For the plots of the current shown here, $E_F = 0$, corresponding to the center of the transmission window. In order to obtain specific units for I (μA), the energy units used in Equation (3-1) are taken to be in eV .

Figure 3-2 shows the results of the I/V calculation for this case, in which the bandgap in the I/V characteristic conducting region can be seen to grow smaller and smaller as V_m increases until it is almost purely ohmic. Interestingly enough, if V_{in} and V_m were to swap values, with V_m set to 0.5 and V_{in} incremented, the bandgap would tend to increase, rather than decrease.

It is also shown through incrementing V_m that resonance effects develop. This is observed in Figure 3-1 through comparing the transmission when V_m is symmetric with respect to the rest of the hopping integral values, at 0.5, and when it is less than or greater than this value, giving an asymmetric set of system coupling parameters.

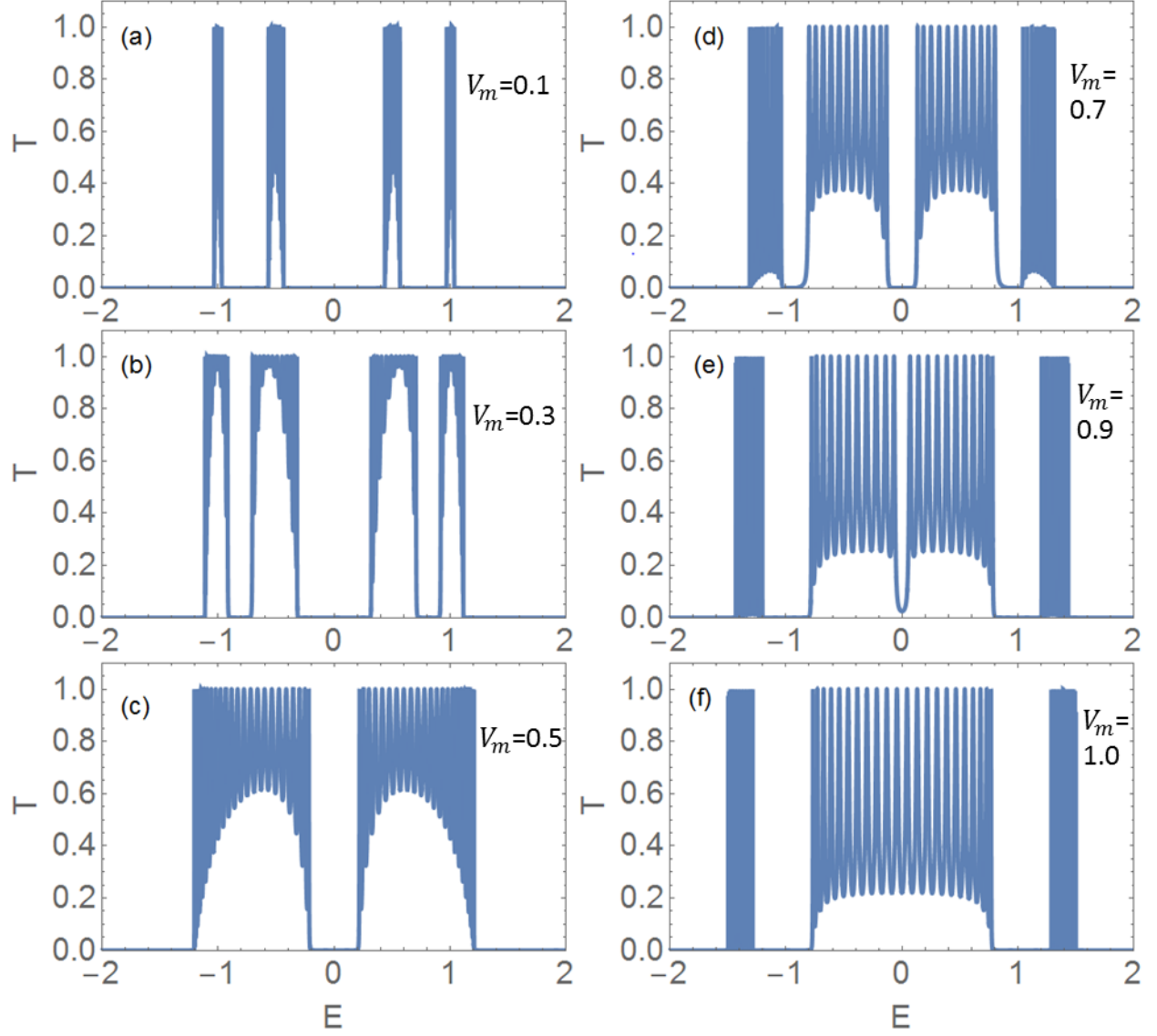


Figure 3-1 Transmission spectrum for a 12 ring system where the site energy parameters are all set at 0. The hopping integrals V_L , V_R , and V_{in} are all at 0.5, and the hopping integral V_m is incremented from 0.1 to 0.9 in increments of 0.2 (with $V_m = 1.0$ added at the end) from (a) - (f).

When V_m is equal to the other hopping integral values at 0.5, the transmission bands and peaks are fullest in their widths, and the valleys between peaks are at their highest, compared to when V_m is greater than the other hopping integral values. As V_m diverges from this symmetric value, the bands and peaks begin to either decrease in width or the valleys drop, indicating narrower transmission resonance conditions. Because of the critical position of this hopping integral, the

entire system wavefunction must pass through it. When it is symmetric, it has a higher probability of passing the same energies as the rest of the nanoring system, and therefore the final transmission peaks have a stronger spectrum. When V_m is asymmetric, its high probability energies are shifted away from those easily passed by the rest of the system. Since the system will no longer easily pass all the same energies, the system transmission conditions become more narrowly constrained within the energy spectrum. This effect is further modulated by the system-leads couplings and the number of rings in series, as discussed later.

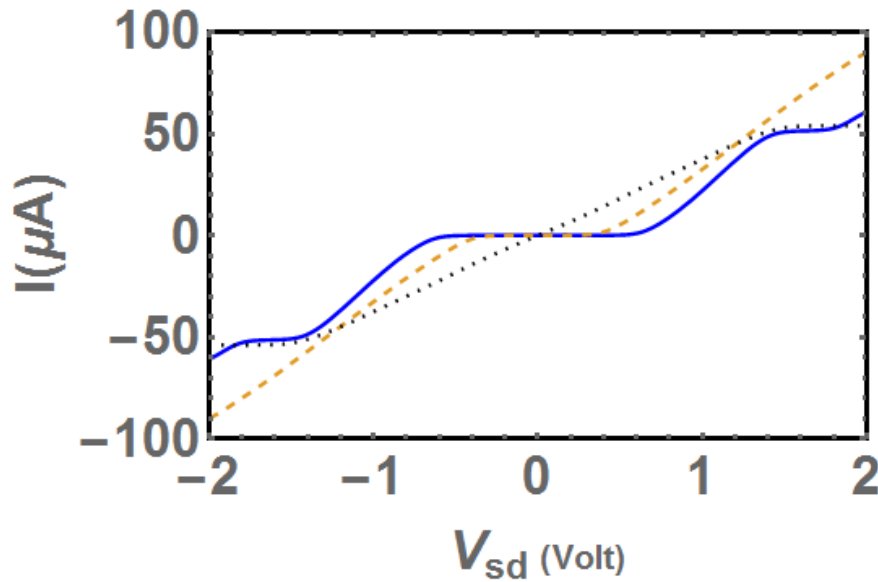


Figure 3-2 Plot of current vs voltage for the 12 ring system of Figure 3-1 where $V_m = 0.3$ (Solid, Blue), 0.5 (Dashed, Orange), and 1.0 (Dotted, Black). Note the central bandgap as well as the ohmic regions. This corresponds to the bandgap in the transmission bands of Figure 3-1. Data modeled at room temperature, or $T=293$ K.

3.2 Changing leads

In Figure 3-3 and Figure 3-4, the effects arising from altering the leads are observed. This is accomplished through incrementing the hopping integral parameters V_L and V_R . When V_L alone

is increased, as in Figure 3-3, the observable effects here are subtle, but important. Changes in the transmission strength due to symmetry conditions are first observed. Similar to the pattern recognized in Figure 3-1, when V_L is asymmetric, below 0.4, it can be seen that the peaks are slightly lower than full transmission. As it increases to 0.4 and becomes symmetric with the rest of the system, the system becomes fully transparent at the resonance peaks, and the valleys between are raised. As V_L increases beyond 0.4 and is again asymmetric, there is a noticeable decrease again in the transmission peaks. This time however, the valleys are further raised. As V_L gets closer and closer to 1.0, we see the peaks again begin to rise towards full transmission. This is due to the fact that at the value 1.0, the hopping integrals are at 100% transmission and the impedance caused by V_L is lost.

Perhaps the most important effect caused by incrementing V_L is the number of transmission peaks per band decreasing from 8 to 7. The transition is not easily observable, however when comparing the number of peaks for the 4 ring system in Figure 3-3 for $V_L = 0.6$ and $V_L = 0.7$, it is clear that a peak has been lost. Although not clear from the figure, when V_L is approximately 0.66, the 3rd and 4th peak from the inside of each band merge to one. The loss of this one peak is the result of the loss of the potential barrier of the left lead. An electron resonates with this barrier and causes a particular energy to be passed. As the hopping integral increments closer to 1.0, the potential barrier becomes smaller and smaller, until its effect is lost, along with the transmission peak associated with it.

In Figure 3-4, a similar system is observed. Here, instead of V_L alone being incremented, both V_L and V_R are incremented together. The effects are similar to Figure 3-3, however, instead of 8 peaks per band being reduced to 7, the number is reduced to 6. This is to be expected, since the peaks correlate to potential barriers which establish resonance conditions. Since both the left

and right leads are varied from largely impeding the electron to becoming perfect transmitters, eventually the resonance effect for both those barriers is lost and the two peaks associated with the leads disappear.

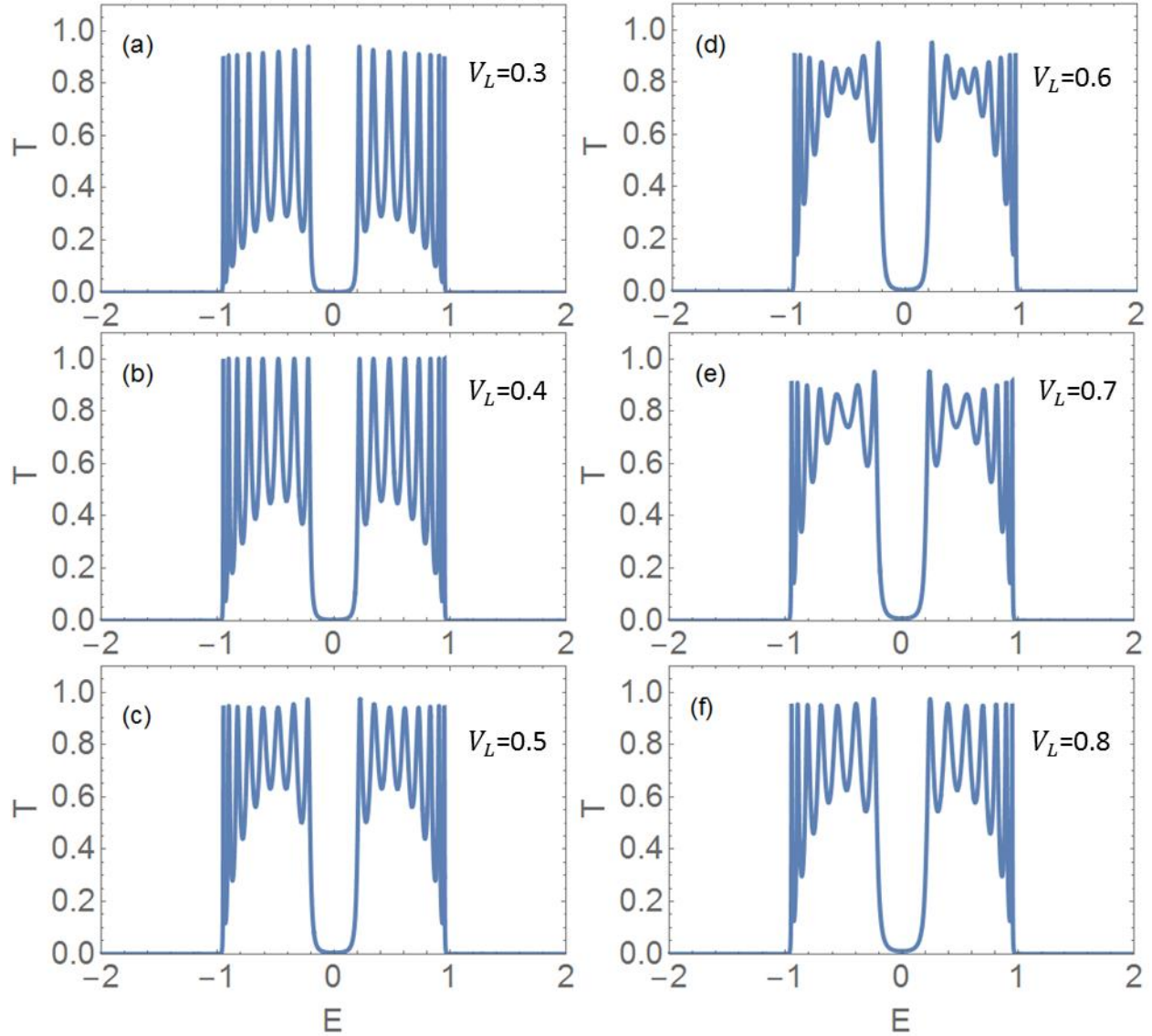


Figure 3-3 Transmission spectrum of a 4 ring system where the site energy parameters are all set at 0 and the hopping integrals V_m , V_{in} , and V_R all are set at 0.4. V_L is incremented from 0.3 to 0.8 in steps of 0.1 from (a) - (f).

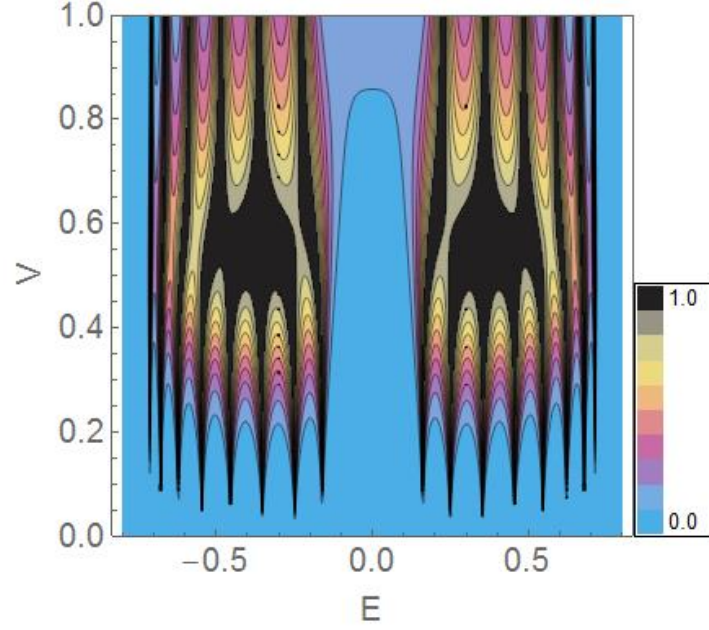


Figure 3-4 Contour plot of 4 ring system of transmission probability over V_L and V_R vs Energy. The site energy parameters are set at 0, while the hopping integrals V_{in} and V_m are both set at 0.3. This plot shows how the transmission spectrum is affected when the two lead values, V_L and V_R , are incremented. Of greatest note is the fact that, as the hopping integrals are increased, the number of peaks per band decreases from 8 to 6.

3.3 Changing system size

While it is seen from the earlier results that varying the hopping integrals significantly affects the transmission resonances and band structure, changing the number of rings in the system also affects the transmission, especially at the quasibound state energy of the QD sites around the rings. Figure 3-5 illustrates the effect of varying of the number of rings connected linearly and their respective transmission spectra. The first and most noticeable effect is the number of resonance peaks per band structure. Beginning with 3 rings connected serially, we observe 4 peaks per band, with a total of 8 peaks, for the case shown here with $V_L = V_R = 1$; if these external couplings are lowered to match V_m and V_{in} , the number of peaks per band

increases by 2, as illustrated in Figure 3-4. As the number of rings increases from 3 to 8 in increments of 1, the number of peaks per band increases by 2 with each successive ring added, ending with 14 per band structure for the case with 8 rings. This pattern of each band structure increasing by 2 peaks (4 peaks for the whole transmission) with each additional ring holds true for almost all conditions. As long as there are discernable band structures with transmission peaks, adding rings will have the same effect. For symmetric rings, this effect is due to the number of QD's per arm. With 2 QDs in each arm, and each ring connected by 2 QDs to neighboring rings, the system provides the electron wavefunction with 4 additional sites with which to reflect, transmit, and otherwise interact, leading to 4 transmission peaks being added for each ring. Also noteworthy is that, even with the increase of the number of peaks per band structure, the bands themselves do not widen. The spectrum of possible transmission values never increases, only the number of transmission peaks within the set boundary of the bands. This also is true for most conditions.

Not only does the number of resonance peaks increase with each additional ring, but also observable is the decreasing of the transmission in the middle of the bandgap. As the number of rings increases from 3 to 8, the central transmission, $T(0)$, decreases from a value of almost 0.5 to close to 0. Interestingly enough, $T(0)$ decays exponentially as a function of the number of rings. This effect shall be discussed more thoroughly along with later results. Of significance is the fact that this drastic decreasing of $T(0)$ with the number of rings in series only occurs for the conditions when V_L and V_R are set at 1.0, giving full transmission through those hopping integrals. This, and the fact that increasing the number of rings causes exponential decay of $T(0)$, leads to the conclusion that the drop in the central transmission (at $E = \epsilon_{QD} = 0.0$) is primarily a boundary effect. If V_L and V_R are changed to lower values, increasing the number of rings causes

less and less of a difference in $T(\varepsilon_{QD})$, and $T(\varepsilon_{QD})$ stays at around 0. With the increase of the size of the system, the boundary conditions influence the results less and less. Thus $T(\varepsilon_{QD})$, starts high, an effect caused the maxing out of V_L and V_R , and then drops exponentially to zero, the value determined by interference effects within the rest of the system.

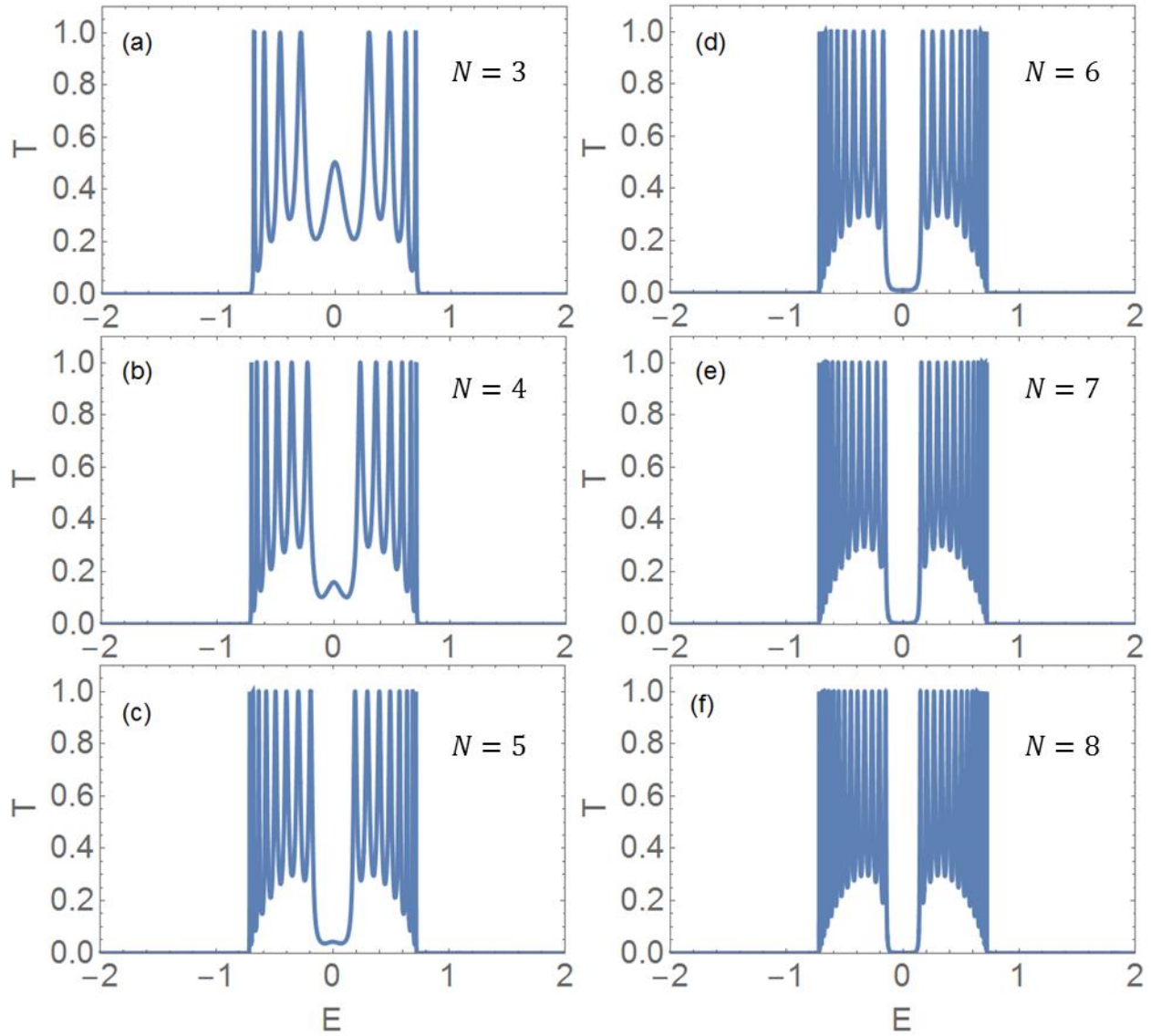


Figure 3-5 Transmission spectrum of nanoring chain with increasing number of rings. The site energy parameters are all set at 0, the hopping integrals V_m and V_{in} are at 0.3, while V_L and V_R are maxed out at 1. The number of rings, N , is incremented in steps of 1 from $N = 3$ to $N = 8$ from (a) - (f).

We next analyze the transmission through the multiple ring structure specifically at the QD resonance energy as a function of inter-ring coupling, V_m , and the number of rings in series. All QD site energy values, ε_{QD} , are set to $\varepsilon_{QD} = 0.0$, and all inter-dot couplings are fixed at $V_{in} = 0.3$. The couplings between the ring system and the leads are also set initially to $V_L = V_R = V_{leads} = 0.3$. We focus here on the transmission with the incoming electron energy tuned to the site energy of the QDs in the rings, $\varepsilon_{QD} = 0$. At this energy, the system transmission exhibits a near-perfect bandgap, unless $V_m > 2V_{in}$. In Figure 3-6, we show the dependence of $T(\varepsilon_{QD})$ on the number of rings, N , for various values of the inter-ring coupling parameter, V_m . For $V_m > 0.6$, $T(\varepsilon_{QD})$, increases to near 100% transmission as the number of rings increases to a critical value, N_{crit} , and then $T(\varepsilon_{QD})$ decreases again for higher numbers of rings. N_{crit} becomes increasingly large as V_m is lowered from $V_m = 1.0$ towards $V_m = 2V_{in} = 0.6$. For more than the critical number of rings, the transmission at $E = \varepsilon_{QD}$ decays exponentially as the number of rings increases. For a large value of V_m , only a relatively few number of rings in series is necessary to allow reflections between rings to produce destructive interference which dampens out $T(\varepsilon_{QD})$ for any higher number of rings [42]. The initial build-up of $T(\varepsilon_{QD})$ as N approaches the critical value indicates that multiple reflections between the rings can also produce constructive interference leading to 100% transmission, at least for inter-ring coupling, $V_m > 0.6$, and system-leads coupling, V_{leads} , less than a critical value (defined below). As V_m approaches 0.6, which is twice the value of the inter-dot couplings, V_{in} , the system transmission, $T(\varepsilon_{QD}) = 0.0861$, becomes independent of ring number, N , but it is still dependent upon the system-leads coupling. For example, the N -independent value of $T(\varepsilon_{QD})$ at $V_m = 0.6$ increases with the strength of the coupling between the multi-ring system and the source and drain leads,

V_{leads} , reaching 100% transmission at a critical value of $V_{leads} = 0.775$. Thereafter, $T(\varepsilon_{QD})$ decreases to $T(\varepsilon_{QD}) = 0.779$ for $V_{leads} = 1.0$ (ideal coupling to the leads).

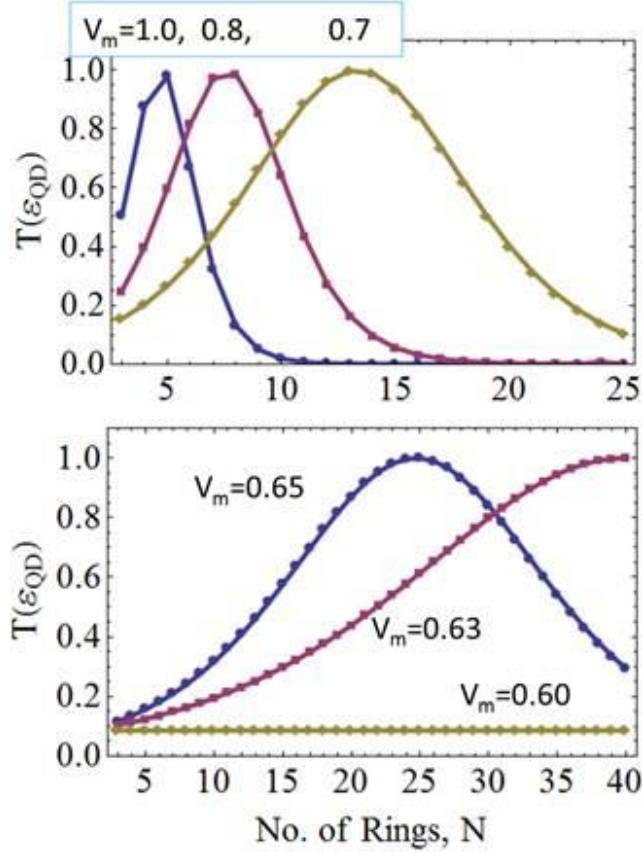


Figure 3-6 Variation of $T(\varepsilon_{QD})$ with the number of series-coupled rings for six different values of inter-ring coupling, V_m . The site energies are all set at 0, while the hopping integrals are all at 0.3, except for V_m .

At the critical value of $V_{leads} = 0.775$, the transmission remains at 100% across a broad range of energies centered around $E = \varepsilon_{QD}$, as depicted in Figure 3-7. In order to sustain transparency for a system composed of multiple rings and QDs across such a wide energy band, there requires a unique confluence of resonance and interference effects. For $V_{leads} = V_m = 0.6$,

which is the case with each ring coupled symmetrically to the left and right, the transmission still manifests distinct resonance peaks across the energy band. As V_{leads} increases to 0.775, however, resonance saturation occurs, in which the anti-resonances merge with resonance maxima across the energy range of approximately $-0.3 < E < 0.3$, for all values of N .

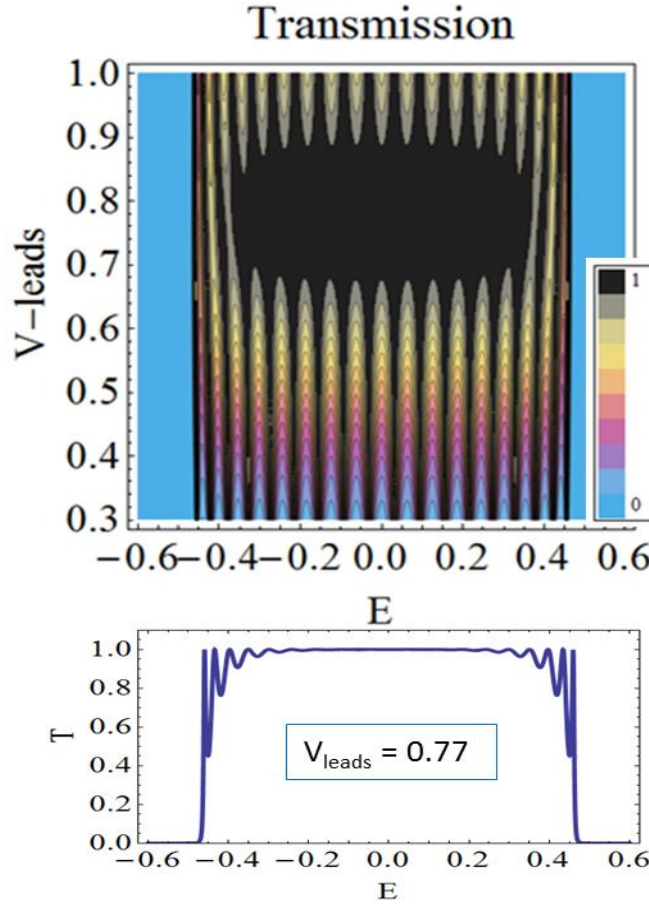


Figure 3-7 The contour plot shows the transmission of the multi-ring system for $N = 10$, as a function of energy and system-leads coupling, V_{leads} . The line plot depicts the broad band of nearly 100% transmission for the particular case of $V_{leads} = 0.77$. The inter-ring coupling is $V_m = 0.6$. The site energies are set at 0, while $V_{in} = 0.3$.

For $V_m < 0.6$, and $V_{leads} < 0.775$, calculations show that $T(\varepsilon_{QD})$ decays exponentially with increasing N ; no critical value of N exists at which $T(\varepsilon_{QD})$ increases from its value for low-ring number ($N = 3$). These effects are shown in Figure 3-8 for three different values of V_m .

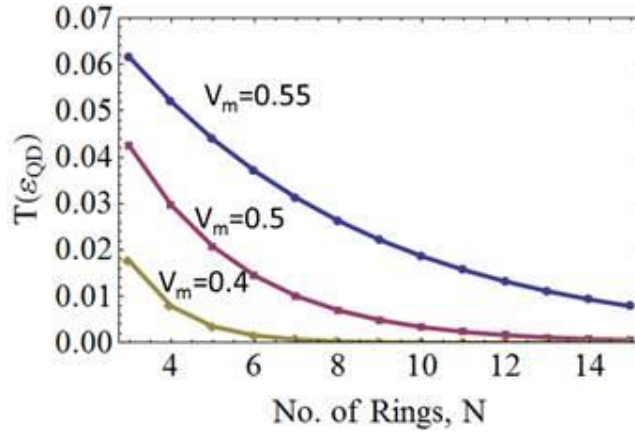


Figure 3-8 Exponential decay of $T(\varepsilon_{QD})$ as the number of rings increases, for $V_m = 0.55, 0.5$, and 0.4 . The site energies are all set at 0 , while $V_{in} = V_{leads} = 0.3$.

With smaller coupling between individual rings in series, each additional ring effectively contributes an attenuation factor into the overall transmission at $E = \varepsilon_{QD}$. Chakrabarti *et al* distinguish between cases in which rings have an even or an odd number of QD sites in each arm [2]. For the case studied here, having an even number of QD sites in each arm, and with no magnetic flux threading the rings, they predict the exponential decay of $T(\varepsilon_{QD})$ with increasing number of rings in series. In contrast, for an equal but odd number of sites in each arm, their results show that $T(\varepsilon_{QD}) = 1.0$, independent of N . Recent work by us for the case with 1 QD in each arm of serially-connected rings verifies this conclusion for an odd number of QD sites per arm [20].

A contour plot showing the transmission as a function of the number of rings in series for the inter-ring coupling, $V_m = 0.8$, is depicted in Figure 3-9(a) and the yellow line plot in Figure 3-6. The maximum transmission at $E = \varepsilon_{QD}$ occurs for $N = 8$ rings in series, and for this case a line plot of the transmission over the same energy range as for the contour plot is shown in Figure 3-9(b). The rise and fall of $T(\varepsilon_{QD})$ as function of the number of rings is clearly seen in

Figure 3-9(a), while the resonance peaks in the two transmission bands on either side of $E = \varepsilon_{QD} = 0.0$ maintain unity amplitude for all values of ring number.

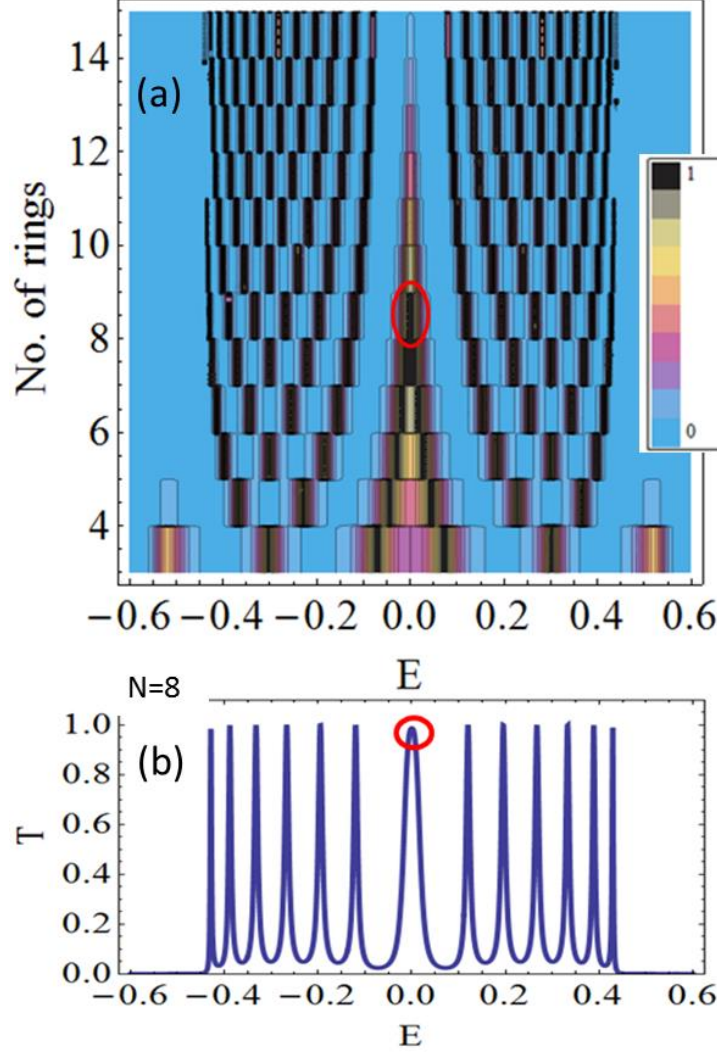


Figure 3-9 (a) Contour plot of the transmission as a function of electron energy for different numbers of rings in series. (b) Line plot of the transmission for the specific case of 8 rings, for which $T(\varepsilon_{QD})$ attains full transmission. Site energies are all set at 0, while $V_m = 0.8$ and $V_{in} = V_{leads} = 0.3$.

Finally, we show in Figure 3-10 the dependence of $T(\varepsilon_{QD})$ on V_m for six different systems in which the number of rings in series varies. For $V_{leads} = 0.3$, and with less than 5 rings in series, our calculations show that $T(\varepsilon_{QD})$ does not reach full transmission for inter-ring

coupling $V_m \leq 1.0$. Figure 3-10(a) shows cases for which $N \geq 5$. For systems with more rings, the transmission transparency at $E = \varepsilon_{QD}$ becomes increasingly limited to a narrowed range of V_m values, the center of which approaches $V_m = 0.6$ as N becomes very large. At exactly $V_m = 0.6$, with $V_{leads} = 0.3$, $T(\varepsilon_{QD})$ has the same value (0.086) regardless of the number of rings in series. As noted above, this value of $T(\varepsilon_{QD})$ can be modulated up to 100% transmission by adjusting V_{leads} to the critical value of 0.775, at which resonance saturation occurs. The dependence of $T(\varepsilon_{QD})$ on V_m for this case is shown in Figure 3-10(b) for several values of N . The ring system is completely transparent at $V_m = 0.6$ and $V_{leads} = 0.775$, independent of the number of rings in series.

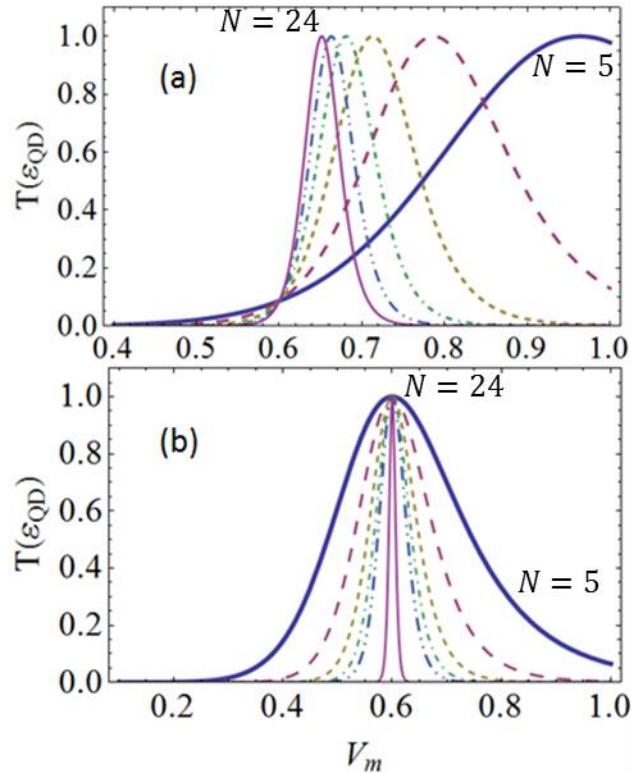


Figure 3-10 Dependence of $T(\varepsilon_{QD})$ on V_m for six different numbers, N , of rings in series. (a) $V_{leads} = 0.3$; $N = 5$ (thick solid), 8 (long dashes), 12 (short dashes), 16 (dash-dot), 20 (dash-double dot), 24 (thin solid). (b) $V_{leads} = 0.775$ (note difference in horizontal scaling). Same values of N , except $N = 80$ (thin solid). The site energies are all set at 0, while $V_{in} = 0.3$.

4. MAGNETIC RESULTS

4.1 Sharpened AB Oscillations

One particular magnetic effect which has been studied previously is sharpened AB oscillations [43]. This effect occurs with a small amount of magnetic flux, and causes a sharp transmission zero to occur around the energy value of the QD quasi-bound state for a symmetric system. It also causes the usually sinusoidal AB oscillations to sharpen into a set of sharp transmission peaks, centered on integer values of Φ/Φ_0 as shown in Figure 4-1. In the transmission spectrum, these appear as sensitive magnetic flux effects, or zeros in the transmission. So far, this has been shown to occur in small systems, with one nanoring and 2 QDs on that ring. Here I will demonstrate the generalization of this effect for a larger system, and explore the effects that different parameters have upon this.

I first wish to show the generalization of results from previous work to a larger system. It has been shown before [43] that with the introduction of a small amount of magnetic flux, for example, around the order of 0.05 flux quanta, small anti-resonances occur at the symmetric QD site energy value or hopping integral, depending on the system. For graphene, a value of 0.05 flux quanta relates to a perpendicular magnetic field of about $4 * 10^3 T$. This is clearly a magnetic field that is not viable to use experimentally. However, these results can be scaled down to a more viable magnetic field and still display these same properties. Previously, for 1 or multiple rings in direct contact, these resonances have simply manifested as a sharp transmission zero interrupting a seemingly continuous line.

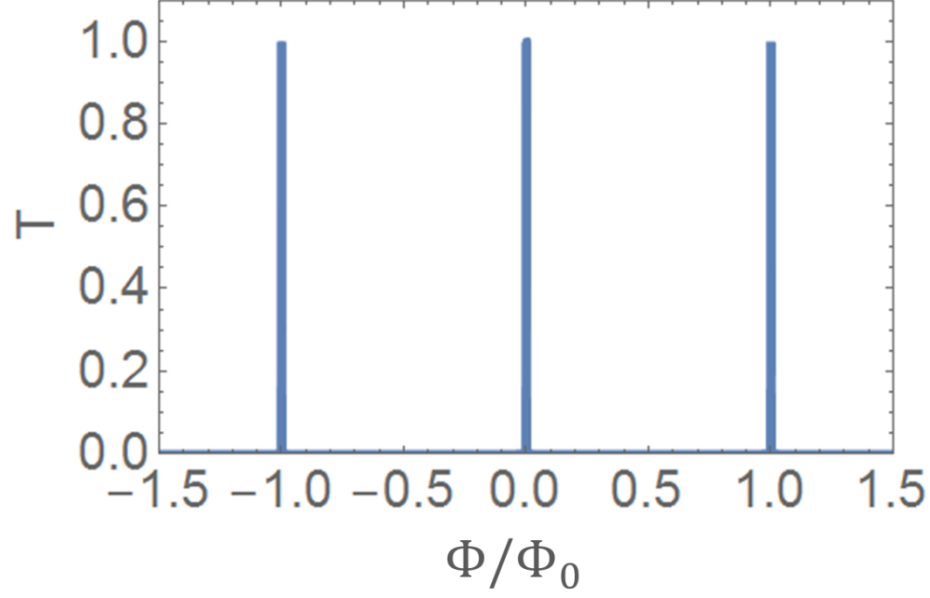


Figure 4-1 Transmission vs flux plot for a system showing sharpened AB oscillations. These can be seen as transmission peaks at integer flux quantum values of the magnetic flux.

In Figure 4-2, we see the results of introducing a small magnetic flux, of 0.05 flux quanta, into a system of 4 nanorings connected by a coupling segment. In Figure 4-2(a), the system has no magnetic flux present. However, in Figure 4-2(b), the small magnetic flux is introduced. For this system, finite flux results in sharp resonances occurring at exactly the hopping integral value of ± 0.4 . For non-zero QD site energy values, the flux-induced transmission zeros occurs at $\varepsilon_{\text{QD}} \pm 0.4$. This deviates from the energy at which the zero appeared in the case of direct-contact rings, but it shows that sharp AB oscillations are a generalized effect applying to nanorings with magnetic flux present.

This effect exhibits additional differences to the previous results, as well. Previously, the resonance was only a sharp transmission zero at the QD site energy value. However, our result shows what appears to be both a transmission zero and peak close together.

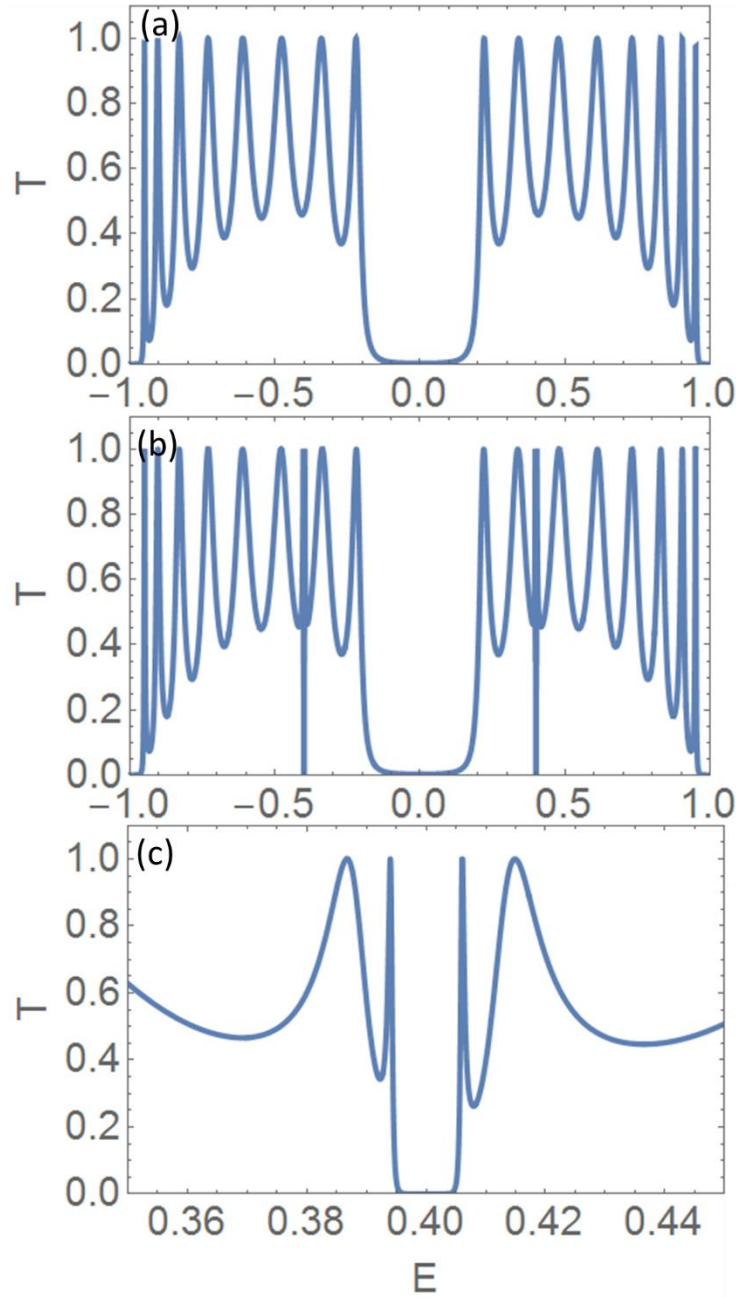


Figure 4-2 Transmission spectrum of a 4 ring system with site energy parameters all set at 0 and hopping integrals all set at $V_n = 0.4$, seen without magnetic flux in (a). A small amount of magnetic flux, at $\Phi/\Phi_0 = 0.05$, results in sensitive magnetic flux effects at the hopping integral value of 0.4, seen in (b) and (c).

Let us change the scale of the figure to investigate this closer. As can be seen from Figure 4-2(c), this resonance is more complicated than at first glance. What appeared to be a transmission peak

and zero, is actually a set of 4 peaks, surrounding a zero at the hopping integral value. This added complexity inspires us to investigate the dynamics of other system parameters and their effects on this transmission phenomenon.

Let us now investigate the effect that varying the number of rings connected in series has upon these sensitive magnetic flux effects. In Figure 4-3, we see a system with the number of rings connected serially varying from 4 to 9. There is again a small magnetic flux of 0.05 flux quanta present through each ring. We notice several interesting aspects of these plots. The most noticeable is the number of added transmission peaks from the sensitive flux response increases directly proportionately to the number of rings connected in series. Before any flux is passed through the system, the plots with an even number of rings have only a smooth valley shown, while the plots with an odd number of rings have a single transmission maximum in the region where the flux effect will occur. With 4 rings, when flux is passed through the system, an extra 4 peaks are added. With 6 rings, an extra 6 peaks are added and so forth. The effect extends to any amount of serially connected rings desired.

Although there is a clear proportionality with the systems with an even amount rings between the ring number and the added peak number, at first glance this does not appear to hold with the systems with an odd number of rings. Observing plot (b), (d), and (f) shows a number of peaks that does not equal the number of rings, but appears to have 1 more peak than ring number. Interestingly, regardless of the number of rings or the value of symmetric hopping integrals, a system with an even numbered amount of rings will always have the sensitive flux effect at a transmission minimum, while a system with an odd number of rings will always have flux effect at a transmission maximum. This means that, before any magnetic flux was passed through the system of odd numbered rings, there was a transmission peak at the value where the sensitive

flux effect would take place. Therefore, this peak is split into the number of peaks that we see in the figures, and the added number of peaks due to the sensitive flux response is always equal to the number of rings connected in series.

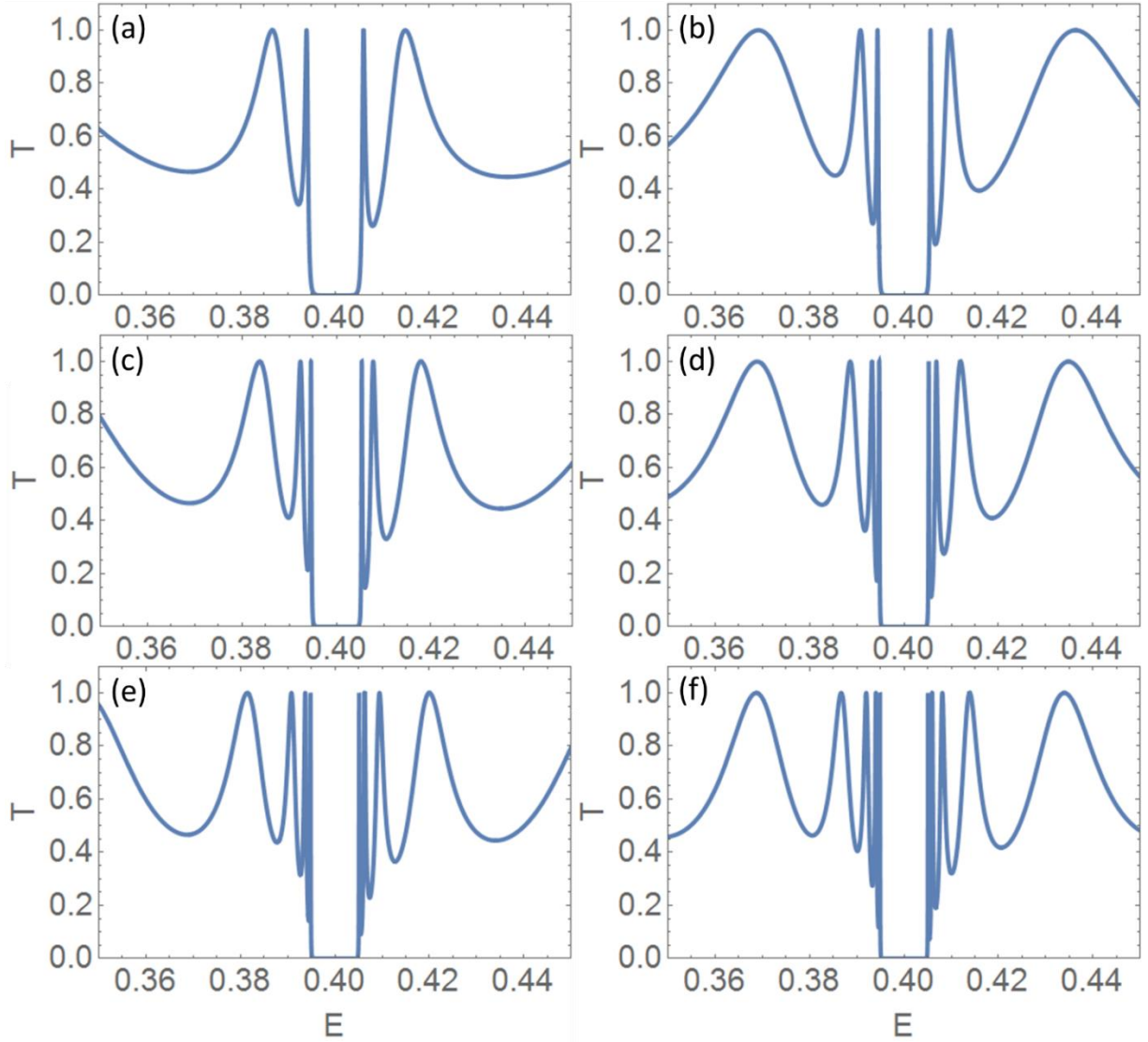


Figure 4-3 Transmission spectrum of nanoring chain with increasing number of rings. The site energy parameters are all set at 0, and the hopping integrals all are set at $V_n = 0.4$. The number of rings, N , is incremented in steps of 1 from $N = 4$ to $N = 9$ from (a) - (f). A small amount of magnetic flux, at $\Phi/\Phi_0 = 0.05$, results in sensitive magnetic flux effects at the hopping integral value of 0.4. Notice the number of peaks added by the AB Effect increases in proportion to the number of rings.

Whenever an incident electron energy coincides with one of the eigenenergy values of the system, there are resonance conditions and the electron achieves a full transmission. The peaks seen in the line plots are results of this. The energy eigenvalues of the system are degenerate proportional to the number of rings in the system when no magnetic flux is present. When flux through the rings becomes non-zero, the degeneracy is lifted and the eigenenergy values split into the transmission peaks. The lead values affect the position of the transmission peaks in relation to the energy state values. By alternating between values symmetric with the rest of the system and transparency (a hopping integral value of 1.0), the transmission peak locations in relation to the energy eigenvalues can be shifted.

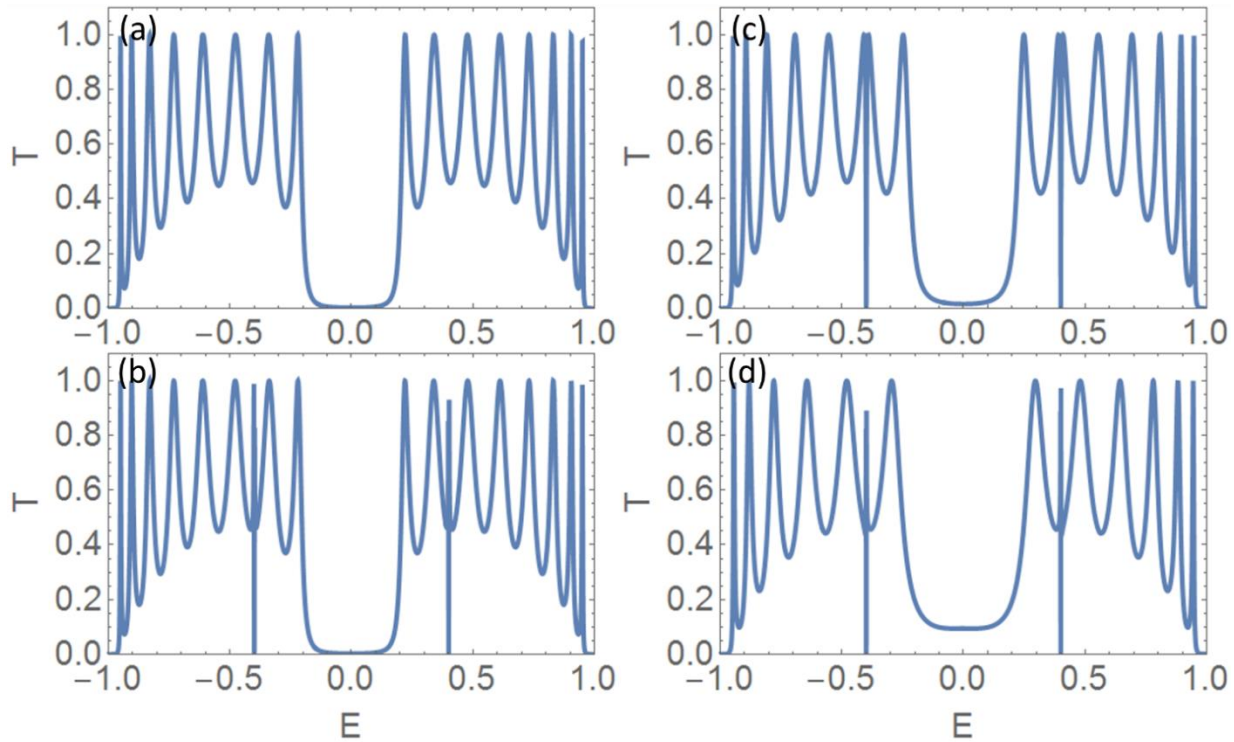


Figure 4-4 Transmission plots of 4 ring system showing sensitive magnetic flux effects with different lead values. (a) has no flux with leads symmetric with the rest of the system. (b) introduces flux, with both leads still symmetric. (c) has 1 lead set at full transparency, while (d) has both leads set to full transparency. Note the switching of peak to valley of the location of the flux effects.

Scattering associated with these junctions leads to deviations from the eigenvalues. By setting either lead to a perfect lead, or to a hopping integral of 1, the flux response is found to switch from occurring at a peak to a valley, and vice-versa. By setting both leads to a value of 1, the site of the sensitive magnetic flux remains at the same type of maxima or minima as can be seen in Figure 4-4.

We will now investigate the effects of varying the different hopping integrals on these sensitive magnetic flux effects. In Figure 4-5, we find that the position of the AB resonances is dependent on V_{in} , the hopping integral value of all the transitions within each QD. As we will see later, this position is completely independent of the coupling between rings. Also notice that the width and shape of the oscillation is unaffected by the changing of V_{in} .

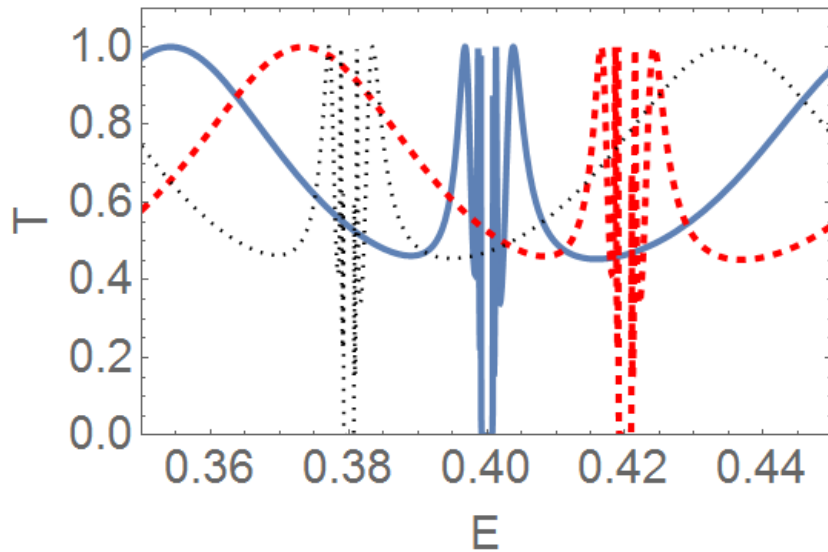


Figure 4-5 Transmission vs Energy plot of a 6 ring system with hopping integrals set at $V_{leads} = V_m = 0.4$ and a magnetic flux of 0.02 flux quanta present. V_{in} is set at 0.38 (Black, Dotted), 0.4 (Blue, Solid), and 0.42 (Red, Dashed). Note the position of the bandgap as V_{in} is altered.

In general, V_{in} has a large effect on the transmission spectrum of an electron, and does not simply shift transmitted energies. However, the magnetic flux responses are shifted along the energy axis to always be centered directly on the V_{in} value.

Along with varying the V_{in} parameter, we also investigate the impact that varying V_m has on these sensitive magnetic flux effects. Figure 4-6 shows a system where this parameter is given several different values. Although complicated and seemingly uncorrelated at first, this plot shows a very clear and linear impact upon the bandgap at the symmetric hopping integral value of 0.4. V_m is given 3 different values, 0.2, 0.4, and 0.8. When $V_m = 0.2$, the bandgap width is approximately $\Delta E = 0.05$. When $V_m = 0.4$, the value of the rest of the system, the bandgap width is approximately $\Delta E = 0.1$. Finally, when $V_m = 0.8$, the bandgap has a value of about $\Delta E = 0.2$. So, where V_m is at the value of the rest of the system, the bandgap is approximately equal in width to 2 times the value of the magnetic flux, 0.05.

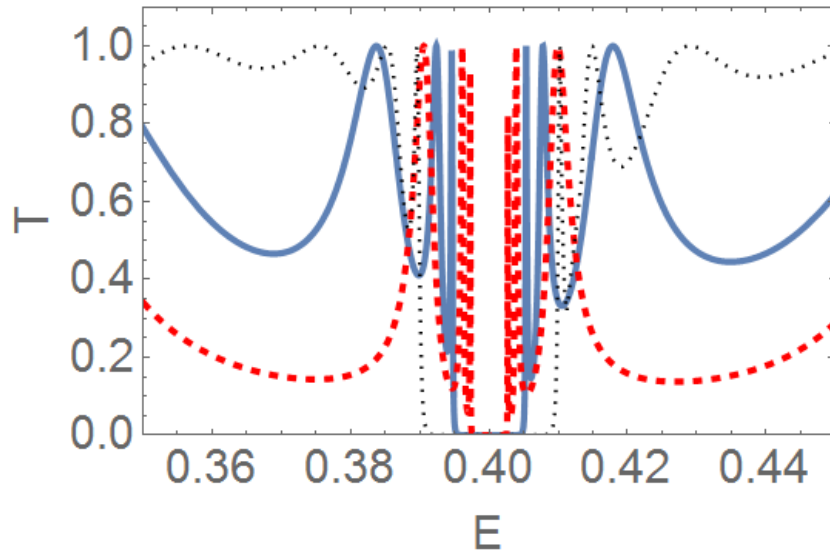


Figure 4-6 Transmission vs Energy plot of a 6 ring system with hopping integrals set at $V_{leads} = V_{in} = 0.4$ and a magnetic flux of 0.05 flux quanta present. V_m is set at 0.2 (Red, Dashed), 0.4 (Blue, Solid), and 0.8 (Black, Dotted). Note the width of the bandgap as V_m is altered.

When V_m is halved, the bandgap width is halved, and when V_m is doubled, the bandgap width is doubled. This shows an approximately linear relationship between the value of the hopping integral V_m and the width of the energy bandgap created by the AB interference, at least for these system parameter values. For different values, this directly linear relationship is altered. However, regardless of value, V_m always has a directly proportional effect upon the width of the energy bandgap. Also, it is clear that this hopping integral value has no effect on the energy position of these magnetic flux effects, affecting only the bandgap.

4.2 Magnetic flux effect on energy bandgaps

As we have seen the effect of varying the different hopping integral parameters of the system, let us now observe the effect of the magnetic flux passing through the system on the energy transmission spectrum. Figure 4-7 and Figure 4-8 show a system of 4 rings in series with increasing flux passed through them. As was shown in the previous results, sharpened AB oscillations can be seen in Figure 4-7(a), with only a small amount of magnetic flux present. It is at these sensitive magnetic flux responses that we see bandgaps appearing at $\pm V_{in}$, which in this case is ± 0.3 . As the magnetic flux through the rings increases, the bandgaps at the hopping integral value increase in width. In earlier results, a linear relationship between the parameter V_m and the width of the added bandgap was shown. In Figure 4-8, a linear relationship between the magnetic flux Φ/Φ_0 and the width of the added bandgap becomes apparent. These results agree with those presented by Deo and Jayannavar [42]. In Figure 4-9, we see the transmission of this system as a function of the imaginary and real parts of the energy. Interestingly, the poles of this

complex system are displaced slightly off the real energy axis, with multiple transmission maxima occurring with negative imaginary energy values.

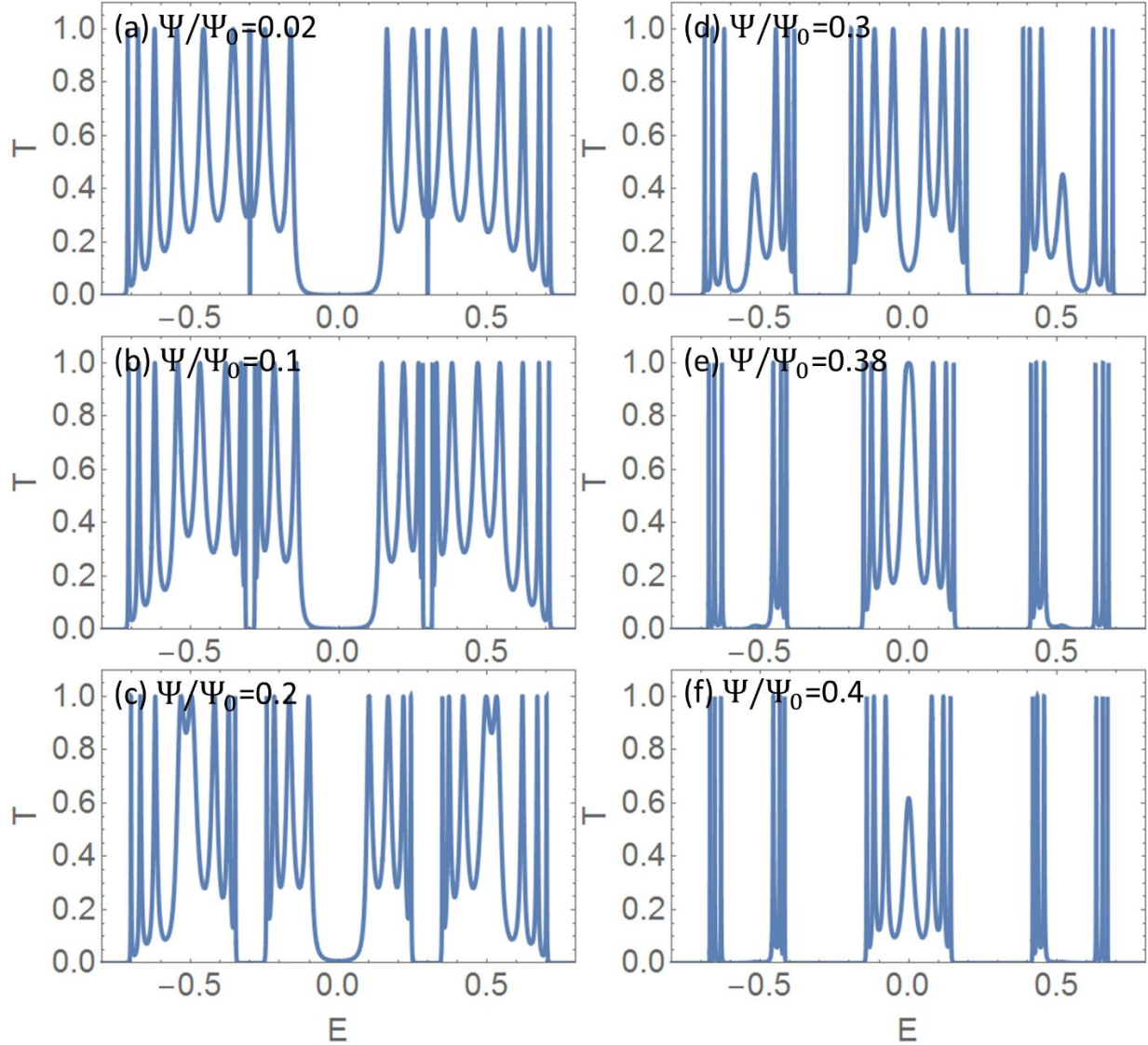


Figure 4-7 Transmission spectrum of nanoring chain with increasing magnetic flux. The site energy parameters are all set at 0, and the hopping integrals all are set at $V_n = 0.3$. The magnetic flux is incremented in uneven steps from $\Phi/\Phi_0 = 0.02$ to $\Phi/\Phi_0 = 0.4$ from (a) - (f). When a small flux is first introduced, sensitive flux effects can be seen as a bandgap is introduced. When $\Phi/\Phi_0 = 0.38$, the middle energy bandgap disappears and merges into a transmission peak.

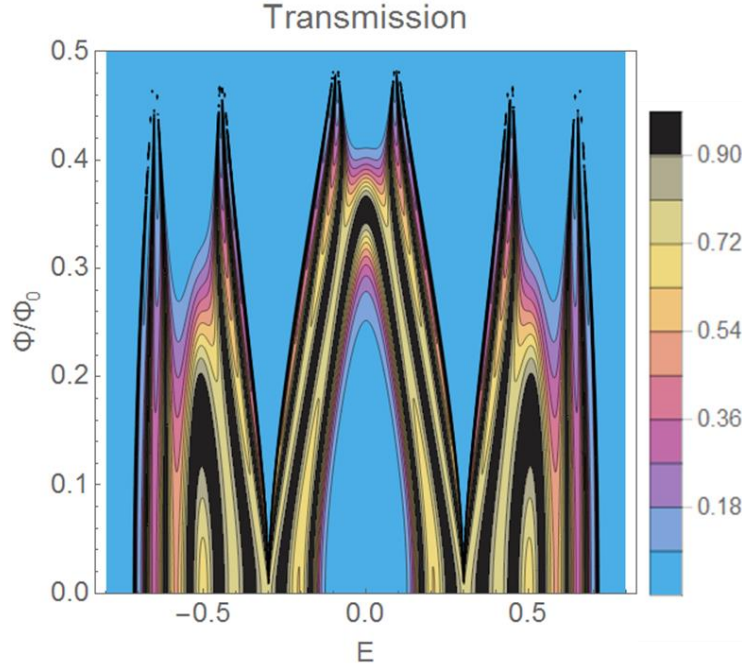


Figure 4-8 Contour plot of transmission as a function of magnetic flux and energy for a system of 4 nanorings. All site energies are set at 0 and all hopping integrals at 0.3. Notice the growing bandgaps at the hopping integral values, and the merging middle bandgap into a peak.

Not only do bandgaps appear and increase in width as the flux increases, but the middle bandgap decreases. This middle bandgap, or semiconducting energy band centered at 0 V, was observed in the non-magnetic results in Chapter 3, as it is a topic of interest in the scientific community and plays a part in determining the conduction properties of a material. In observing Figure 4-7 and Figure 4-8, we see the middle bandgap is greatly affected by the increase of magnetic flux. It appears that at a value of $\Phi/\Phi_0 = 0.38$, the middle bandgap completely merges and becomes a transmission peak. In Figure 4-10 we see this point plotted in the complex energy plane, with the several middle transmission poles merging into 1 with negative imaginary energy values. After this optimal value of $\Phi/\Phi_0 = 0.38$, the middle transmission peak quickly drops off and becomes a zero. The changing and disappearing of this middle bandgap affects the

conductance properties of this system, causing it to be a semiconductor until the optimal flux value, where it has normal metallic properties, as can be seen in Figure 4-11. This shows that the magnetic flux present in the system can alter and control the metallic nature over a certain energy window.

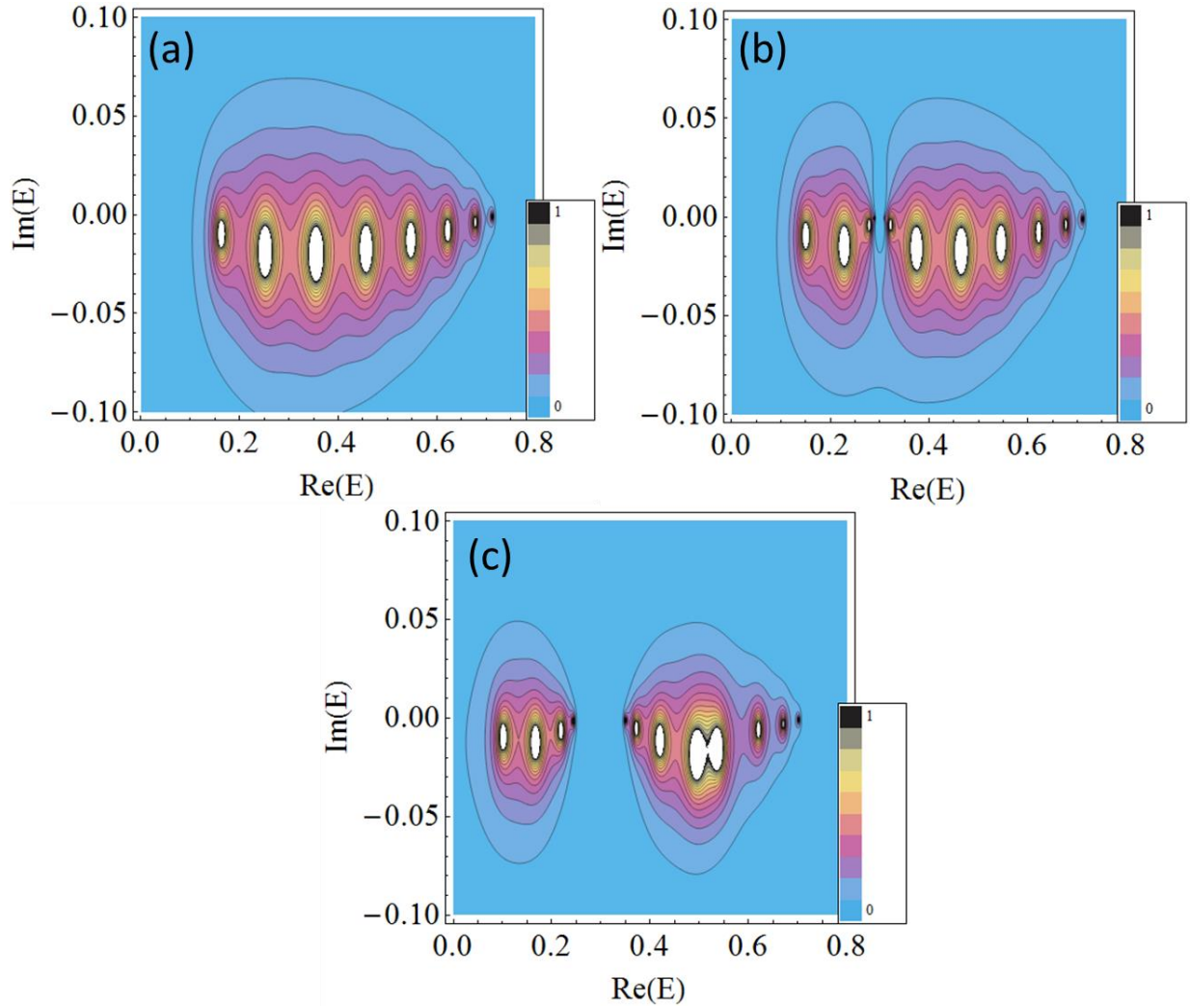


Figure 4-9 Contour plots of Figure 4-8 showing transmission as a function of the imaginary and real portions of energy, with increasing magnetic flux from $\Phi/\Phi_0 = 0.0$ (a), to $\Phi/\Phi_0 = 0.08$ (b), to $\Phi/\Phi_0 = 0.2$ (c). Notice a bandgap appearing, flanked by multiple peaks. The white portions represent poles in the complex energy going to infinity.

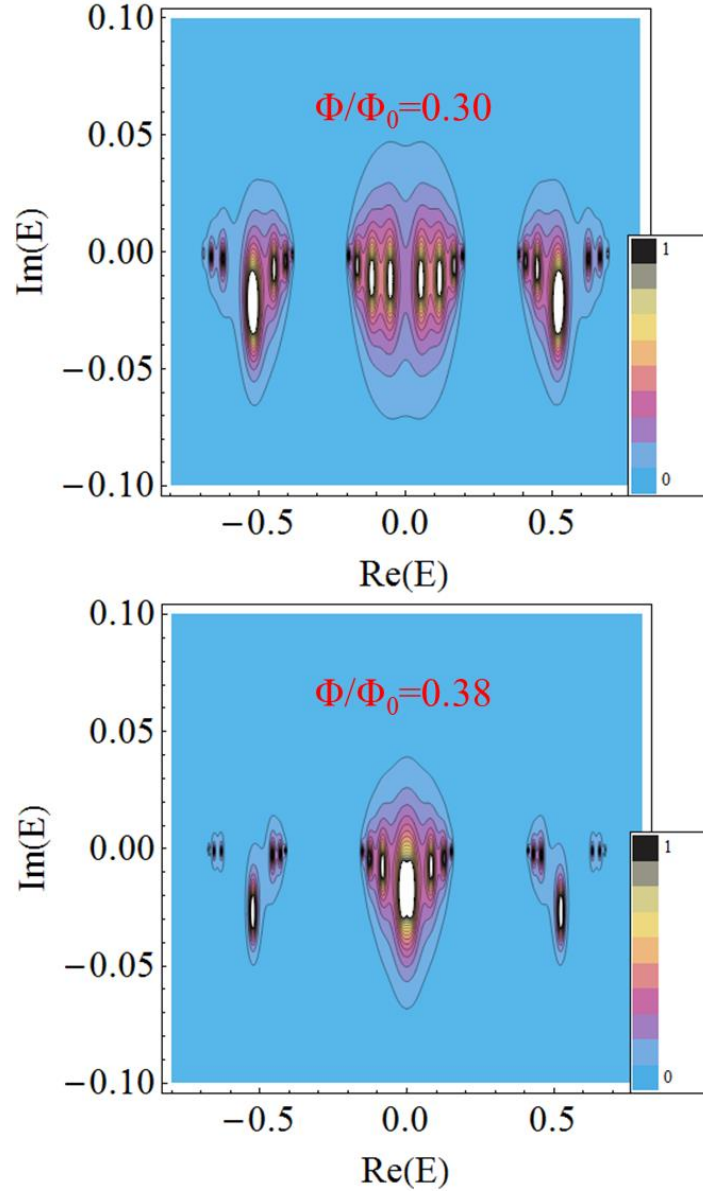


Figure 4-10 Contour plots of Figure 4-8 showing the transmission as a function of the imaginary and real portions of energy, with increasing flux. Notice for the second plot, the merging of the middle bandgap into a peak. The white portions represent poles in the complex energy going to infinity.

Other effects of the magnetic flux on the bandgap, band structures, and sets of transmission peaks have been observed by other groups. Notably, Li *et al* presented results for a 3 ring system of 8 sites per ring, without leads coupling the rings.

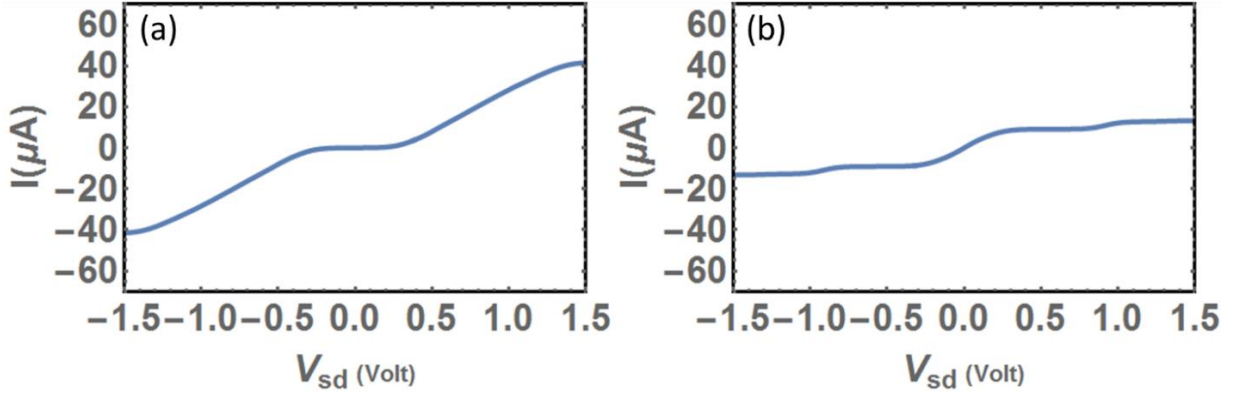


Figure 4-11 IV plots of the system of Figure 4-8, with the magnetic flux set at $\Phi/\Phi_0 = 0$ (a) and $\Phi/\Phi_0 = 0.38$ (b). Notice that the system goes from a semi-conductor to being ohmic over the middle region.

It was shown that when magnetic flux is applied to the system, the number of rings does not affect the overall structure of the energy spectrum [11]. I wish to show the generalization of this effect to our system, comprised of rings with 6 sites with leads coupling the rings. It is important to note the rise of a bandgap due to the coupling leads. Figure 4-12 shows a system of 3 rings in series. It is clear that, as the magnetic flux is increased through the system, the transmission bands split from 2 distinct bands, to 6 sets of transmission peaks, or 6 bands. As was seen previously, the middle bandgap merges to a single band, while additional bandgaps arise due to interference effects from the AB phase shift. The number of these added bands corresponds to the number of sites per nanoring. Note from the same figure, that there are 2 transmission peaks per band, as can be seen more clearly in Figure 4-13.

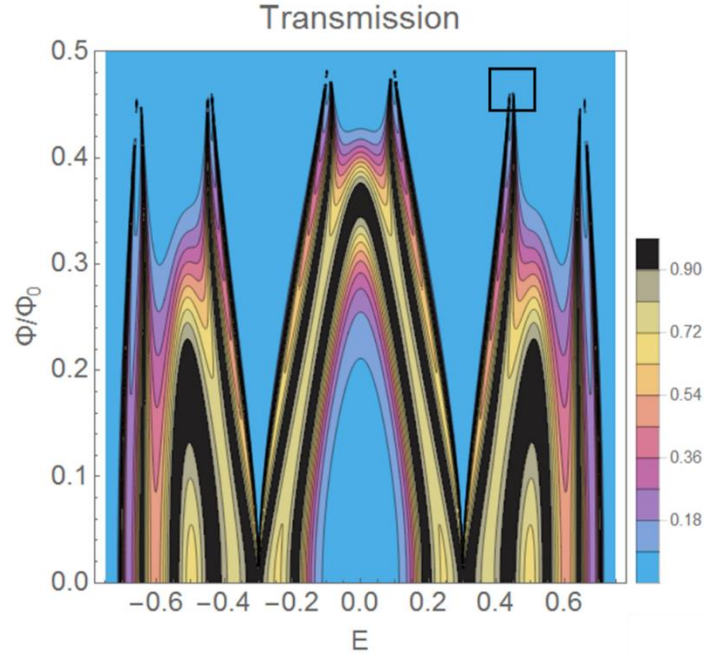


Figure 4-12 Contour plot of transmission as a function of electron energy and magnetic flux. This is a system of 3 nanorings, with site energies set at 0 and hopping integrals at 0.3. Notice the 6 sets of transmission peaks created by the increasing flux. Black boxed area expanded to show detail in next figure.

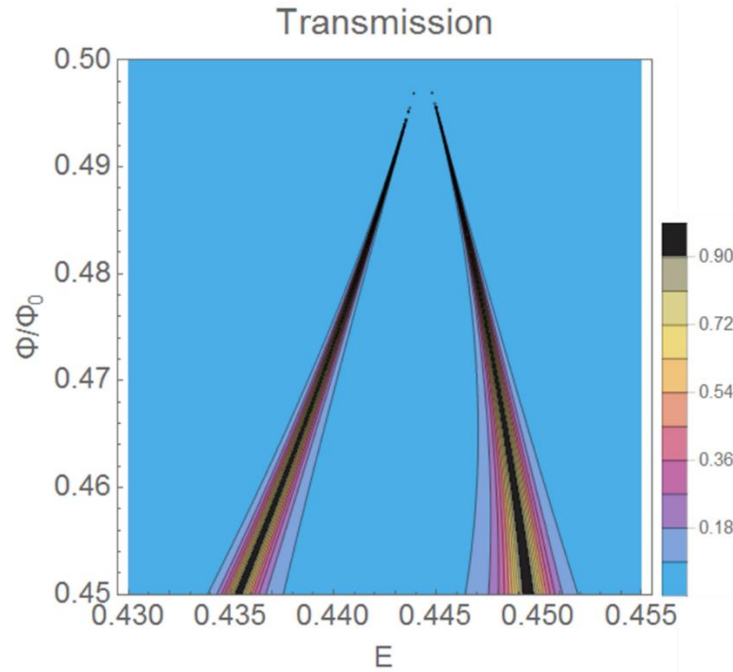


Figure 4-13 Contour plot of transmission as a function of energy and magnetic flux. This is for the system of Figure 4-12, zoomed in on a set of peaks to show detail.

In Figure 4-14, we see a similar system, but with 6 rings in series. With the increase of magnetic flux through the system, we see the initial 2 transmission bands merge and split into 6 sets of peaks, the same as the previous system. As predicted by Li *et al*, the structure of the energy spectrum is preserved, remaining unchanged with the addition of 3 rings. Also observed is the increase of the number of peaks per added band. Whereas in the system with 3 rings there were 2 peaks per band, in this system of 6 rings there are 5 peaks per band. This shows, and is indeed confirmed, that the number of peaks per band added by the increase of magnetic flux is equal to 1 less than the number of rings in series. This result, however, only holds for systems with rings coupled by a lead between each.

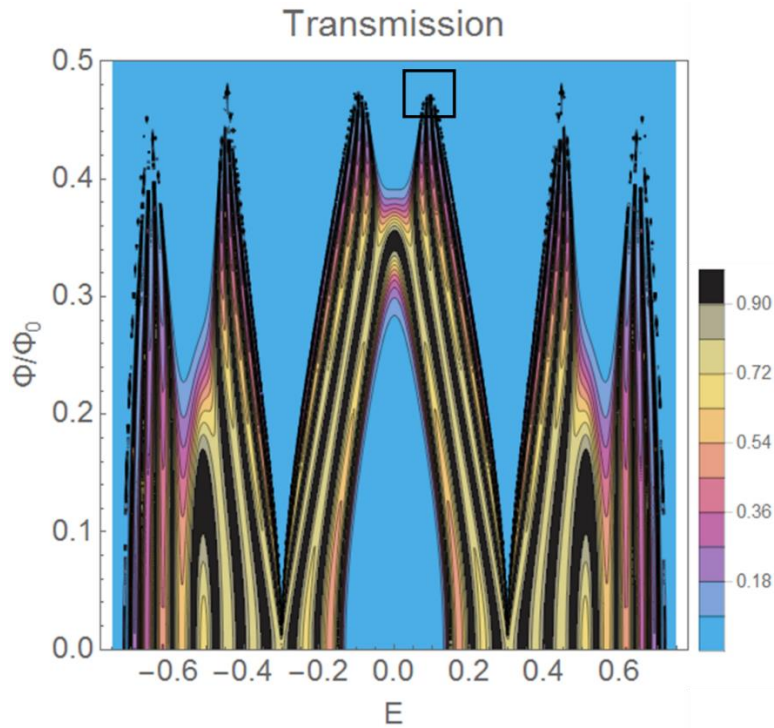


Figure 4-14 Contour plot of transmission as a function of energy and magnetic flux. This is for a 6 ring system with site energies at and hopping integrals at 0.3. Notice the preserved overall structure, and the increased peaks per set. Black box area expanded in next figure to show detail.

transmission through the system. As we see in both plots, increasing the flux decreases the lead coupling values needed to achieve full transmission. For higher values of Φ/Φ_0 , the value of V_{leads} needs to be less and less in order for $T(0)$ to be transparent. This is indicated by the diagonal line seen in Figure 4-16. Also observed in these plots is the effect of the ring coupling and the lead coupling on the system's sensitivity to the magnetic flux. As you can see, as the lead coupling parameters increase, the sensitivity to the magnetic flux increases as well. This effect is amplified by increasing the ring coupling parameter. In Figure 4-16(a), with a ring coupling parameter of $V_m = 0.3$, there is not much increase in flux sensitivity as the lead parameter increases. However, in Figure 4-16(b), with $V_m = 0.6$, as the V_{leads} increases, the transmission becomes highly impacted by increase in magnetic flux. Recall in Chapter 3, when $V_{in} = 0.3$, $V_m = 0.6$ and $V_{leads} = 0.775$, a unique transmission structure was observed, with an extended energy eigenstate.

This effect is similar when the system parameters being varied are switched. In Figure 4-17 we see the resonant transmission as a function of the magnetic flux and the ring coupling parameter V_m . Similar to the previous figure, the higher the magnetic flux, the lower the ring coupling needs to be in order to achieve resonant transmission transparency. So as we increase magnetic flux, the lead coupling needed for full transmission is decreased. We also observe the ring coupling V_m and its impact on the system's sensitivity to the magnetic flux. As V_m increases, the flux has a greater and greater impact on the transmission. When the lead coupling V_{leads} is increased, this effect is again amplified. Comparing Figure 4-17(a) and Figure 4-17(b) shows that, when V_{leads} is increased from 0.3 to 0.775, the system shows a much higher sensitivity to a varying magnetic flux.

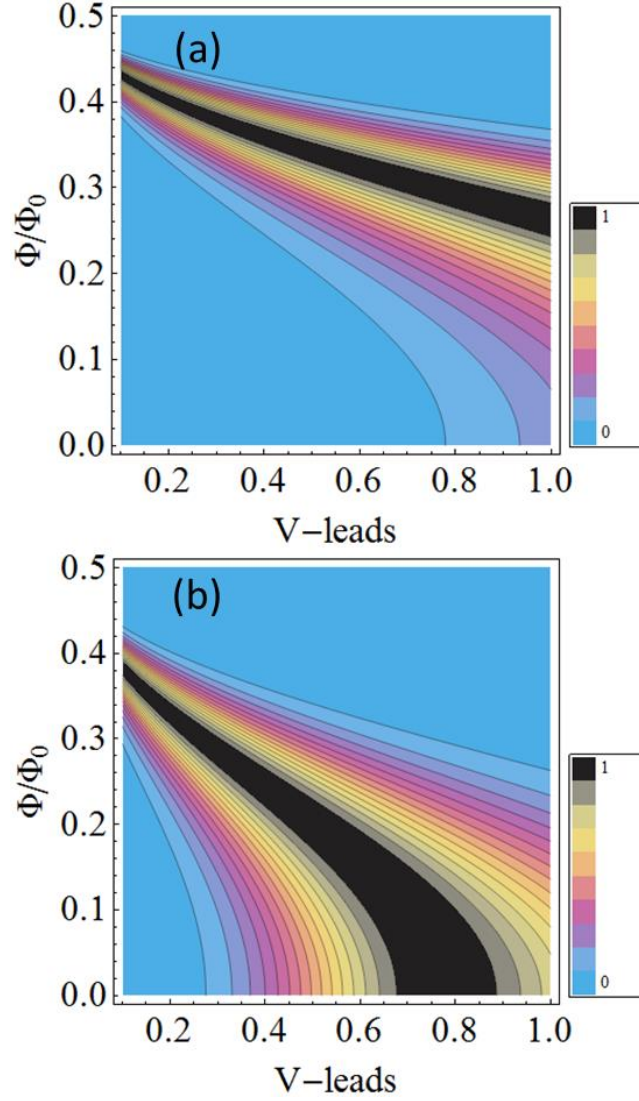


Figure 4-16 Contour plots showing the transmission, $T(\epsilon_{QD})$, as a function of magnetic flux and the lead couplings. This is a 4 ring system, with all site energies set to 0 and hopping integrals at 0.3. The plots have different ring coupling values, of $V_m = 0.3$ (a) and $V_m = 0.6$ (b). Notice that the larger coupling causes a greater flux sensitivity.

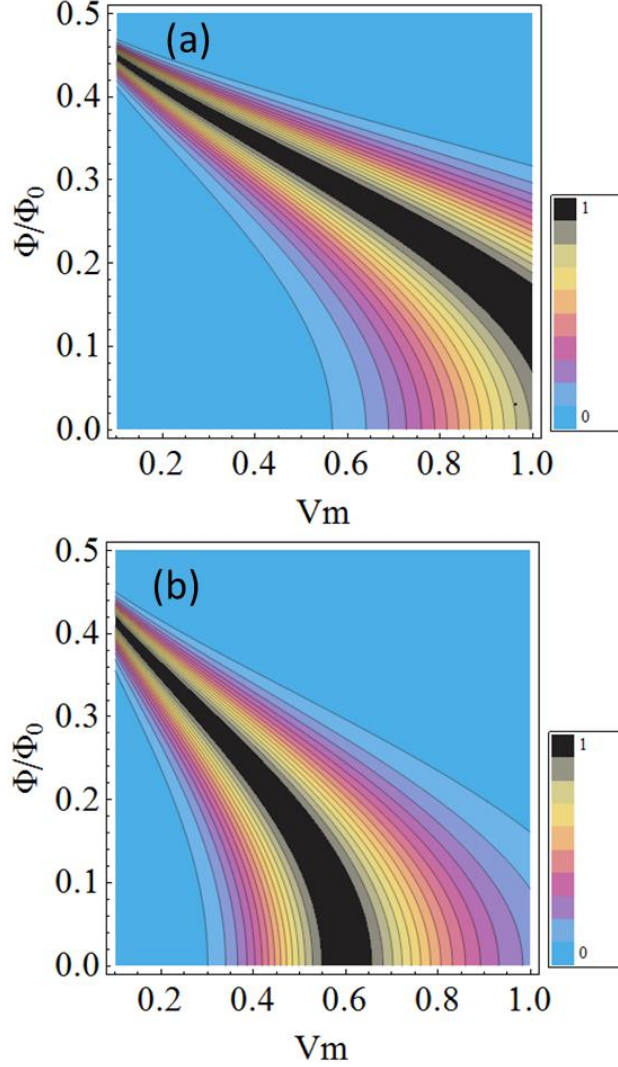


Figure 4-17 Contour plots showing the transmission, $T(\varepsilon_{QD})$, as a function of magnetic flux and the ring couplings. This is a 4 ring system, with all site energies set to 0 and hopping integrals at 0.3. The plots have different lead coupling values, of $V_{leads} = 0.3$ (a) and $V_{leads} = 0.775$ (b). Notice that the larger coupling causes a greater flux sensitivity.

Let us again observe the resonant transmission, at $\varepsilon_{QD} = 0$, where all the hopping integrals are set equal to V_0 , such that $V_{in} = V_m = V_{leads} = V_0 = 1$. In Figure 4-18 and Figure 4-19, we see plots where conditions are enforced, showing the resonant transmission as a function of flux and one of the coupling parameters V_m or V_{leads} . As shown previously, for higher coupling values, a lower magnetic flux is needed to achieve full resonant transmission

value. Here it can be seen that the resonant transmission peaks center around the half flux quantum value, diverging from it as the coupling parameter increases. As can be observed in both figures, when all hopping integrals are equal to $V_0 = 1$, resonant transmission peaks occur at exactly $\Phi/\Phi_0 = 1/3$ and $\Phi/\Phi_0 = 2/3$. If the plot ranges were extended, this effect would be seen to be periodic for each flux quantum.

In addition to this effect, it is also found that this periodic location of resonant transmission peaks does not change with the addition of more rings to the system. As can be seen in Figure 4-20, the full transmission peaks remain stationary at exactly $\Phi/\Phi_0 = 1/3$ and $\Phi/\Phi_0 = 2/3$. The resonant transmission for magnetic flux not equal to these arbitrary values decays exponentially with the addition of more rings, as can be seen by the sharpening of the peaks. This effect also holds for different coupling parameter values, revealing what can be referred to as an extended eigenstate of the system under the influence of a magnetic field [42] [44] [45]. This allows for totally ballistic transport of the electron, where it is completely unaffected by the size of the system and travels without reflection at the resonant energy. These results confirm those presented by Chakrabarti *et al* for similar systems [2].

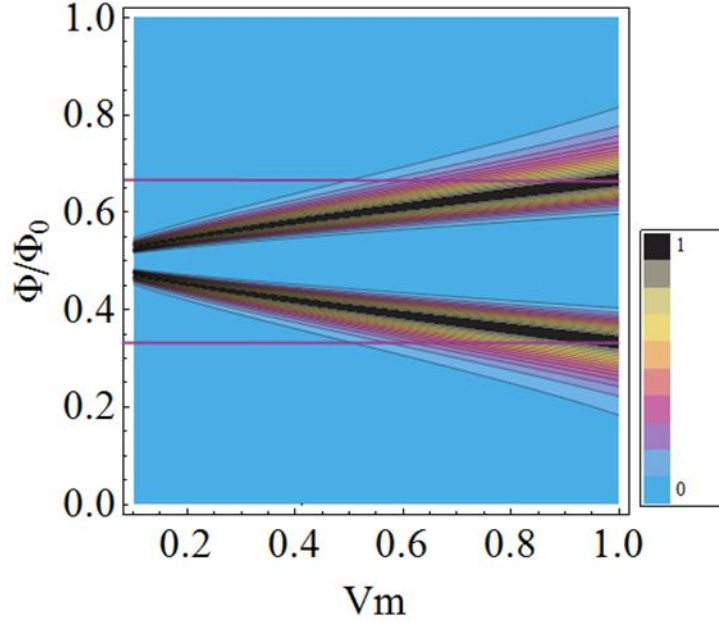


Figure 4-18 Resonant transmission, $T(0)$, as a function of flux and ring coupling parameter V_m . Notice the effect that changing the ring coupling strength has, and that, when $V_m = V_0 = 1$, the peaks are at flux values of $\Phi/\Phi_0 = 1/3$ and $\Phi/\Phi_0 = 2/3$ indicated by the purple lines. This is a 4 ring system, with all site energies set at 0 and hopping integrals $V_n = V_0 = 1$.

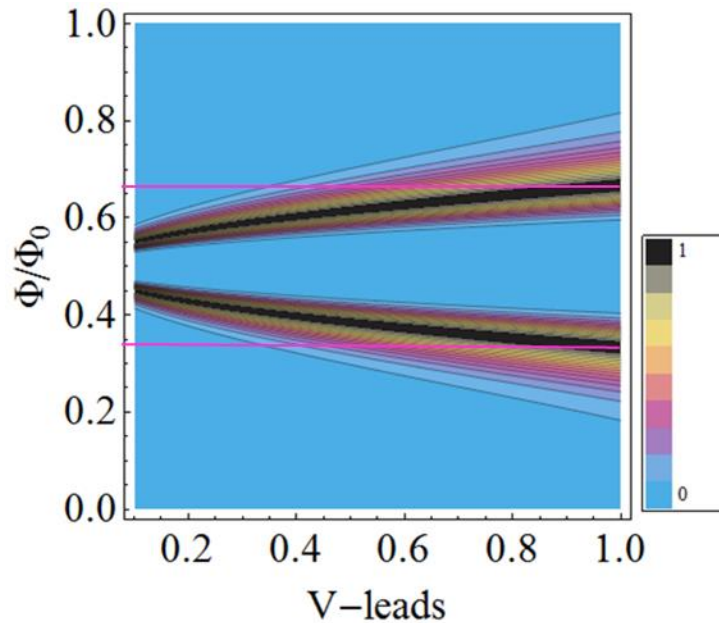


Figure 4-19 Resonant transmission, $T(0)$, as a function of flux and leads parameter V_{leads} . Notice the effect that changing the lead strength has, and that, when $V_{leads} = V_0 = 1$, the peaks are at flux values of $\Phi/\Phi_0 = 1/3$ and $\Phi/\Phi_0 = 2/3$, indicated by the purple lines. This is a 4 ring system, with all site energies set at 0 and hopping integrals $V_n = V_0 = 1$.

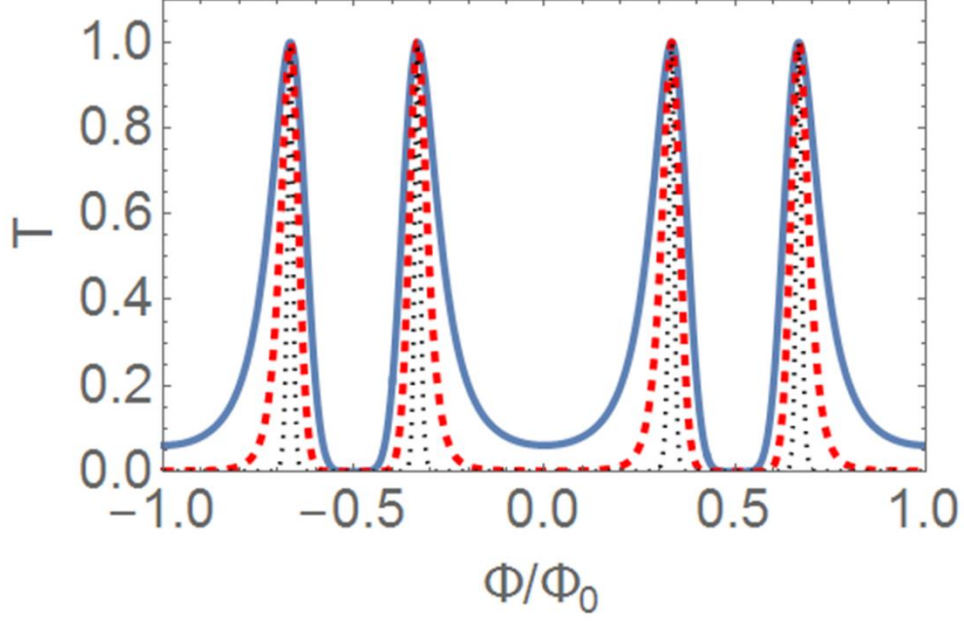


Figure 4-20 Transmission of resonant energy $T(0)$ as a function of magnetic flux for systems of 3 rings (Blue, Solid), 6 rings (Red, Dashed), and 20 rings (Black, Dotted). Site energies as set at 0, and all hopping integrals are set at $V_0 = 1$. Notice the transmission peaks are found at values of $\Phi/\Phi_0 = 1/3$ and $\Phi/\Phi_0 = 2/3$, and the locations of the peaks does not change with system size.

4.4 Zeeman Effect impact on bandgap

Let us now turn our attention to toward the Zeeman Effect and its impact upon the electron transmission through this system. As was shown in the earlier methods section, the Zeeman Effect spin-splits the electron's resonant energy levels by the energy difference $\pm\epsilon_Z$. It will be shown here how the Zeeman Effect can use an applied external magnetic field to alter the metallic nature of a material, as well as manipulate the conduction of spin states. As has been documented previously and in this thesis, the energy transmission spectrum of a nanoring with symmetric parameters contains an energy bandgap centered on the symmetric QD site energies. The width of this bandgap can be altered through manipulation of the ring coupling and inter-

ring coupling parameters. However, earlier, it was shown that the presence of magnetic flux in the system can also change the width of this bandgap, even causing it to completely merge into a transmission peak via the AB Effect. This could only be achieved through a perpendicular magnetic field, as it is the magnetic flux through the rings which brings about this effect. However, utilizing the Zeeman Effect, a similar behavior can be observed using a parallel magnetic field.

As can be seen in Figure 4-21, increasing the Zeeman Energy ϵ_Z causes the transmission bands to clearly separate in proportion to the increase in ϵ_Z . In this system with all site energies set at 0, all hopping integrals set at 0.3, and no magnetic flux present, the middle bandgap can be seen to drastically diminish with the increasing parallel magnetic field. From the ϵ_Z values of about 0.16 to 0.7, the bandgap completely disappears. Since the bands are being spin-split with increasing Zeeman Energy, with the spin up bands decreasing in energy and the spin down bands increasing in energy, this new middle transmission band becomes a mixed spin state band. This happens as a spin down and spin up band have merged into one as they cross paths in the energy spectrum. In Figure 4-22(a), we see a line plot showing this merged spin peak.

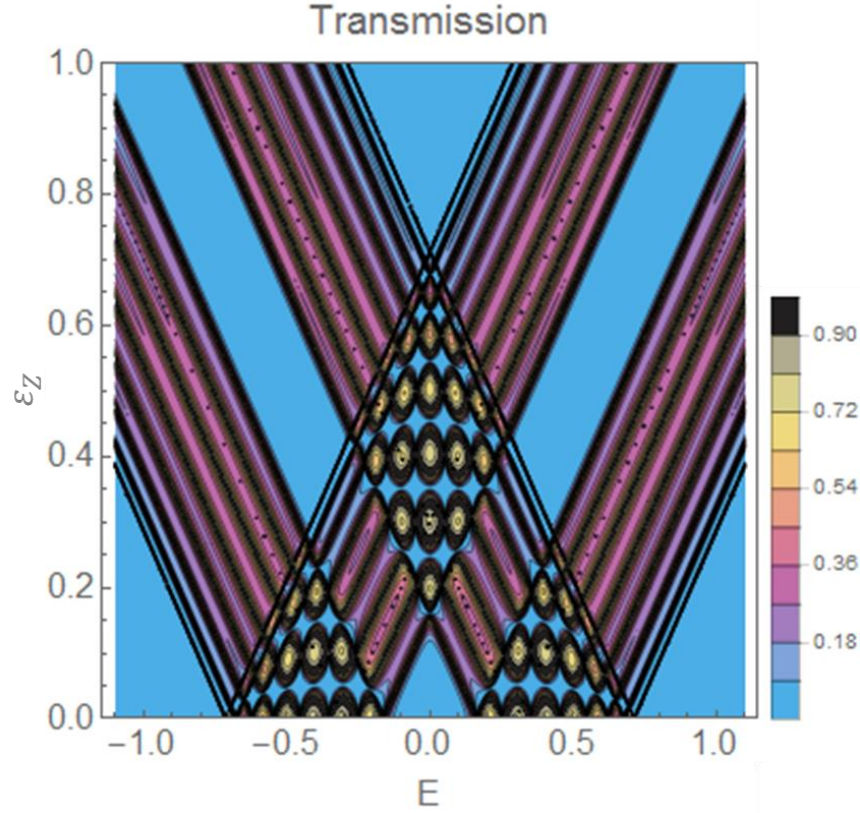


Figure 4-21 Contour plot of electron transmission as a function of energy and Zeeman Energy ε_z . This is for a 4 ring system with all QD site energies set at 0 and all hopping integrals set at 0.3. Notice the spin up and spin down bands merging and creating mixed spin state bands with the increase of the Zeeman Energy. Also notice the pure spin state bands diverging from center.

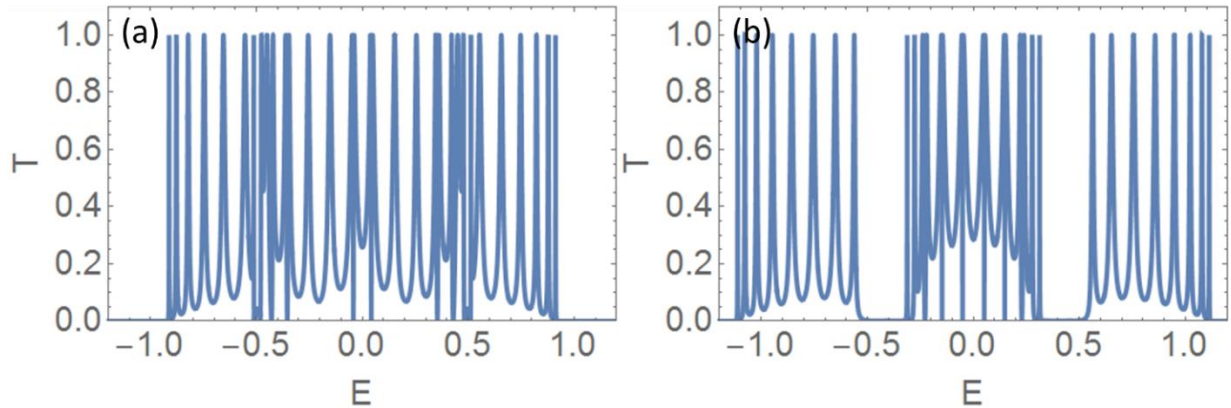


Figure 4-22 Transmission vs energy line plots for the system described in Figure 4-21. The Zeeman Energy is changed from $\varepsilon_z = 0.2$ (a) to $\varepsilon_z = 0.4$ (b). Notice in (a) there is no middle bandgap, while in (b), there are clear bandgaps, with band structures on either side.

Not only does the Zeeman splitting produced by the parallel magnetic field cause the middle bandgap to merge, but it also causes 2 spin-polarized band structures to separate energetically. Able to be seen in Figure 4-21 and Figure 4-22(b), above a Zeeman Energy of about 0.3, the bands become separated by bandgaps. These peaks are spin-polarized, based on the material. For a GaAs heterostructures with a negative g-factor, the spin up band has the lower energy, while the spin down band has the higher energy. However, for graphene, which has a positive g-factor, this is reversed. In graphene, the spin up band has the higher energy, while the spin down band has the lower. This means that there are now transmission bands which are completely spin-polarized, and have ohmic properties.

The spin-splitting described by the Zeeman Effect influences the conducting nature of the material. As mentioned above, the middle bandgap normally found in these system is completely eliminated with a Zeeman Energy of $\varepsilon_Z = 0.2$. This means that the semi-conducting nature of the system has been effectively changed to be completely ohmic. In Figure 4-23, we see that this is the case, as the IV relationship is basically linear over the allowed energy spectrum. Here, the Fermi Energy is set at 0, which in this application sets the center of integration, or where our zero voltage point is. If one considers also the case of Figure 4-22(b), where the Zeeman Energy is set at $\varepsilon_Z = 0.4$, the conducting nature has been changed again. Bandgaps have again formed, indicating the possibility of semi-conducting. However, the outer bands are completely spin-polarized, meaning a single spin state is ohmic over a certain voltage band. This is seen in Figure 4-24. Although mixed with ohmic and semi-conducting regions, the ohmic portions centered around $\pm 1.5 V$ correspond to the spin-polarized transmission bands which separated from the merged states due to the Zeeman splitting. Therefore, it is shown that the Zeeman Effect can

effectively alter the conducting nature of a material, such as graphene, changing it from a semiconductor to metallic, as well as polarizing entire transmission bands in separate electron spins.

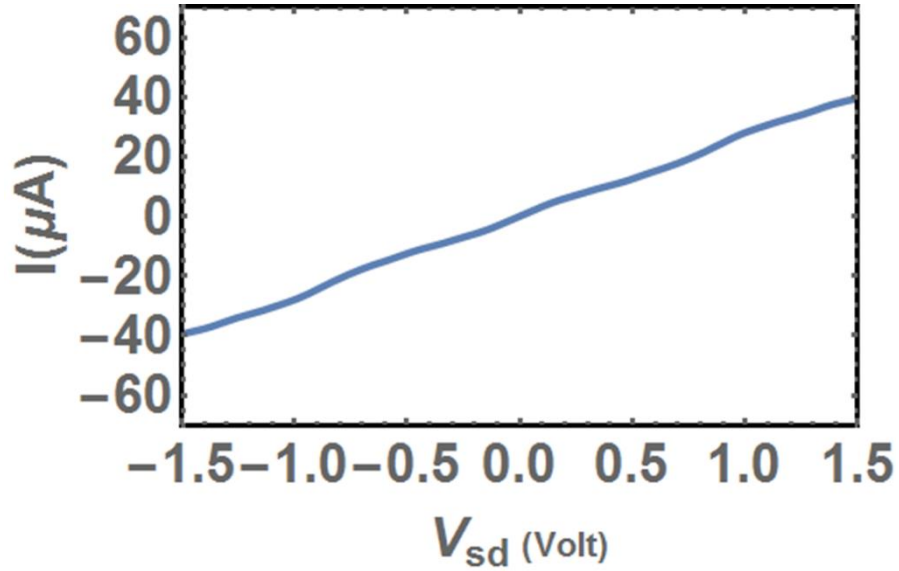


Figure 4-23 IV plot of the system of Figure 4-21 with a Zeeman Energy of $\varepsilon_Z = 0.2$ and Fermi Energy set at 0. The system is completely ohmic, but with portions that are spin-polarized, such as the outer edges, and portions that are mixed, such as the center.

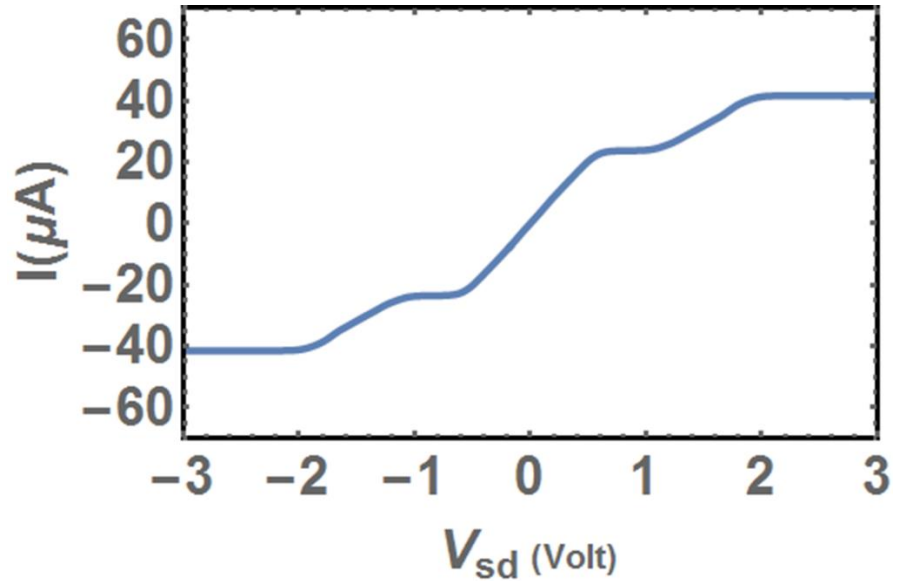


Figure 4-24 IV plot of the system of Figure 4-21 with the Zeeman Energy set to $\varepsilon_Z = 0.4$ and Fermi Energy set at 0. Notice the ohmic and conducting regions, especially the spin-polarized ohmic regions centered around ± 1.5 V.

5. CONCLUSION

In this thesis the electron transport properties of a chain of serially connected, hexagonal nanorings were explored. This transmission has been investigated with and without the presence of a magnetic field and magnetic flux. Using the Tight-Binding Approximation, a system of equations for each system has been created and solved with aid of the software Mathematica. Taking a new computational approach, we did not create one large matrix to solve. Instead, we solved the system iteratively, and achieved much more optimized results. When analyzing nanoring chains with an applied external magnetic field, the Aharonov-Bohm Effect and Zeeman Effect were included. The Aharonov-Bohm Effect added a phase shift to the electrons, while the Zeeman Effect spin-split the electron resonant energy levels.

In a non-magnetic system, these results have shown several important effects of varying different system parameters of a chain of serially connected nanorings. When all other hopping integrals are equal, it was found that increasing the inter-ring coupling parameter (allowing the electron to transmit more freely between rings) causes the energy transmission bandgap to decrease, to the point of disappearing. This eliminates the semiconducting nature of the system. The effects arising from altering the coupling to the leads were also investigated, showing that the number of peaks per band structure could be decreased or increased by allowing the lead hopping integrals to be above or below the symmetric value of the rest of the system. The number of rings connected serially was shown to affect the number of peaks per band. For each

ring added, the number of peaks increased according to the number of QDs per arm of each nanoring.

For specific system parameter values, the transmission at the site energy values, $T(\epsilon_{QD})$, shows a gaussian and exponential decaying trend. A critical value is found for the optimal number of rings, and this value shows dependence on the inter-ring coupling, V_m . By tuning the leads to the particular value of $V_{leads} = 0.775$, a combination of interference and resonance effects can be used to produce a broad range of transparency, where the system shows full transmission over a range of values, rather than a narrow peak. Finally, when the inter-ring coupling, $V_m = 2V_{in}$, $T(\epsilon_{QD})$ will be fixed at a single value, regardless of the number of rings in series. The specific value of $T(\epsilon_{QD})$ can be modulated up to full transmission by increasing the system-leads coupling to the critical value of $V_{leads} = 0.775$.

When a magnetic field was introduced to the system, the AB and Zeeman Effects were used to observe the transmission properties. Small amounts of magnetic flux through the rings were shown to produce sharpened AB oscillations, an effect demonstrated in smaller systems. These oscillations were found to introduce small bandgaps located at certain hopping integral values, bounded by peaks. The amount of peaks was found to directly correspond to the number of rings connected in series. The coupling parameter between rings, V_m , was shown to affect the width of the added energy bandgap, being directly proportional for certain sets of values. The position of these sensitive magnetic flux effects was found to be directly equal to the inter-ring coupling value V_{in} , the hopping integral governing electron transition between sites with each ring, while the lead values directly determined whether these effects were found at transmission peaks or valleys.

Through investigation of these sensitive flux responses, other effects of magnetic flux were investigated. It was shown that as magnetic flux is increased through the system, the small energy bandgaps introduced in the AB oscillations increased in width, becoming large bandgaps which compare in size to the middle bandgap typically found in these nanoring systems. This middle bandgap was also found to decrease in width with the addition of magnetic flux. It eventually decreases to the point where it merges and becomes a transmission peak. With the increasing magnetic flux, the system was found to coalesce into sets of transmission peaks, or transmission bands. The number of bands was found to be constant, being dependent on the number of sites per ring, while the number of peaks per band increased with the number of rings in series. It was also found that increasing the magnetic flux through the system decreased the coupling parameter strength needed to achieve maximum resonant transmission, $T(\varepsilon_{QD})$. This applies to the ring coupling and lead coupling parameters V_m and V_{leads} . As these two parameters were increased, it was shown to amplify the system's response to the magnetic flux. This increased the system's sensitivity to the presence of magnetic flux. If all hopping integrals were set to $V_0 = 1$, the resonant transmission $T(\varepsilon_{QD})$ was found to be at maximum for flux values of $\Phi/\Phi_0 = 1/3$ and $\Phi/\Phi_0 = 2/3$. The location of these maxima were shown to be independent of the system size, remaining stationary for an increasing value of ring number. This allowed the electron to achieve totally ballistic transport through the system.

The Zeeman Effect was also investigated, and found to have a profound impact on the metallic nature of the material, as well spin polarization effects. Normally, in these symmetric nanoring systems, there is a middle energy bandgap where there is no transmission. However, increasing the parallel magnetic field, which increased the Zeeman Energy ε_z , showed the width of the bandgap decreasing until it merged in a mixed spin state transmission band. This changed

the material from a semiconductor to a metal, where it exhibited ohmic properties. As the Zeeman Energy was increased, and the spin-splitting increased, spin-polarized peaks energetically separated by bandgaps appeared at the higher and lower energies of the system. These are transmission bands where electrons which are completely spin-polarized exhibit ohmic properties.

These results only analyze and discuss a very small amount of the intricacies of these systems. Much more work is needed to fully understand the electron transport properties and the effect that magnetic fields have on these. Much of this work is needed in order to further the field of spintronics. Many of these results have been, or are able to be, generalized to apply to graphene. Although many of the flux values required in this paper are impractical to use with graphene, the sensitive flux effects all scale to values of flux that are reasonable, given the size of graphene. This is a topic of much research in modern day physics, and the electron transport properties of this material have been shown to be of much practical use. Future work would include, along with the analysis of more results, a 2-dimensional generalization of the current system. While the system described and observed in this thesis is a 1-dimensional chain of hexagonal nanorings, work is currently being done to extend this hexagonal unit structure into 2 dimensions. This would effectively and directly model graphene, even allowing the analysis of carbon nanotubes.

6. REFERENCES

- [1] G. Cohen, O. Hod and E. Rabani, "Resonant transport properties of tight-binding mesoscopic rings," *Phys Rev. B*, vol. 76, pp. 235-120, 2007.
- [2] A. Chakrabarti, R. Römer and M. Schreiber, "Magnetotransport in periodic and quasiperiodic arrays of mesoscopic rings," *Phys. Rev. B*, vol. 68, p. 195417, 2003.
- [3] J. Chen, A. Chang and M. Melloch, *Phys. Rev. Lett.*, vol. 92, p. 176801, 2004.
- [4] J. Zhou, M. Wu and M. Weng, *Phys. Lett. A*, vol. 349, p. 393, 2006.
- [5] J. Xia and S. Li, *Phys. Rev. B*, vol. 66, p. 035311, 2002.
- [6] P. Cedraschi and M. Büttiker, *Phys. Rev. B*, vol. 63, p. 165312, 2001.
- [7] S. Maiti, *Physica E*, vol. 36, p. 199, 2007.
- [8] S. Wolf, D. Awschalom, R. Buhrman, J. Daughton, S. v. Molnar, M. Roukes, A. Chtchelkanova and D. Treger, *Science*, vol. 294, p. 1488, 2001.
- [9] W. Rabaud, L. Saminadayar, D. Mailly, K. Hasselbach, A. Benoît and B. Etienne, "Persistent currents in mesoscopic connected rings," *Phys. Rev. Lett.*, vol. 86, p. 3124, 2001.
- [10] A. Holleitner, C. Decker, H. Qin, K. Eberl and R. Blick, *Phys. Rev. Lett.*, vol. 87, p. 256802, 2001.
- [11] J. Li, Z. Zhang and Y. Liu, "Resonant transport properties of tight-binding mesoscopic rings," *Phys. Rev. B*, vol. 55, p. 5337, 1997.
- [12] J. Folk, R. Potok, C. Marcus and V. Umansky, *Science*, vol. 299, p. 679, 2003.
- [13] R. Hanson, L. Vandersypen, L. W. v. Beveren, J. Elzerman, I. Vink and L. Kouwenhoven, *Phys. Rev. B*, vol. 70, p. 241304(R), 2004.
- [14] P. Dutta, S. K. Maiti and S. Karmakar, "Quantum transport in an array of mesoscopic rings: Effect of interface geometry," *Solid State Communications*, vol. 150, pp. 1056-1061, 2010.
- [15] Y. Liu and P. M. Hui, "Electronic-transport properties of tight-binding multiring systems," *Phys. Rev. B*, vol. 57, p. 12994, 1998.
- [16] W. Cui, S. Wu, G. Jin, X. Zhao and Y. Ma, "Analytic study of electron transmission through serial mesoscopic metallic rings," *Eur. Phys. J. B*, vol. 59, p. 47–54, 2007.

- [17] E. R. Hedin, A. C. Perkins and Y. S. Joe, "Combined Aharonov–Bohm and Zeeman spin-polarization effects in a double quantum dot ring," *Physics Letters A*, vol. 375, p. 651–656, 2011.
- [18] E. R. Hedin and Y. S. Joe, "Spin-polarized Transmission through Single and Double Aharonov-Bohm Rings with Embedded Quantum Dots," Chapter 4 of a review volume entitled "Spintronics in Nanoscale Devices," 2013.
- [19] E. R. Hedin and Y. S. Joe, "Spin-polarized current from multiply-coupled rings with Zeeman-split quantum dots," *Journal of Applied Physics*, vol. 115, p. 113701, 2014.
- [20] E. R. Hedin and Y. S. Joe, "Serially-connected Aharonov-Bohm rings with embedded quantum dots," in *17th International Workshop on Computational Electronics (IWCE)*, 2014.
- [21] S. Datta, *Quantum Transport: Atom to Transistor*, New York: Cambridge University Press, 2005.
- [22] J. B. Cutright, "Analysis of Electron Transport through Novel Nanoelectronic and Spintronic Devices," Master's thesis, Ball State University, 2012.
- [23] N. Rognerud, "Free Fall of Elementary particles: On moving bodies and their electromagnetic forces," 1994.
- [24] Y. Aharonov and D. Bohm, *Phys. Rev.*, vol. 115, p. 485, 1963.
- [25] Abigail C. Perkins, E. R. Hedin, and Y. S. Joe, "Electron Spin-Polarization via nano-Electronics Circuits: Spintronics Applications of Zeeman and Aharonov-Bohm Effects on Electron Transport in a Double Quantum Dot Ring," (Lambert Academic Publishing, Saarbrücken, Germany, 2011).
- [26] J. Davies, *The Physics of Low-Dimensional Semiconductors*, Cambridge University Press, 2005.
- [27] R. G. Chambers, *Phys. Rev. Lett.*, vol. 5, p. 3, 1960.
- [28] M. Büttiker, *Phys. Rev. Lett.*, vol. 57, p. 1761, 1986.
- [29] D. R. Cooper, B. D’Anjou, N. Ghattamaneni, B. Harack, M. Hilke, A. Horth, N. Majlis, M. Massicotte, L. Vandsburger, E. Whiteway and V. Yu, "Experimental Review of Graphene," *ISRN Condensed Matter Physics*, vol. 2012, p. 1–56, 2012.
- [30] R. A. Serway, C. J. Moses and C. A. Moyer, *Modern Physics*, 3rd Ed, Thomson Bookstore, 2005.

- [31] D. Griffiths, Introduction to Quantum Mechanics (2nd edition), Pearson: Prentice Hall, 2005.
- [32] W. Gerlach and O. Stern, "Das magnetische Moment des Silberatoms," *Zeitschrift für Physik*, vol. 9, p. 353–355, 1922.
- [33] P. Tipler and R. Llewellyn, Modern Physics, New York: W.H. Freeman, 2003.
- [34] M. Valin-Rodriguez, A. Puente and L. Serra, *Eur. Phys. J. B*, vol. 39, p. 87 , 2004.
- [35] C. Kittel, Introduction to Solid State Physics: 8th Edition, John Wiley and Sons, Inc., 2005.
- [36] P. Recher, E. V. Sukhorukov and D. Loss, *Phys. Rev. Lett.* , vol. 85, p. 1962 , 2000.
- [37] S. Ihnatsenka and I. V. Zozoulenko, "Spin polarization and g-factor enhancement in graphene nanoribbons in magnetic field," *Solid State Electronics*, vol. 601, p. 74, 2012.
- [38] C. Roh, "Electron Transport through Double Quantum Dots in an Aharonov-Bohm Ring," 2008.
- [39] J. C. Slater and G. F. Koster, *Phys. Rev.* , vol. 94, p. 1498 , 1954.
- [40] D. A. Bahamon and V. M. Pereira, "Conductance across strain junctions in graphene nanoribbons," *Phys Rev. B*, vol. 88, p. 195416 , 2013.
- [41] S. Malakooti, E. R. Hedin and Y. S. Joe, "Tight-binding approach to strain-dependent DNA electronics," *Jnl. of Appl. Physics*, vol. 114, p. 014701 , 2013.
- [42] P. S. Deo and A. M. Jayannavar, "Quantum waveguide transport in serial stub and loop structures," *Phys. Rev. B*, vol. 50, p. 11629 , 1994.
- [43] E. R. Hedin, Y. S. Joe and A. M. Satanin, "Sharpened Aharonov-Bohm oscillations near resonance in a balanced ring with double quantum dots," *J Comput Electron*, vol. 10825, p. 201, 2008.
- [44] A. Aldea, P. Gartner and I. Corcotoi, *Phys. Rev. B*, vol. 45, p. 14122, 1992.
- [45] A. M. Jayannavar and P. S. Deo, *Phys. Rev. B*, vol. 51, p. 10175, 1995.

2 Quantum dots per arm - lead in between

No AB and no Zeeman

Matt Orvis

· This program uses the Tight-Binding approximation to model electron transmission through a linearly connected chain of nanorings. Each of these rings contains 2 branches, with 2 quantum dots in each branch, a quantum dot at the splitting of those two branches, and a quantum dot at the rejoining of them. This give a total of 6 quantum dots per ring. Each ring is connected by a lead, and there are leads entering and exiting the system.

·There are no magnetic effects included in this program.

Section 1 shows the full matrix for a system of 4 rings with the quantum dots at the entrance and exit of the system set at 0, and the hopping integrals next to them at 1.

Section 2 shows the full matrix for a system of 4 rings with the quantum dots at the entrance and exit of the system nonzero, and the hopping integrals inside of them nonzero.

• Section 3 shows the manual breaking of the full matrix into 4 smaller matrices, each corresponding to 1 nanoring.

·Section 4 shows the smaller matrices put into a loop which will allow the iterating of the inner ring to an arbitrary length.

2. 4 rings - manual with outer dots and outer V non-zero

```
Clear["Global`*"]      (*Clears all variables so that not affected by
previous evaluations*)
```

$$\theta[EE_]:=ArcCos[-EE/2]; \quad (*Dispersion\ relationship*)$$

```
(*Compute entire matrix hand*)
```

$$S[EE_ , V1_ , VL_ , VR_ , VB_ , \epsilon L_ , \epsilon TL_ , \epsilon TR_ , \epsilon BL_ , \epsilon BR_ , \epsilon R_] :=$$
[illegible]


```

PlotRange->{{lb,rb},{0.,1.1}},PlotStyle->{AbsoluteThickness[2.8]},
FrameLabel-> {"E","R"},
BaseStyle->{"Times",20}]
Plot[{Abs[t1[EE,.3,.3,.3,.3,.5,.5,.5,.5,.5,.5]]^2+Abs[r[EE,.3,.3,.3,.3,.5,.5,.5,.5,.5,.5]]^2},{EE,lb,rb},Axes->False,Frame->True,
PlotRange->{{lb,rb},{0.,1.1}},PlotStyle->{AbsoluteThickness[2.8]},
FrameLabel-> {"E","R + T"},
BaseStyle->{"Times",20}]
(*Create plots of transmission as a function of energy to manipulate
and look for results*)
Manipulate[Plot[{Abs[t1[EE,V1,VL,VR,VB,εL,εTL,εTR,εBL,εBR,εR]]^2},{EE,lb,rb},Axes->False,Frame->True,
PlotRange->{{lb,rb},{0.,1.1}},PlotStyle->{AbsoluteThickness[2.8]},
FrameLabel-> {"E","T"},
BaseStyle->{"Times",20},PlotLabel->"Transmission vs
Energy"],{{V1,.3},0,1},{VL,.3},0,1},{VR,.3},0,1},{VB,.3},0,1},{εL,.5},0,3},{εTL,.5},0,3},{εTR,.5},0,3},{εBL,.5},0,3},{εBR,.5},0,3},{εR,.5},0,3]]

```

3.4 rings - manual matrices w/indices

```

Clear["Global`*"]      (*Clears all variables so that not affected by
previous evaluations*)
θ[EE_]:=ArcCos[-EE/2];  (*Dispersion relationship*)
(*Break larger matrix up into 4 smaller matrices, each corresponding
to 1 nanoring. Each ring besides the first has functions in it which
call terms from the previous matrix, allowing information to be passed
from ring to ring. Columns have been rearranged in order to all row
reducing to be effective*)
A[0]=RowReduce[({
{-VL, 0, 0, 0, 0, 0, Exp[-I θ[EE]], 0, -Exp[I θ[EE]]},
{εL-EE, -V1, 0, -V1, 0, 0, -VL, 0, VL},
{-V1, εTL-EE, -V1, 0, 0, 0, 0, 0, 0},
{0, -V1, εTR-EE, 0, 0, -V1, 0, 0, 0},
{-V1, 0, 0, εBL-EE, -V1, 0, 0, 0, 0},

```

```

      {0, 0, 0, -v1, εBR-EE, -v1, 0, 0, 0},
      {0, 0, -v1, 0, -v1, εR-EE, 0, -VB, 0}
    }]];
(*A[0]//Simplify//MatrixForm*)
A[1]=RowReduce[({
      {εL-EE+VB A[0][[6]][[8]], -v1, 0, -v1, 0, 0, 0, 0, VB
A[0][[6]][[9]]},
      {-v1, εTL-EE, -v1, 0, 0, 0, 0, 0, 0},
      {0, -v1, εTR-EE, 0, 0, -v1, 0, 0, 0},
      {-v1, 0, 0, εBL-EE, -v1, 0, 0, 0, 0},
      {0, 0, 0, -v1, εBR-EE, -v1, 0, 0, 0},
      {0, 0, -v1, 0, -v1, εR-EE, 0, -VB, 0}
    }]);
A[1]//Simplify//MatrixForm
A[2]=RowReduce[({
      {εL-EE+VB A[1][[6]][[8]], -v1, 0, -v1, 0, 0, 0, 0, VB
A[1][[6]][[9]]},
      {-v1, εTL-EE, -v1, 0, 0, 0, 0, 0, 0},
      {0, -v1, εTR-EE, 0, 0, -v1, 0, 0, 0},
      {-v1, 0, 0, εBL-EE, -v1, 0, 0, 0, 0},
      {0, 0, 0, -v1, εBR-EE, -v1, 0, 0, 0},
      {0, 0, -v1, 0, -v1, εR-EE, 0, -VB, 0}
    }]);
(*A[2]//Simplify//MatrixForm*)
A[3]=RowReduce[({
      {εL-EE+VB A[2][[6]][[8]], -v1, 0, -v1, 0, 0, 0, 0, VB
A[2][[6]][[9]]},
      {-v1, εTL-EE, -v1, 0, 0, 0, 0, 0, 0},
      {0, -v1, εTR-EE, 0, 0, -v1, 0, 0, 0},
      {-v1, 0, 0, εBL-EE, -v1, 0, 0, 0, 0},

```

```

{0, 0, 0, -V1,  $\epsilon_{BR-EE}$ , -V1, 0, 0},
{0, 0, -V1, 0, -V1,  $\epsilon_{R-EE}$ , -VR Exp[I  $\theta_{EE}$ ], 0},
{0, 0, 0, 0, 0, -VR, 1, 0}
}]];

(*Transmission coefficient is final term of last matrix*)
t2[EE_,V1_,VL_,VR_,VB_, $\epsilon_L$ _, $\epsilon_{TL}$ _, $\epsilon_{TR}$ _, $\epsilon_{BL}$ _, $\epsilon_{BR}$ _, $\epsilon_R$ _]=A[3][[7]][[8]];

{lb=2,rb=-2}; (*Set bounds of plot*)

(*Plot transmission coefficient for same parameters as large matrix.
Calculating a reflection coefficient is far more difficult in this
method, so the only internal consistency check to use is to compare it
with the method done by hand*)
Plot[Abs[t2[EE,.3,.3,.3,.3,.5,.5,.5,.5,.5]]^2,{EE,lb,rb},Axes-
>False,Frame->True,
PlotRange->{{lb,rb},{0.,1.1}},PlotStyle->{AbsoluteThickness[2.8]},
FrameLabel-> {"E","T"},
BaseStyle->{"Times",20}]

(*Create plots of transmission as a function of energy to manipulate
and look for results*)
Manipulate[Plot[Abs[t2[EE,V1,VL,VR,VB, $\epsilon_L$ _, $\epsilon_{TL}$ _, $\epsilon_{TR}$ _, $\epsilon_{BL}$ _, $\epsilon_{BR}$ _, $\epsilon_R$ ]]^2,{EE,lb,
rb},Axes->False,Frame->True,
PlotRange->{{lb,rb},{0.,1.1}},PlotStyle->{AbsoluteThickness[2.8]},
FrameLabel-> {"E","T"},
BaseStyle->{"Times",20},PlotLabel->"Transmission vs
Energy"],{{V1,.3},0,1},{{VL,.3},0,1},{{VR,.3},0,1},{{VB,.3},0,1},{{ $\epsilon_L$ ,
.5},0,3},{{ $\epsilon_{TL}$ ,.5},0,3},{{ $\epsilon_{TR}$ ,.5},0,3},{{ $\epsilon_{BL}$ ,.5},0,3},{{ $\epsilon_{BR}$ ,.5},0,3},{{ $\epsilon_R$ ,
.5},0,3}]

```

4. NN rings with matrices

```

Clear["Global`*"] (*Clears all variables so that not affected by
previous evaluations*)

(*Create module which calculates and returns the transmission
coefficient*)

tCalculator[EE_,V1_,VL_,VR_,VB_, $\epsilon_L$ _, $\epsilon_{TL}$ _, $\epsilon_{TR}$ _, $\epsilon_{BL}$ _, $\epsilon_{BR}$ _, $\epsilon_R$ _,NN_]:=Module
[{ $\theta$ ,A,t},

```

```

θ=ArcCos[-EE/2];(*Dispersion relationship*)
(*Initialize loop with manually inputting first matrix for as many
rings as you want*)
A[1]=RowReduce[({
  {-VL, 0, 0, 0, 0, 0, Exp[-I θ], 0, -Exp[I θ]},
  {εL-EE, -V1, 0, -V1, 0, 0, -VL, 0, VL},
  {-V1, εTL-EE, -V1, 0, 0, 0, 0, 0, 0},
  {0, -V1, εTR-EE, 0, 0, -V1, 0, 0, 0},
  {-V1, 0, 0, εBL-EE, -V1, 0, 0, 0, 0},
  {0, 0, 0, -V1, εBR-EE, -V1, 0, 0, 0},
  {0, 0, -V1, 0, -V1, εR-EE, 0, -VB, 0}
})];
(*Run a do loop that iterates the middle matrix *)
Do[
  A[i]=RowReduce[({
    {εL-EE+VB A[i-1][[6]][[8]], -V1, 0, -V1, 0, 0, 0, 0, VB A[i-
1][[6]][[9]]},
    {-V1, εTL-EE, -V1, 0, 0, 0, 0, 0, 0},
    {0, -V1, εTR-EE, 0, 0, -V1, 0, 0, 0},
    {-V1, 0, 0, εBL-EE, -V1, 0, 0, 0, 0},
    {0, 0, 0, -V1, εBR-EE, -V1, 0, 0, 0},
    {0, 0, -V1, 0, -V1, εR-EE, 0, -VB, 0}
  })];
  x=i;
  ,{i,2,NN-1}
];
(*Finish system by manually inputting final ring*)
A[x+1]=RowReduce[({
  {εL-EE+VB A[x][[6]][[8]], -V1, 0, -V1, 0, 0, 0, 0, VB
A[x][[6]][[9]]},
  {-V1, εTL-EE, -V1, 0, 0, 0, 0, 0, 0},

```

```

{0, -V1,  $\epsilon_{TR-EE}$ , 0, 0, -V1, 0, 0},
{-V1, 0, 0,  $\epsilon_{BL-EE}$ , -V1, 0, 0, 0},
{0, 0, 0, -V1,  $\epsilon_{BR-EE}$ , -V1, 0, 0},
{0, 0, -V1, 0, -V1,  $\epsilon_{R-EE}$ , -VR Exp[I  $\theta$ ], 0},
{0, 0, 0, 0, 0, -VR, 1, 0}
}]];
(*Transmission coefficient is last term of last matrix*)
t=A[x+1][[7]][[8]];
t]

{lb=2,rb=-2};(*Set bounds of plot*)
(*Plot transmission coefficient for same parameters as large matrix.
Calculating a reflection coefficient is far more difficult in this
method, so the only internal consistency check to use is to compare it
with the method done by hand*)
Plot[{Abs[tCalculator[EE,.3,.3,.3,.3,.5,.5,.5,.5,.5,.5,4]]^2,Abs[tCalcu
lator[EE,.3,.9,.3,.3,.5,.5,.5,.5,.5,.5,4]]^2},{EE,lb,rb},Axes-
>False,Frame->True,
PlotRange->{{-.3,1.3},{0.,1.1}},PlotStyle->{AbsoluteThickness[2.8]},
FrameLabel-> {"E","T"},PlotLabel->"Transmission vs Energy",
BaseStyle->{"Times",20}]
(*Create plots of transmission as a function of energy to manipulate
and look for results*)
Manipulate[Plot[{Abs[tCalculator[EE,V1,VL,VR,VB, $\epsilon_L$ , $\epsilon_{TL}$ , $\epsilon_{TR}$ , $\epsilon_{BL}$ , $\epsilon_{BR}$ , $\epsilon_R$ ,NN
]]^2},{EE,lb,rb},Axes->False,Frame->True,
PlotRange->{{-2,2},{0.,1.1}},PlotStyle->{AbsoluteThickness[2.8]},
FrameLabel-> {"E","T"},
BaseStyle-
>{"Times",20}],{{V1,.5},0,1},{VL,.5},0,1},{VR,.5},0,1},{VB,.5},0,1
,{ $\epsilon_L$ ,0.0},-2,2},{ $\epsilon_{TL}$ ,0.0},-2,2},{ $\epsilon_{TR}$ ,0.0},-2,2},{ $\epsilon_{BL}$ ,0.0},-
2,2},{ $\epsilon_{BR}$ ,0.0},-2,2},{ $\epsilon_R$ ,0.0},-2,2},{NN,4},3,20,1]]
Needs["PlotLegends`"]
ShowLegend[ContourPlot[{Abs[tCalculator[EE,.5,.5,.5,VR,.0,.0,.0,.0,.0,
.0,4]]^2},{EE,-1.5,1.5},{VR,0.0,1},Contours->10,PlotPoints-
>80,PlotRange->{0.,1},FrameTicks-
```

```
>{Automatic, Automatic, None, None}, FrameLabel->{"E", "V"}, ColorFunction->
>"CMYKColors", BaseStyle->{"Times", 16}], {ColorData["CMYKColors"][1-
#1]&, 10, " 1.0", " 0.0", LegendLabel->None, LegendShadow-
>None, LegendPosition->{.97, -.705}}]
```

8. APPENDIX B

2 Quantum dots per arm - lead in between

With Zeeman and AB

Matt Orvis

·This program uses the Tight-Binding approximation to model electron transmission through a linearly connected chain of nanorings. Each of these rings contains 2 branches, with 2 quantum dots in each branch, a quantum dot at the splitting of those two branches, and a quantum dot at the rejoining of them. This give a total of 6 quantum dots per ring. Each ring is connected by a lead, and there are leads entering and exiting the system.

- This models magnetic effects, the Aharonov-Bohm Effect and Zeeman Effect

Section 1 shows the full matrix for a system of 3 rings with leads into the system and leads between rings.

Section 2 shows the smaller matrices put into a loop which will allow the iterating of the inner ring to an arbitrary length.

1. 3 rings - manual with outer dots and outer V non-zero - with Zeeman and AB

```
Clear["Global`*"] (*Clears all variables so that not affected by
previous evaluations*)
```

$$\theta[EE_]:=ArcCos[-EE/2]; \quad (*Dispersion\ relationship*)$$
$$\varphi[\Psi_-] := 2\pi \Psi_- / 1; (*\phi_0 = 1*) \quad (*\text{Variable which changes AB Effect, in the exponential terms of the matrix}*)$$
$$S[EE_,\Psi_,\text{Vin}_,\text{Vout}_,\text{VB}_,\text{V}_,\epsilon\text{L}_,\epsilon\text{TL}_,\epsilon\text{TR}_,\epsilon\text{BL}_,\epsilon\text{BR}_,\epsilon\text{R}_,\epsilon\text{Z}_] :=$$
[illegible]

$\{-V \exp[I \varphi[\Psi]/6], 0, \epsilon_{TL}-\epsilon_Z-EE, 0, -V \exp[-I \varphi[\Psi]/6], 0\},$

$\{0, -V \exp[I \varphi[\Psi]/6], 0, \epsilon_{TL}+\epsilon_Z-EE, 0, -V \exp[-I \varphi[\Psi]/6], 0\},$

$\{0, 0, -V \exp[I \varphi[\Psi]/6], 0, \epsilon_{TR}-\epsilon_Z-EE, 0, 0, 0, 0, 0, -V \exp[-I \varphi[\Psi]/6], 0\},$

$\{0, 0, 0, -V \exp[I \varphi[\Psi]/6], 0, \epsilon_{TR}+\epsilon_Z-EE, 0, 0, 0, 0, 0, -V \exp[-I \varphi[\Psi]/6], 0\},$

$\{-V \exp[-I \varphi[\Psi]/6], 0, 0, 0, 0, 0, \epsilon_{BL}-\epsilon_Z-EE, 0, -V \exp[I \varphi[\Psi]/6], 0\},$

$\{0, -V \exp[-I \varphi[\Psi]/6], 0, 0, 0, 0, 0, \epsilon_{BL}+\epsilon_Z-EE, 0, -V \exp[I \varphi[\Psi]/6], 0\},$

$\{0, 0, 0, 0, 0, 0, -V \exp[-I \varphi[\Psi]/6], 0, \epsilon_{BR}-\epsilon_Z-EE, 0, -V \exp[I \varphi[\Psi]/6], 0\},$

$\{0, 0, 0, 0, 0, 0, 0, -V \exp[-I \varphi[\Psi]/6], 0, \epsilon_{BR}+\epsilon_Z-EE, 0, -V \exp[I \varphi[\Psi]/6], 0\},$

$\{0, 0, 0, 0, -V \exp[I \varphi[\Psi]/6], 0, 0, 0, -V \exp[-I \varphi[\Psi]/6], 0, \epsilon_R-\epsilon_Z-EE, 0, -VB, 0\},$

$\{0, 0, 0, 0, 0, -V \exp[I \varphi[\Psi]/6], 0, 0, 0, -V \exp[-I \varphi[\Psi]/6], 0, \epsilon_R+\epsilon_Z-EE, 0, -VB, 0\},$

$\{0, 0, 0, 0, 0, 0, 0, 0, 0, 0, 0, -VB, 0, \epsilon_L-\epsilon_Z-EE, 0, -V \exp[-I \varphi[\Psi]/6], 0, 0, 0, -V \exp[I \varphi[\Psi]/6], 0, 0, 0, 0, 0, 0, 0, 0, 0, 0, 0, 0, 0, 0, 0, 0\},$

$\{0, 0, 0, 0, 0, 0, 0, 0, 0, 0, 0, -VB, 0, \epsilon_L+\epsilon_Z-EE, 0, -V \exp[-I \varphi[\Psi]/6], 0, 0, 0, -V \exp[I \varphi[\Psi]/6], 0, 0, 0, 0, 0, 0, 0, 0, 0, 0, 0, 0, 0, 0, 0, 0\},$


```

(*Pull out final transmission term*)
t[EE_,Ψ_,Vin_,Vout_,VB_,V_,εL_,εTL_,εTR_,εBL_,εBR_,εR_,εZ_] := Part[v[EE,Ψ,
,Vin,Vout,VB,V,εL,εTL,εTR,εBL,εBR,εR,εZ],38][[1]]//Simplify;

(*Pull out initial reflection term*)
r[EE_,Ψ_,Vin_,Vout_,VB_,V_,εL_,εTL_,εTR_,εBL_,εBR_,εR_,εZ_] := Part[v[EE,Ψ,
,Vin,Vout,VB,V,εL,εTL,εTR,εBL,εBR,εR,εZ],37][[1]]//Simplify;

{l b=-2,rb=2}; (*Set bounds of plot*)

(*Plot transmission and reflection coefficients. Then sum them to
check internal consistency. They should always add to 1*)
Plot[{Abs[t[EE,.25,.3,.3,.3,.3,.5,.5,.5,.5,.5,.5,.2]]^2},{EE,l b,rb},Axe
s->False,Frame->True,
  PlotRange->{{l b,rb},{0.,1.1}},PlotStyle->{AbsoluteThickness[2.8]},
  FrameLabel-> {"E","T"},
  BaseStyle->{"Times",20}]
Plot[{Abs[r[EE,.25,.3,.3,.3,.3,.5,.5,.5,.5,.5,.5,.2]]^2},{EE,l b,rb},Axe
s->False,Frame->True,
  PlotRange->{{l b,rb},{0.,1.1}},PlotStyle->{AbsoluteThickness[2.8]},
  FrameLabel-> {"E","R"},
  BaseStyle->{"Times",20}]
Plot[{Abs[t[EE,.25,.3,.3,.3,.3,.5,.5,.5,.5,.5,.5,.2]]^2+Abs[r[EE,.25,.3
,.3,.3,.3,.5,.5,.5,.5,.5,.5,.2]]^2},{EE,l b,rb},Axes->False,Frame->True,
  PlotRange->{{l b,rb},{0.,1.1}},PlotStyle->{AbsoluteThickness[2.8]},
  FrameLabel-> {"E","R + T"},
  BaseStyle->{"Times",20}]

(*Create a plot of transmission as a function of energy and flux to
manipulate and look for results*)
Manipulate[Plot[{Abs[t[EE,Ψ,Vin,Vout,VB,V,εL,εTL,εTR,εBL,εBR,εR,εZ]]^2},{
EE,l b,rb},Axes->False,Frame->True,
  PlotRange->{{l b,rb},{0.,1.1}},PlotStyle->{AbsoluteThickness[2.8]},
  FrameLabel-> {"E","T"},
  BaseStyle->{"Times",20},PlotLabel->"Transmission vs
Energy"],{{Ψ,.25},0,1},{{Vin,.3},0,1},{{Vout,.3},0,1},{{VB,.3},0,1},{{
V,.3},0,1},{{εL,.5},0,3},{{εTL,.5},0,3},{{εTR,.5},0,3},{{εBL,.5},0,3},{{
εBR,.5},0,3},{{εR,.5},0,3},{{εZ,.2},0,2}]

```

```

Manipulate[Plot[Abs[t[EE, $\Psi$ ,Vin,Vout,VB,V, $\epsilon$ L, $\epsilon$ TL, $\epsilon$ TR, $\epsilon$ BL, $\epsilon$ BR, $\epsilon$ R, $\epsilon$ Z]]2},{
 $\Psi$ ,0,1},Axes->False,Frame->True,
  PlotRange->{{0,1},{0.,1.1}},PlotStyle->{AbsoluteThickness[2.8]},
  FrameLabel-> {" $\Psi$ ","T"},
  BaseStyle->{"Times",20},PlotLabel->"Transmission vs Flux",{EE,-
.1},-
2,2},{Vin,.3},0,1},{Vout,.3},0,1},{VB,.3},0,1},{V,.3},0,1},{ $\epsilon$ L,.5
},0,3},{ $\epsilon$ TL,.5},0,3},{ $\epsilon$ TR,.5},0,3},{ $\epsilon$ BL,.5},0,3},{ $\epsilon$ BR,.5},0,3},{ $\epsilon$ R,
.5},0,3},{ $\epsilon$ Z,.2},0,2}]

```

2. NN rings with matrices

```

Clear["Global`*"] (*Clears all variables so that not affected by
previous evaluations*)

(*Create module which calculates and returns the transmission
coefficient*)

tCalculator[EE_, $\Psi$ _,Vin_,Vout_,VB_,V_, $\epsilon$ L_, $\epsilon$ TL_, $\epsilon$ TR_, $\epsilon$ BL_, $\epsilon$ BR_, $\epsilon$ R_, $\epsilon$ Z_,NN_
]:=Module[{ $\theta$ , $\phi$ ,A,t},
   $\theta$ =ArcCos[-EE/2]; (*Dispersion relationship*)
   $\phi$ =2 $\pi$   $\Psi$ /1; (*Variable which changes AB Effect, in the exponential
terms of the matrix*)
  (*Initialize loop with manually inputting first matrix for as many
rings as you want*)
  A[1]=RowReduce[({
    {-Vin, -Vin, 0, 0, 0, 0, 0, 0, 0, 0, 0, 0, 0, Exp[-I  $\theta$ ], 0, 0, -
Exp[I  $\theta$ ]},
    { $\epsilon$ L- $\epsilon$ Z-EE, 0, -V Exp[-I  $\phi$ /6], 0, 0, 0, -V Exp[I  $\phi$ /6], 0, 0, 0, 0,
0, -Vin, 0, 0, Vin},
    {0,  $\epsilon$ L+ $\epsilon$ Z-EE, 0, -V Exp[-I  $\phi$ /6], 0, 0, 0, -V Exp[I  $\phi$ /6], 0, 0, 0,
0, -Vin, 0, 0, Vin},
    {-V Exp[I  $\phi$ /6], 0,  $\epsilon$ TL- $\epsilon$ Z-EE, 0, -V Exp[-I  $\phi$ /6], 0, 0, 0, 0, 0,
0, 0, 0, 0, 0, 0},
    {0, -V Exp[I  $\phi$ /6], 0,  $\epsilon$ TL+ $\epsilon$ Z-EE, 0, -V Exp[-I  $\phi$ /6], 0, 0, 0, 0,
0, 0, 0, 0, 0, 0},
    {0, 0, -V Exp[I  $\phi$ /6], 0,  $\epsilon$ TR- $\epsilon$ Z-EE, 0, 0, 0, 0, 0, -V Exp[-I
 $\phi$ /6], 0, 0, 0, 0, 0},

```

```

    {0, 0, 0, -V Exp[I φ/6], 0, εTR+εZ-EE, 0, 0, 0, 0, 0, -V Exp[-I
φ/6], 0, 0, 0, 0},
    {-V Exp[-I φ/6], 0, 0, 0, 0, 0, εBL-εZ-EE, 0, -V Exp[I φ/6], 0,
0, 0, 0, 0, 0, 0},
    {0, -V Exp[-I φ/6], 0, 0, 0, 0, 0, εBL+εZ-EE, 0, -V Exp[I φ/6],
0, 0, 0, 0, 0, 0},
    {0, 0, 0, 0, 0, 0, -V Exp[-I φ/6], 0, εBR-εZ-EE, 0, -V Exp[I
φ/6], 0, 0, 0, 0, 0},
    {0, 0, 0, 0, 0, 0, 0, -V Exp[-I φ/6], 0, εBR+εZ-EE, 0, -V Exp[I
φ/6], 0, 0, 0, 0},
    {0, 0, 0, 0, -V Exp[I φ/6], 0, 0, 0, -V Exp[-I φ/6], 0, εR-εZ-EE,
0, 0, -VB, 0, 0},
    {0, 0, 0, 0, 0, -V Exp[I φ/6], 0, 0, 0, -V Exp[-I φ/6], 0, εR+εZ-
EE, 0, 0, -VB, 0}
  });

```

(*Run a do loop that iterates the middle matrix, calling terms from the previous matrix, passing information from ring to ring*)

```

Do[
  A[i]=RowReduce[({
    {εL-εZ-EE+VB A[i-1][[11]][[14]], VB A[i-1][[11]][[15]], -V Exp[-
I φ/6], 0, 0, 0, -V Exp[I φ/6], 0, 0, 0, 0, 0, 0, 0, VB A[i-
1][[11]][[16]]},
    {VB A[i-1][[12]][[14]], εL+εZ-EE+VB A[i-1][[12]][[15]], 0, -V
Exp[-I φ/6], 0, 0, 0, -V Exp[I φ/6], 0, 0, 0, 0, 0, 0, 0, VB A[i-
1][[12]][[16]]},
    {-V Exp[I φ/6], 0, εTL-εZ-EE, 0, -V Exp[-I φ/6], 0, 0, 0, 0, 0,
0, 0, 0, 0, 0},
    {0, -V Exp[I φ/6], 0, εTL+εZ-EE, 0, -V Exp[-I φ/6], 0, 0, 0, 0,
0, 0, 0, 0, 0},
    {0, 0, -V Exp[I φ/6], 0, εTR-εZ-EE, 0, 0, 0, 0, 0, -V Exp[-I
φ/6], 0, 0, 0, 0},
    {0, 0, 0, -V Exp[I φ/6], 0, εTR+εZ-EE, 0, 0, 0, 0, 0, -V Exp[-I
φ/6], 0, 0, 0},
    {-V Exp[-I φ/6], 0, 0, 0, 0, 0, εBL-εZ-EE, 0, -V Exp[I φ/6], 0,
0, 0, 0, 0, 0}
  ]);

```

{0, -V Exp[-I $\varphi/6$], 0, 0, 0, 0, 0, $\epsilon_{BL}+\epsilon_Z-EE$, 0, -V Exp[I $\varphi/6$],
0, 0, 0, 0, 0, 0},

{0, 0, 0, 0, 0, 0, -V Exp[-I $\varphi/6$], 0, $\epsilon_{BR}-\epsilon_Z-EE$, 0, -V Exp[I
 $\varphi/6$], 0, 0, 0, 0, 0},

{0, 0, 0, 0, 0, 0, 0, -V Exp[-I $\varphi/6$], 0, $\epsilon_{BR}+\epsilon_Z-EE$, 0, -V Exp[I
 $\varphi/6$], 0, 0, 0, 0},

{0, 0, 0, 0, -V Exp[I $\varphi/6$], 0, 0, 0, -V Exp[-I $\varphi/6$], 0, $\epsilon_R-\epsilon_Z-EE$, 0, 0, -VB, 0, 0},

{0, 0, 0, 0, 0, -V Exp[I $\varphi/6$], 0, 0, 0, -V Exp[-I $\varphi/6$], 0,
 $\epsilon_R+\epsilon_Z-EE$, 0, 0, -VB, 0}

}}];

x=i;

,{i,2,NN-1}

];

(*Finish system by manually inputting final ring*)

A[x+1]=RowReduce[({

{ $\epsilon_L-\epsilon_Z-EE+VB$ A[x][[11]][[14]], VB A[x][[11]][[15]], -V Exp[-I
 $\varphi/6$], 0, 0, 0, -V Exp[I $\varphi/6$], 0, 0, 0, 0, 0, 0, VB A[x][[11]][[16]]},

{VB A[x][[12]][[14]], $\epsilon_L+\epsilon_Z-EE+VB$ A[x][[12]][[15]], 0, -V Exp[-I
 $\varphi/6$], 0, 0, 0, -V Exp[I $\varphi/6$], 0, 0, 0, 0, 0, 0, VB A[x][[12]][[16]]},

{-V Exp[I $\varphi/6$], 0, $\epsilon_{TL}-\epsilon_Z-EE$, 0, -V Exp[-I $\varphi/6$], 0, 0, 0, 0, 0,
0, 0, 0, 0},

{0, -V Exp[I $\varphi/6$], 0, $\epsilon_{TL}+\epsilon_Z-EE$, 0, -V Exp[-I $\varphi/6$], 0, 0, 0, 0,
0, 0, 0, 0},

{0, 0, -V Exp[I $\varphi/6$], 0, $\epsilon_{TR}-\epsilon_Z-EE$, 0, 0, 0, 0, 0, -V Exp[-I
 $\varphi/6$], 0, 0, 0},

{0, 0, 0, -V Exp[I $\varphi/6$], 0, $\epsilon_{TR}+\epsilon_Z-EE$, 0, 0, 0, 0, 0, -V Exp[-I
 $\varphi/6$], 0, 0},

{-V Exp[-I $\varphi/6$], 0, 0, 0, 0, 0, $\epsilon_{BL}-\epsilon_Z-EE$, 0, -V Exp[I $\varphi/6$], 0,
0, 0, 0, 0},

{0, -V Exp[-I $\varphi/6$], 0, 0, 0, 0, 0, $\epsilon_{BL}+\epsilon_Z-EE$, 0, -V Exp[I $\varphi/6$],
0, 0, 0, 0},

{0, 0, 0, 0, 0, 0, -V Exp[-I $\varphi/6$], 0, $\epsilon_{BR}-\epsilon_Z-EE$, 0, -V Exp[I
 $\varphi/6$], 0, 0, 0},

```

{0, 0, 0, 0, 0, 0, 0, -V Exp[-I  $\varphi/6$ ], 0,  $\epsilon_{BR} + \epsilon_Z - \epsilon_{EE}$ , 0, -V Exp[I
 $\varphi/6$ ], 0, 0},

{0, 0, 0, 0, -V Exp[I  $\varphi/6$ ], 0, 0, 0, -V Exp[-I  $\varphi/6$ ], 0,  $\epsilon_R - \epsilon_Z - \epsilon_{EE}$ ,
0, -Vout Exp[I  $\theta$ ], 0},

{0, 0, 0, 0, 0, -V Exp[I  $\varphi/6$ ], 0, 0, 0, -V Exp[-I  $\varphi/6$ ], 0,  $\epsilon_R + \epsilon_Z -$ 
 $\epsilon_{EE}$ , -Vout Exp[I  $\theta$ ], 0},

{0, 0, 0, 0, 0, 0, 0, 0, 0, 0, 0, -Vout, -Vout, 1, 0}
}]];

(*Transmission coefficient is last term of last matrix*)
t=A[x+1][[13]][[14]];
t]

```

```

{l b=-2, r b=2}; (*Set bounds of plot*)

```

(*Plot transmission coefficient for same parameters as large matrix. Calculating a reflection coefficient is far more difficult in this method, so the only internal consistency check to use is to compare it with the method done by hand*)

```

Plot[{Abs[tCalculator[EE,0,.3,.3,.3,.3,0,0,0,0,0,0,4]]^2},{EE,l b,r b},
Axes->False,Frame->True,

PlotRange->{{l b,r b},{0.,1.1}},PlotStyle->{AbsoluteThickness[2.8]},

FrameLabel-> {"E","T"},

BaseStyle->{"Times",20}]

```

(*Create plots of transmission as a function of energy and flux to manipulate and look for results*)

```

Manipulate[Plot[{Abs[tCalculator[EE, $\Psi$ ,VL/\[Sqrt]2,VR/\[Sqrt]2,Vm,Vin, $\epsilon_L$ , $\epsilon_{TL}$ , $\epsilon_{TR}$ , $\epsilon_{BL}$ , $\epsilon_{BR}$ , $\epsilon_R$ , $\epsilon_Z$ ,NN]]^2},{EE,l b,r b},Axes->False,Frame->True,

PlotRange->{{l b,r b},{0.,1.1}},PlotStyle->{AbsoluteThickness[2.8]},

FrameLabel-> {"E","T"},

BaseStyle->{"Times",20}(*,PlotLabel->"Transmission vs
Energy"*)(*,MaxRecursion->12*)],{{NN,12},3,15,1},{ $\Psi$ ,0.25},0,1},{ $\epsilon_Z$ ,0.
2},0,2},{VL,.5},0,1},{VR,.5},0,1},{Vm,.5},0,1},{Vin,.5},0,1},{ $\epsilon_L$ ,
0},-2,2},{ $\epsilon_{TL}$ ,0},-2,2},{ $\epsilon_{TR}$ ,0},-2,2},{ $\epsilon_{BL}$ ,0},-2,2},{ $\epsilon_{BR}$ ,0},-
2,2},{ $\epsilon_R$ ,0},-2,2}]

```

```

Manipulate[Plot[{Abs[tCalculator[EE, $\Psi$ ,Vin,Vout,VB,V, $\epsilon_L$ , $\epsilon_{TL}$ , $\epsilon_{TR}$ , $\epsilon_{BL}$ , $\epsilon_{BR}$ , $\epsilon_R$ , $\epsilon_Z$ ,NN]]^2},{ $\Psi$ ,0,1},Axes->False,Frame->True,

```



```

PlotRange->{{0,1},{0.,1.1}},PlotStyle->{AbsoluteThickness[2.8]},
FrameLabel-> {"Ψ","T"},
BaseStyle->{"Times",20},PlotLabel->"Transmission vs Flux",{EE,-
.1},-
2,2},{Vin,.3},0,1},{Vout,.3},0,1},{VB,.3},0,1},{V,.3},0,1},{εL,0},
-2,2},{εTL,0},-2,2},{εTR,0},-2,2},{εBL,0},-2,2},{εBR,0},-
2,2},{εR,0},-2,2},{εz,0},0,2},{NN,4},3,15,1]]
Needs["PlotLegends`"]
ShowLegend[ContourPlot[{Abs[tCalculator[EE,Ψ,.3,.3,.3,.3,.5,.5,.5,.5,.
5,.5,.2,4]]^2},{EE,-.5,1.5},{Ψ,0.00,1.},Contours->10,PlotPoints->
50,PlotRange->{0.,1.},FrameTicks->
{Automatic,Automatic,None,None},FrameLabel->{"E","Φ/Φ0"},PlotLabel->
"Transmission",ColorFunction->"CMYKColors",BaseStyle->
{"Times",16}],{ColorData["CMYKColors"][1-#1]&,10," 1.0","
0.0",LegendLabel->None,LegendShadow->None,LegendPosition->{1.,-.7}}]
ContourPlot[{Abs[tCalculator[EE,\[CapitalPhi],.3,.3,.3,.3,0,0,0,0,0,0,
0,6]]^2},{EE,0.07,.12},{\[CapitalPhi],.45,0.5},Contours->
10,PlotPoints->50,PlotRange->{0.,1.},FrameTicks->
{Automatic,Automatic,None,None},FrameLabel->
{"E","\[CapitalPhi]/Subscript[\[CapitalPhi], 0]"},PlotLabel->
"Transmission",ColorFunction->"CMYKColors",BaseStyle->
{"Times",16},PlotLegends->Automatic]

```

9. APPENDIX C

IV Calculation of Chain of NN Nanorings, 2 Branches, 2 QD Arms. No Magnetic Effects

By Matt Orvis

This program calculates the Current vs voltage for a chain of linearly connected nanorings. Each ring has 6 QDs, with 2 on each branch and 1 at each end of the ring. Each ring is coupled to the next by a lead, and leads enter and exit the system. In essence, this program finds the transmission coefficient as a function of energy, then integrates over it to find the area under the curve. It needs much more physical system values in order to calculate an actual current and voltage.

```
Clear["Global`*"] (*Clears all variables so that not affected by
previous evaluations*)
```

```
(*Create module which calculates and returns the transmission
coefficient*)
```

```
tCalculator[EE_,V1_,VL_,VR_,VB_,εL_,εTL_,εTR_,εBL_,εBR_,εR_,NN_] := Module
[{θ,A,t},
```

```
θ=ArcCos[-EE/2];(*Dispersion relationship*)
```

```
(*Initialize loop with manually inputting first matrix for as many
rings as you want*)
```

```
A[1]=RowReduce[({
  {-VL, 0, 0, 0, 0, 0, Exp[-I θ], 0, -Exp[I θ]},
  {εL-EE, -V1, 0, -V1, 0, 0, -VL, 0, VL},
  {-V1, εTL-EE, -V1, 0, 0, 0, 0, 0, 0},
  {0, -V1, εTR-EE, 0, 0, -V1, 0, 0, 0},
  {-V1, 0, 0, εBL-EE, -V1, 0, 0, 0, 0},
  {0, 0, 0, -V1, εBR-EE, -V1, 0, 0, 0},
  {0, 0, -V1, 0, -V1, εR-EE, 0, -VB, 0}
})];
```

```
(*Run a do loop that iterates the middle matrix, calling terms from
the previous matrix, passing information from ring to ring*)
```

```
Do[
```

```
A[i]=RowReduce[({
```

```

        {εL-EE+VB A[i-1][[6]][[8]], -v1, 0, -v1, 0, 0, 0, 0, VB A[i-
1][[6]][[9]]},
        {-v1, εTL-EE, -v1, 0, 0, 0, 0, 0, 0},
        {0, -v1, εTR-EE, 0, 0, -v1, 0, 0, 0},
        {-v1, 0, 0, εBL-EE, -v1, 0, 0, 0, 0},
        {0, 0, 0, -v1, εBR-EE, -v1, 0, 0, 0},
        {0, 0, -v1, 0, -v1, εR-EE, 0, -VB, 0}
    }]);
x=i;
,{i,2,NN-1}
];
(*Finish system by manually inputting final ring*)
A[x+1]=RowReduce[({
        {εL-EE+VB A[x][[6]][[8]], -v1, 0, -v1, 0, 0, 0, VB
A[x][[6]][[9]]},
        {-v1, εTL-EE, -v1, 0, 0, 0, 0, 0, 0},
        {0, -v1, εTR-EE, 0, 0, -v1, 0, 0, 0},
        {-v1, 0, 0, εBL-EE, -v1, 0, 0, 0, 0},
        {0, 0, 0, -v1, εBR-EE, -v1, 0, 0, 0},
        {0, 0, -v1, 0, -v1, εR-EE, -VR Exp[I θ], 0},
        {0, 0, 0, 0, 0, -VR, 1, 0}
    }]);
(*Transmission coefficient is last term of last matrix*)
t=A[x+1][[7]][[8]];
t]
(*Set Physical Parameters*)
(*ef:=0.1;*)κ:=0.5;
kb:=8.6174*10^(-5); (*Boltzmann Constant*)
q:=293; (*Temperaure in K. Room Temp*)
β:=1/(kb*q); (*Fermi Energy*)

```

```

(*Begin integration technique, using Simpson's Numerical Integration
Technique*)

IV=Function[{EE,ef,V1,VL,VR,VB,εL,εTL,εTR,εBL,εBR,εR,NN},77.37*(Abs[tCa]
culator[EE,V1,VL,VR,VB,εL,εTL,εTR,εBL,εBR,εR,NN]]^2)*(1/(Exp[β*{EE-ef-
(1-κ)*v}]+1)-1/(Exp[β*{EE-ef+(κ*v)}]+1))];

Simpson1[a0_,b0_,m0_,efe_,V1a_,VLa_,VRa_,VBa_,εLa_,εTLa_,εTRA_,εBLa_,εBR
a_,εRa_,NNa_]:=

Module[{a=N[a0],b=N[b0],m=m0,ef=efe,V1=V1a,VL=VLa,VR=VRa,VB=VBa,εL=εLa,
εTL=εTLa,εTR=εTRA,εBL=εBLa,εBR=εBRa,εR=εRa,NN=NNa},

h=(b-a)/(2m);
SumEven=0;
For[k=1,k<=m-1,k++,
SumEven=SumEven+IV[a+h 2
k,ef,V1,VL,VR,VB,εL,εTL,εTR,εBL,εBR,εR,NN];];
SumOdd=0;
For[k=1,k<=m,k++,
SumOdd=SumOdd+IV[a+h (2 k-
1),ef,V1,VL,VR,VB,εL,εTL,εTR,εBL,εBR,εR,NN];];
Return[h/3
(IV[a,ef,V1,VL,VR,VB,εL,εTL,εTR,εBL,εBR,εR,NN]+IV[b,ef,V1,VL,VR,VB,εL,εT
L,εTR,εBL,εBR,εR,NN]+2 SumEven+4 SumOdd)];];

(*Create plot of Current vs voltage that is able to be manipulated*)
Manipulate[

current=Simpson1[a,b,m,ef,V1,VL,VR,VB,εL,εTL,εTR,εBL,εBR,εR,NN];

Plot[current,{v,-1.5,1.5},Axes->False,Frame->True,FrameStyle-
>Thick,FrameLabel->{"Vsd (V)", "I(μA)"},BaseStyle-
>{"Helvetica",22,Bold},PlotStyle->{AbsoluteThickness[3]}, PlotRange-
>{{-1.5,1.5},{-70.,70.}}]

,{a,-1,-10,10},{b,1,-10,10},{m,50},1,100},{ef,0.0},-
2,2},{V1,.301},0,1},{VL,.3},0,1},{VR,.3},0,1},{VB,.3},0,1},{εL,0.
0},-2,2},{εTL,0.0},-2,2},{εTR,0.0},-2,2},{εBL,0.0},-
2,2},{εBR,0.0},-2,2},{εR,0.0},-2,2},{NN,4},3,20,1}

]

```

```
(*Needs["PlotLegends`"]

ShowLegend[ContourPlot[Simpson1[-1., 1., 100, ezz, 0, 0], {v, -
1, 1}, {ezz, 0.00, .5}, PlotPoints->25, Contours->15, PlotRange->{-
20., 20.}, FrameTicks->{Automatic, Automatic, None, None}, FrameLabel->{"V", "e
z"}, PlotLabel->"Current", BaseStyle->{"Times", 16}], {ColorData["LakeColors
"][[1-#1]&, 10, " 20", " -
20", LegendLabel->None, LegendShadow->None, LegendPosition->{1., -.7}]}]*)

current1=Simpson1[-1, 1, 50, 0, .501, .5, .5, .3, 0, 0, 0, 0, 0, 0, 12];
current2=Simpson1[-1, 1, 50, 0, .501, .5, .5, .5, 0, 0, 0, 0, 0, 0, 12];
current3=Simpson1[-1, 1, 50, 0, .501, .5, .5, 1.0, 0, 0, 0, 0, 0, 0, 12];
Plot[{current1, current2, current3}, {v, -2.0, 2.0}, Axes->False, Frame-
>True, FrameStyle->Thick, FrameLabel->{"Vsd (Volt)", "I(μA)"}, BaseStyle-
>{"Helvetica", 22, Bold}, PlotStyle->{Blue, Dashed, {Dotted, Black}}
, PlotStyle->{AbsoluteThickness[3]}, PlotRange->{{-2.0, 2.0}, {-
100., 100.}}]
```

10. APPENDIX D

IV Calculation of Chain of NN Nanorings, 2 Branches, 2 QD Arms. With Magnetic Effects

By Matt Orvis

This program calculates the Current vs voltage for a chain of linearly connected nanorings. Each ring has 6 QDs, with 2 on each branch and 1 at each end of the ring. Each ring is coupled to the next by a lead, and leads enter and exit the system. In essence, this program finds the transmission coefficient as a function of energy, then integrates over it to find the area under the curve. It needs much more physical system values in order to calculate an actual current and voltage. This contains the Aharonov Bohm Effect and Zeeman Effect to incorporate magnetic flux.

```
Clear["Global`*"] (*Clears all variables so that not affected by previous evaluations*)
```

```
(*Create module which calculates and returns the transmission coefficient*)
```

```
tCalculator[EE_,Ψ_,Vin_,Vout_,VB_,V_,εL_,εTL_,εTR_,εBL_,εBR_,εR_,εZ_,NN_] := Module[{θ,φ,A,t},
```

```
  θ = ArcCos[-EE/2]; (*Dispersion relationship*)
```

```
  φ = 2π Ψ/1; (*Magnetic Flux for AB Effect*)
```

```
(*Initialize loop with manually inputting first matrix for as many rings as you want*)
```

```
  A[1] = RowReduce[{
    {-Vin, -Vin, 0, 0, 0, 0, 0, 0, 0, 0, 0, 0, 0, Exp[-I θ], 0, 0, -
    Exp[I θ]},
    {εL-εZ-EE, 0, -V Exp[-I φ/6], 0, 0, 0, -V Exp[I φ/6], 0, 0, 0, 0,
    0, -Vin, 0, 0, Vin},
    {0, εL+εZ-EE, 0, -V Exp[-I φ/6], 0, 0, 0, -V Exp[I φ/6], 0, 0, 0,
    0, -Vin, 0, 0, Vin},
    {-V Exp[I φ/6], 0, εTL-εZ-EE, 0, -V Exp[-I φ/6], 0, 0, 0, 0, 0, 0,
    0, 0, 0, 0, 0},
    {0, -V Exp[I φ/6], 0, εTL+εZ-EE, 0, -V Exp[-I φ/6], 0, 0, 0, 0, 0,
    0, 0, 0, 0, 0},
    {0, 0, -V Exp[I φ/6], 0, εTR-εZ-EE, 0, 0, 0, 0, 0, 0, -V Exp[-I
    φ/6], 0, 0, 0, 0, 0},
    {0, 0, 0, -V Exp[I φ/6], 0, εTR+εZ-EE, 0, 0, 0, 0, 0, -V Exp[-I
    φ/6], 0, 0, 0, 0},
```

```

    {-V Exp[-I φ/6], 0, 0, 0, 0, 0, εBL-εZ-EE, 0, -V Exp[I φ/6], 0,
0, 0, 0, 0, 0, 0},
    {0, -V Exp[-I φ/6], 0, 0, 0, 0, 0, εBL+εZ-EE, 0, -V Exp[I φ/6],
0, 0, 0, 0, 0, 0},
    {0, 0, 0, 0, 0, 0, -V Exp[-I φ/6], 0, εBR-εZ-EE, 0, -V Exp[I
φ/6], 0, 0, 0, 0, 0},
    {0, 0, 0, 0, 0, 0, 0, -V Exp[-I φ/6], 0, εBR+εZ-EE, 0, -V Exp[I
φ/6], 0, 0, 0, 0, 0},
    {0, 0, 0, 0, -V Exp[I φ/6], 0, 0, 0, -V Exp[-I φ/6], 0, εR-εZ-EE,
0, 0, -VB, 0, 0},
    {0, 0, 0, 0, 0, -V Exp[I φ/6], 0, 0, 0, -V Exp[-I φ/6], 0, εR+εZ-
EE, 0, 0, -VB, 0}
  }]);

```

(*Run a do loop that iterates the middle matrix, calling terms from the previous matrix, passing information from ring to ring*)

```

Do[
  A[i]=RowReduce[({
    {εL-εZ-EE+VB A[i-1][[11]][[14]], VB A[i-1][[11]][[15]], -V Exp[-
I φ/6], 0, 0, 0, -V Exp[I φ/6], 0, 0, 0, 0, 0, 0, 0, 0, VB A[i-
1][[11]][[16]]},
    {VB A[i-1][[12]][[14]], εL+εZ-EE+VB A[i-1][[12]][[15]], 0, -V
Exp[-I φ/6], 0, 0, 0, -V Exp[I φ/6], 0, 0, 0, 0, 0, 0, 0, 0, VB A[i-
1][[12]][[16]]},
    {-V Exp[I φ/6], 0, εTL-εZ-EE, 0, -V Exp[-I φ/6], 0, 0, 0, 0, 0,
0, 0, 0, 0, 0, 0},
    {0, -V Exp[I φ/6], 0, εTL+εZ-EE, 0, -V Exp[-I φ/6], 0, 0, 0, 0,
0, 0, 0, 0, 0, 0},
    {0, 0, -V Exp[I φ/6], 0, εTR-εZ-EE, 0, 0, 0, 0, 0, 0, -V Exp[-I
φ/6], 0, 0, 0, 0, 0},
    {0, 0, 0, -V Exp[I φ/6], 0, εTR+εZ-EE, 0, 0, 0, 0, 0, 0, -V Exp[-I
φ/6], 0, 0, 0, 0},
    {-V Exp[-I φ/6], 0, 0, 0, 0, 0, εBL-εZ-EE, 0, -V Exp[I φ/6], 0,
0, 0, 0, 0, 0, 0},
    {0, -V Exp[-I φ/6], 0, 0, 0, 0, 0, εBL+εZ-EE, 0, -V Exp[I φ/6],
0, 0, 0, 0, 0, 0},
    {0, 0, 0, 0, 0, 0, -V Exp[-I φ/6], 0, εBR-εZ-EE, 0, -V Exp[I
φ/6], 0, 0, 0, 0, 0},

```

{0, 0, 0, 0, 0, 0, 0, -V Exp[-I $\varphi/6$], 0, $\epsilon_{BR+\epsilon Z-EE}$, 0, -V Exp[I $\varphi/6$], 0, 0, 0, 0},

{0, 0, 0, 0, -V Exp[I $\varphi/6$], 0, 0, 0, -V Exp[-I $\varphi/6$], 0, $\epsilon_{R-\epsilon Z-EE}$, 0, 0, -VB, 0, 0},

{0, 0, 0, 0, 0, -V Exp[I $\varphi/6$], 0, 0, 0, -V Exp[-I $\varphi/6$], 0, $\epsilon_{R+\epsilon Z-EE}$, 0, 0, -VB, 0}

}}];

x=i;

,{i,2,NN-1}

];

(*Finish system by manually inputting final ring*)

A[x+1]=RowReduce[({

{ $\epsilon_{L-\epsilon Z-EE}+VB A[x][[11]][[14]]$, $VB A[x][[11]][[15]]$, -V Exp[-I $\varphi/6$], 0, 0, 0, -V Exp[I $\varphi/6$], 0, 0, 0, 0, 0, 0, $VB A[x][[11]][[16]]$ },

{ $VB A[x][[12]][[14]]$, $\epsilon_{L+\epsilon Z-EE}+VB A[x][[12]][[15]]$, 0, -V Exp[-I $\varphi/6$], 0, 0, 0, -V Exp[I $\varphi/6$], 0, 0, 0, 0, 0, 0, $VB A[x][[12]][[16]]$ },

{-V Exp[I $\varphi/6$], 0, $\epsilon_{TL-\epsilon Z-EE}$, 0, -V Exp[-I $\varphi/6$], 0, 0, 0, 0, 0, 0, 0, 0},

{0, -V Exp[I $\varphi/6$], 0, $\epsilon_{TL+\epsilon Z-EE}$, 0, -V Exp[-I $\varphi/6$], 0, 0, 0, 0, 0, 0, 0},

{0, 0, -V Exp[I $\varphi/6$], 0, $\epsilon_{TR-\epsilon Z-EE}$, 0, 0, 0, 0, 0, -V Exp[-I $\varphi/6$], 0, 0, 0},

{0, 0, 0, -V Exp[I $\varphi/6$], 0, $\epsilon_{TR+\epsilon Z-EE}$, 0, 0, 0, 0, 0, -V Exp[-I $\varphi/6$], 0, 0},

{-V Exp[-I $\varphi/6$], 0, 0, 0, 0, 0, $\epsilon_{BL-\epsilon Z-EE}$, 0, -V Exp[I $\varphi/6$], 0, 0, 0, 0},

{0, -V Exp[-I $\varphi/6$], 0, 0, 0, 0, 0, $\epsilon_{BL+\epsilon Z-EE}$, 0, -V Exp[I $\varphi/6$], 0, 0, 0, 0},

{0, 0, 0, 0, 0, 0, -V Exp[-I $\varphi/6$], 0, $\epsilon_{BR-\epsilon Z-EE}$, 0, -V Exp[I $\varphi/6$], 0, 0, 0},

{0, 0, 0, 0, 0, 0, 0, -V Exp[-I $\varphi/6$], 0, $\epsilon_{BR+\epsilon Z-EE}$, 0, -V Exp[I $\varphi/6$], 0, 0},

{0, 0, 0, 0, -V Exp[I $\varphi/6$], 0, 0, 0, -V Exp[-I $\varphi/6$], 0, $\epsilon_{R-\epsilon Z-EE}$, 0, -Vout Exp[I θ], 0},

{0, 0, 0, 0, 0, -V Exp[I $\varphi/6$], 0, 0, 0, -V Exp[-I $\varphi/6$], 0, $\epsilon_{R+\epsilon Z-EE}$, -Vout Exp[I θ], 0},


```

{0, 0, 0, 0, 0, 0, 0, 0, 0, 0, 0, -Vout, -Vout, 1, 0}
}]];
(*Transmission coefficient is last term of last matrix*)
t=A[x+1][[13]][[14]];
t]
(*Set Physical Parameters*)
(*ef:=0.1;*)κ:=0.5;
kb:=8.6174*10^(-5);(*Boltzmann Constant*)
q:=293; (*Temperaure in K. Room Temp*)
β:=1/(kb*q); (*Fermi Energy*)
(*Begin integration technique, using Simpson's Numerical Integration
Technique*)
IV=Function[{EE,Ψ,ef,v1,vL,vR,vB,εL,εTL,εTR,εBL,εBR,εR,εZ,NN},77.37*(Abs
[tCalculator[EE,Ψ,vL/\[Sqrt]2,vR/\[Sqrt]2,vB,v1,εL,εTL,εTR,εBL,εBR,εR,εZ
,NN]]^2)*(1/(Exp[β*{EE-ef-(1-κ)*v}]+1)-1/(Exp[β*{EE-ef+(κ*v)}]+1))];
Simpson1[a0_,b0_,m0_,efe_,v1a_,vLa_,vRa_,vBa_,εLa_,εTLa_,εTRA_,εBLa_,εBR
a_,εRa_,Ψa_,εza_,NNa_] :=
Module[{a=N[a0],b=N[b0],m=m0,ef=efe,v1=v1a,vL=vLa,vR=vRa,vB=vBa,εL=εLa,
εTL=εTLa,εTR=εTRA,εBL=εBLa,εBR=εBRa,εR=εRa,Ψ=Ψa,εZ=εza,NN=NNa},

h=(b-a)/(2m);
SumEven=0;
For[k=1,k<=m-1,k++,
SumEven=SumEven+IV[a+ h 2
k,Ψ,ef,v1,vL,vR,vB,εL,εTL,εTR,εBL,εBR,εR,εZ,NN];];
SumOdd=0;
For[k=1,k<=m,k++,
SumOdd=SumOdd+IV[a+h (2 k-
1),Ψ,ef,v1,vL,vR,vB,εL,εTL,εTR,εBL,εBR,εR,εZ,NN];];
Return[h/3
(IV[a,Ψ,ef,v1,vL,vR,vB,εL,εTL,εTR,εBL,εBR,εR,εZ,NN]+IV[b,Ψ,ef,v1,vL,vR,v
B,εL,εTL,εTR,εBL,εBR,εR,εZ,NN]+2 SumEven+4 SumOdd)];];
(*Create plot of Current vs voltage that is able to be manipulated*)
Manipulate[

```

```

current=Simpson1[a,b,m,ef,V1,VL,VR,VB,εL,εTL,εTR,εBL,εBR,εR,Ψ,εZ,NN];

Plot[current,{v,-1.5,1.5},Axes->False,Frame->True,FrameStyle->Thick,
FrameLabel->{"Vsd (Volt)","I(μA)"},BaseStyle->{"Helvetica",22,Bold},
PlotStyle->{AbsoluteThickness[3]},PlotRange->{{-1.5,1.5},{-70.,70.}}]

,{a,-1,-10,10},{b,1,-10,10},{m,50},1,100},{ef,0.0},-2,2},
{{V1,.301},0,1},{VL,.3},0,1},{VR,.3},0,1},{VB,.3},0,1},{εL,0.0},-2,2},
{{εTL,0.0},-2,2},{εTR,0.0},-2,2},{εBL,0.0},-2,2},{εBR,0.0},-2,2},
{{εR,0.0},-2,2},{Ψ,0.0},0,1},{εZ,0.0},0,2},{NN,4},3,20,1]

]

(*Needs["PlotLegends`"]

ShowLegend[ContourPlot[Simpson1[-1., 1.,100,ezz,0,0],{v,-1,1},
{ezz,0.00,.5},PlotPoints→25,Contours→15,PlotRange→{-20.,20.},
FrameTicks→{Automatic,Automatic, None, None},FrameLabel→{"V","ezz"},
PlotLabel→"Current",BaseStyle→{"Times",16}],{ColorData["LakeColors"]
[1-#1]&,10," 20"," - 20",LegendLabel→None,LegendShadow→None,
LegendPosition→{1.,-.7}}]*)

current1=Simpson1[-1,1,50,0,.501,.5,.5,.3,0,0,0,0,0,0,0,12];
current2=Simpson1[-1,1,50,0,.501,.5,.5,.5,0,0,0,0,0,0,0,12];
current3=Simpson1[-1,1,50,0,.501,.5,.5,1.0,0,0,0,0,0,0,0,12];

Plot[{current1,current2,current3},{v,-2.0,2.0},Axes->False,Frame->True,
FrameStyle->Thick,FrameLabel->{"Vsd (Volt)","I(μA)"},BaseStyle->{"Helvetica",22,Bold},
PlotStyle->{Blue,Dashed,{Dotted,Black}},PlotStyle->{AbsoluteThickness[3]},
PlotRange->{{-2.0,2.0},{-100.,100.}}]

```